6 EARTH RESOURCE SATELLITES OPERATING IN THE OPTICAL SPECTRUM

6.1 INTRODUCTION

Probably no combination of two technologies has generated more interest and application over a wider range of disciplines than the merger of remote sensing and space exploration. Although many aspects of the process are still in the developmental stage, studying the earth from space has evolved from the realm of pure research to that of worldwide, day-to-day application. Currently we depend on spaceborne sensors to assist in tasks ranging from weather prediction, crop forecasting, and mineral exploration to applications as diverse as pollution detection, rangeland monitoring, and commercial fishing. All this has happened in a very short period of time, and the status of remote sensing from space continues to change as new and/or improved spacecraft are placed into earth orbit.

Without question, the most important outcome of development in space exploration and remote sensing has been the role these technologies have played in conceiving of the earth as a system. Space remote sensing has brought a new dimension to understanding not only the natural wonders and processes operative on our planet but also the impacts of humankind on earth's fragile and interconnected resource base.

This chapter emphasizes satellite systems that operate within the *optical spectrum*, which extends from approximately 0.3 to 14 μm. This range includes UV, visible, near-, mid-, and thermal IR wavelengths. (It is termed the optical spectrum because lenses and mirrors can be used to refract and reflect such energy.) Substantial remote sensing from space is also performed using systems that operate in the *microwave* portion of the spectrum (approximately 1 mm to 1 m wavelength). Microwave remote sensing is the subject of Chapter 8.

The subject of remote sensing from space is a rapidly changing one, with numerous countries and commercial firms developing and launching new systems on a regular basis. In this dynamic environment, it is more important than ever that potential users of data from spaceborne remote sensing systems understand the basic design characteristics of these systems and the various trade-offs that determine whether a particular sensor will be suitable for a given application. Hence, we begin this discussion with an overview of the general characteristics common to all satellite systems. We then examine a wide range of satellite systems, with reference to the ways their designs exemplify the fundamental characteristics discussed in this section.

Although we aim to be current in our coverage of spaceborne remote sensing systems, the rapid pace of change in this field suggests that some of the material in this chapter about certain specific systems will likely be dated rapidly. At the same time, as researchers and practitioners focus on regional to global change issues, knowledge about the characteristics of many of the early systems that are no longer in operation is essential. Thus, after a brief historical overview of the early development of remote sensing from space, we treat the U.S. Landsat and French SPOT satellite systems in some degree of detail. These were the first and most robust global monitoring systems to acquire moderate resolution data on a systematic basis. Also, many of their principles of operation apply to the numerous other systems available today and planned for the future.

After our discussion of the Landsat and SPOT satellite systems and their future counterparts, we describe briefly numerous other earth resources satellites, including high resolution systems and hyperspectral sensors. We then discuss meteorological satellites, ocean monitoring satellites, the Earth Observing System, and space station remote sensing. Depending upon one's academic or work setting, one may wish to "skip over" certain of the sections in this chapter. We have written this discussion with this possibility in mind.

There are many characteristics that describe any given satellite remote sensing system and determine whether or not it will be suitable for a particular application. Among the most fundamental of these characteristics is the satellite's orbit. A satellite in orbit about a planet moves in an elliptical path with the planet at one of the foci of the ellipse. Important elements of the orbit include its *altitude*, *period*, *inclination*, and *equatorial crossing time*. For most earth observation satellites, the orbit is approximately circular, with al-

titudes more than 400 km above the earth's surface. The period of a satellite, or time to complete one orbit, is related to its altitude according to the formula (Elachi, 1987)

$$T_o = 2\pi(R_p + H') \sqrt{\frac{R_p + H'}{g_s R_p^2}} \tag{6.1}$$

where

T_o = orbital period, sec
R_p = planet radius, km (about 6380 km for earth)
H' = orbit altitude (above planet's surface), km
g_s = gravitational acceleration at planet's surface (0.00981 km/sec^2 for earth)

The inclination of a satellite's orbit refers to the angle at which it crosses the equator. An orbit with an inclination close to 90° is referred to as near polar because the satellite will pass near the north and south poles on each orbit. An equatorial orbit, in which the spacecraft's ground track follows the line of the equator, has an inclination of 0°. Two special cases are *sun-synchronous* orbits and *geostationary* orbits. A sun-synchronous orbit results from a combination of orbital period and inclination such that the satellite keeps pace with the sun's westward progress as the earth rotates. Thus, the satellite always crosses the equator at precisely the same local sun time (the local clock time varies with position within each time zone). A geostationary orbit is an equatorial orbit at the altitude (approximately 36,000 km) that will produce an orbital period of exactly 24 hr. A geostationary satellite thus completes one orbit around the earth in the same amount of time needed for the earth to rotate once about its axis and remains in a constant relative position over the equator.

The above elements of a satellite's orbit are illustrated in Figure 6.1, for the Landsat-4 and -5 satellites. As discussed in Section 6.5, the Landsat-4 and -5 satellites were launched into circular, near-polar orbits at an altitude of 705 km above the earth's surface. Solving Eq. 6.1 for this altitude yields an orbital period of about 98.9 min, which corresponds to approximately 14.5 orbits per day. The orbital inclination chosen for Landsat-4 and -5 was 98.2°, resulting in a sun-synchronous orbit. (The orbit for Landsat-7 is nearly identical to that of Landsat-4 and -5).

Another important characteristic of a satellite remote sensing system is its spatial resolution. The principles discussed in Chapter 5 that determine the spatial resolution for airborne sensors also apply to spaceborne systems. Thus, at nadir the spatial resolution is determined by the orbital altitude and the instantaneous field of view, while off nadir the ground resolution cell size increases in both the along-track and across-track dimensions. However, for spaceborne systems the curvature of the earth further degrades the spatial resolution for off-nadir viewing. This becomes particularly important for pointable systems and for systems with a wide total field of view.

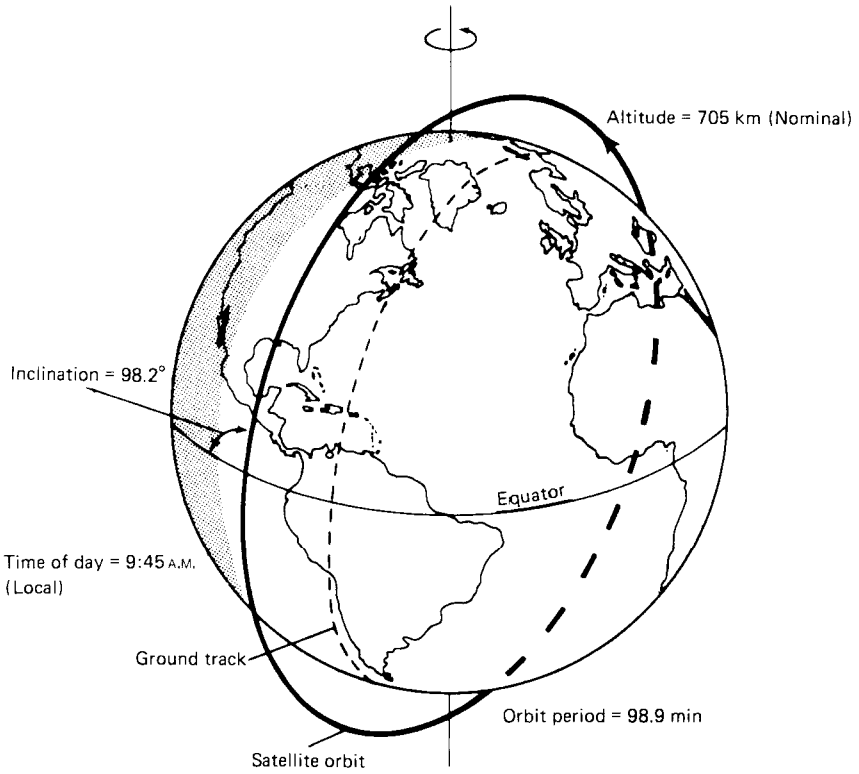

Figure 6.1 Sun-synchronous orbit of Landsat-4 and -5. (Adapted from NASA diagram.)

The spectral characteristics of a satellite remote sensing system include the number, width, and position of the sensor's spectral bands. The extreme cases are panchromatic sensors, with a single broad spectral band, and hyperspectral sensors, with a hundred or more narrow, contiguous spectral bands. During sensor calibration, the relative sensitivity of each band as a function of wavelength may be determined.

The radiometric properties of a remote sensing system include the radiometric resolution, typically expressed as the number of data bits used to record the observed radiance. They also include the gain setting (Section 7.2) that determines the range of variation in brightness over which the system will be sensitive, and the signal-to-noise ratio of the sensor. In some cases, the gain setting on one or more bands may be programmable from the ground, to permit the acquisition of data under different conditions, such as over the dark ocean and the bright polar ice caps. It should be noted that increasing the spatial and spectral resolution both result in a decrease in the energy available to be sensed. A high spatial resolution means that each detector is receiving energy from a smaller area, while a high spectral resolution means

that each detector is receiving energy in a narrower range of wavelengths. Thus, there are trade-offs among the spatial, spectral, and radiometric properties of a spaceborne remote sensing system.

Some other factors to consider in evaluating a satellite system include its coverage area, revisit period (time between successive coverages), and off-nadir imaging capabilities. For sensors that cannot be steered to view off nadir, the swath width is determined by the orbital altitude and the sensor's total field of view, while the revisit period is determined by the orbital period and the swath width. For example, the Landsat-7 ETM+ and Terra/Aqua MODIS instruments are on satellite platforms that share the same orbital altitude and period, but MODIS has a much wider field of view. This gives it a much greater swath width, which in turn means that any given point on the earth will appear in MODIS imagery more frequently. If across-track pointing is used, both the swath width and revisit period will be affected. For certain time-sensitive applications, such as monitoring the effects of flooding, fires, and other natural disasters, a frequent revisit cycle is particularly important. Either across-track or along-track pointing can be used to collect stereoscopic imagery, which can assist in image interpretation and topographic analysis. The primary advantage of along-track pointing for stereoscopic image acquisition is that both images of the stereopair will be acquired within a very brief period of time, typically no more than seconds or minutes apart. Across-track stereoscopic images are often acquired several days apart (with the attendant changes in atmospheric and surface conditions between dates).

Many other practical considerations determine the potential utility of any given satellite remote sensing system in any given application context. These include such factors as the procedures for tasking the satellite, data delivery options, data archiving, license/copyright restrictions, and data cost. These characteristics, many of which are often overlooked by prospective users of satellite imagery, have the potential to radically alter the usability of the imagery from any given system.

6.2 EARLY HISTORY OF SPACE IMAGING

Remote sensing from space received its first impetus through remote sensing from rockets. As early as 1891, a patent was granted to Ludwig Rahrmann of Germany for a "New or Improved Apparatus for Obtaining Bird's Eye Photographic Views." The apparatus was a rocket-propelled camera system that was recovered by parachute. By 1907, another German, Alfred Maul, had added the concept of gyrostabilization to rocket–camera systems. In 1912, he successfully boosted a 41-kg payload containing a 200 × 250-mm format camera to a height of 790 m (ASP, 1983).

Space remote sensing began in earnest during the period 1946 to 1950 when small cameras were carried aboard captured V-2 rockets that were fired

from the White Sands Proving Ground in New Mexico. Over the succeeding years, numerous flights involving photography were made by rockets, ballistic missiles, satellites, and manned spacecraft. However, the photographs produced during early space flights were generally of inferior quality because early missions were made primarily for purposes other than photography. But crude as they were by today's standards, the early photographs demonstrated the potential value of remote sensing from space.

In many respects, the initial efforts aimed at imaging the earth's surface from space were rather incidental outgrowths of the development of meteorological satellites. Beginning with the first Television and Infrared Observation Satellite (TIROS-1) in 1960, early weather satellites returned rather coarse views of cloud patterns and virtually indistinct images of the earth's surface. With refinements in the imaging sensors aboard the meteorological satellites, images of both atmospheric and terrestrial features became more distinct. Eventually, meteorologists began intensive study of surface areas to collect data on water, snow, and ice features. Looking *through*, not just *at*, the earth's atmosphere was becoming possible.

Also beginning in 1960 was an early U.S. military space imaging reconnaissance program, called Corona. This program went through many developments during its lifetime (its final mission was flown in 1972), but the entire effort was classified until 1995 (ASPRS, 1997a).[1] Consequently, the exciting future for remote sensing from space only became apparent to the civilian community as part of the manned space programs of the 1960s: Mercury, Gemini, and Apollo. On May 5, 1961, Alan B. Shepard, Jr., made a 15-min suborbital Mercury flight on which 150 excellent photographs were taken. These pictures were shot with an automatic Mauer 70-mm camera. Because of the trajectory of Shepard's flight, the photographs showed only sky, clouds, and ocean, but the images did indeed substantiate Shepard's statement, "What a beautiful view." On February 20, 1962, John Glenn, Jr., made three historic orbits around the earth and took 48 color photographs during Mercury mission MA-6. The photographs were taken on color negative film with a 35-mm camera and showed mostly clouds and water, although several pictured the deserts of northwest Africa. On later Mercury missions, color pho-

[1]Since 1995, the U.S. government has released two sets of formerly classified imagery taken from photo-reconnaissance satellites. *Declass-1* imagery includes approximately 880,000 frames of photography from the years 1959–1972. *Declass-2* imagery includes approximately 50,000 images taken from 1963–1980. Much of this declassified imagery was taken with various panoramic camera systems. The geographic areas covered by photographs in the Declass-1 and -2 archives are quite extensive, though the images do not provide systematic or complete coverage of the earth. One of the most valuable contributions of these data today is to provide a record of space observations prior to the launch of Landsat-1 in 1972. Historical trends in coastal erosion, glacier movement, urbanization, land use and land cover change, and numerous other time-sensitive phenomena can be studied using these images. Additional information about these data sources may be obtained by consulting the relevant URLs listed in Appendix B.

tographs were taken with 70-mm Hasselblad cameras. A specially modified Hasselblad camera, with an 80-mm lens, soon became the standard for the photographic experiments conducted in the Gemini program. Mission GT-4 of this program included the first formal photographic experiment from space specifically directed at geology. Coverage included nearly vertical overlapping photographs of the southwestern United States, northern Mexico, and other areas of North America, Africa, and Asia. These images soon led to new and exciting discoveries in tectonics, volcanology, and geomorphology.

With the success of the Gemini GT-4 photographic experiments in geology, subsequent missions included a host of similar experiments aimed at investigating various geographic and oceanographic phenomena. Photography comparable to that of the GT-4 experiments was acquired over areas extending between approximately 32° north and south latitudes. Each image had a nominal scale of about 1 : 2,400,000 and included about 140 km on a side. By the end of the Gemini program, some 1100 high quality color photographs had been taken for earth resource applications, and the value of remote sensing from space had become well recognized. Serious thinking began about systematic, repetitive image coverage of the globe.

The scientific community's knowledge and experience with space photography was further extended with the Apollo program. One of the Apollo earth orbit flights (Apollo 9) made prior to the lunar landings included the first controlled experiment involving the acquisition of *multispectral* orbital photography for earth resource studies. A four-camera array of electrically driven and triggered 70-mm Hasselblad cameras was used in the experiment. Photographs were produced using panchromatic film with green and red filters, black and white IR film, and color IR film. Some 140 sets of imagery were thus obtained over the course of 4 days. The imagery covered parts of the southwestern, south central, and southeastern United States as well as parts of Mexico and the Caribbean–Atlantic area.

In 1973, Skylab, the first American space workshop, was launched and its astronauts took over 35,000 images of the earth with the *Earth Resources Experiment Package* (*EREP*) on board. The EREP included a six-camera multispectral array, a long focal length "earth terrain" camera, a 13-channel multispectral scanner, a pointable spectroradiometer, and two microwave systems. The EREP experiments were the first to demonstrate the complementary nature of photography and electronic imaging from space.

Another early (1975) space station experiment having a remote sensing component was the joint *U.S.–USSR Apollo–Soyuz Test Project* (*ASTP*). Regrettably—because earth resource imaging was not a primary goal of this venture—hand-held 35- and 70-mm cameras were again used. For various reasons, the overall quality of most of the images from the ASTP was disappointing. However, like Skylab, the ASTP mission demonstrated that trained crew members could obtain useful, and sometimes unique, earth resource data from visual observation and discretionary imaging. The results

of training crew members to look for specific earth resource phenomena and selectively record important events crystallized the complementary nature of manned and unmanned observation systems.

6.3 LANDSAT SATELLITE PROGRAM OVERVIEW

With the exciting glimpses of earth resources being provided by the early meteorological satellites and the manned spacecraft missions, NASA, with the cooperation of the U.S. Department of the Interior, began a conceptual study of the feasibility of a series of *Earth Resources Technology Satellites* (*ERTSs*). Initiated in 1967, the program resulted in a planned sequence of six satellites that were given before-launch designations ERTS-A, -B, -C, -D, -E, and -F. (After a successful launch into prescribed orbits, they were to become ERTS-1, -2, -3, -4, -5, and -6.)

ERTS-1 was launched by a Thor-Delta rocket on July 23, 1972, and it operated until January 6, 1978. The platform used for the ERTS-1 sensors was a Nimbus weather satellite, modified for the ERTS mission objectives. It represented the first unmanned satellite specifically designed to acquire data about earth resources on a systematic, repetitive, medium resolution, multispectral basis. It was primarily designed as an *experimental* system to test the *feasibility* of collecting earth resource data from unmanned satellites. All data would be collected in accordance with an *"open skies"* principle, meaning there would be nondiscriminatory access to data collected anywhere in the world. All nations of the world were invited to take part in evaluating ERTS-1 data, and the results of this worldwide experimentation with the system were overwhelmingly favorable. In fact, these results probably exceeded most of the expectations of the scientific community. About 300 individual ERTS-1 experiments were conducted in 43 U.S. states and 36 nations.

Just prior to the launch of ERTS-B on January 22, 1975, NASA officially renamed the ERTS program the "Landsat" program (to distinguish it from the planned Seasat oceanographic satellite program). Hence, ERTS-1 was retroactively named Landsat-1 and all subsequent satellites in the series carried the Landsat designation. As of the time of this writing (2002), six Landsat satellites have been launched successfully, namely Landsat-1 to -5 and Landsat-7. Landsat-6 suffered a launch failure.

Table 6.1 highlights the characteristics of the Landsat-1 through -7 missions. It should be noted that five different types of sensors have been included in various combinations on these missions. These are the *Return Beam Vidicon* (*RBV*), the *Multispectral Scanner* (*MSS*), the *Thematic Mapper* (*TM*), the *Enhanced Thematic Mapper* (*ETM*), and the *Enhanced Thematic Mapper Plus* (*ETM+*). Table 6.2 summarizes the spectral sensitivity and spatial resolution of each of these systems as included on the various missions.

TABLE 6.1 Characteristics of Landsat-1 to -7 Missions

Satellite	Launched	Decommissioned	RBV Bands	MSS Bands	TM Bands	Orbit
Landsat-1	July 23, 1972	January 6, 1978	1–3 (simultaneous images)	4–7	None	18 days/900 km
Landsat-2	January 22, 1975	February 25, 1982	1–3 (simultaneous images)	4–7	None	18 days/900 km
Landsat-3	March 5, 1978	March 31, 1983	A–D (one-band side-by-side images)	4–8[a]	None	18 days/900 km
Landsat-4	July 16, 1982[b]	—	None	1–4	1–7	16 days/705 km
Landsat-5	March 1, 1984	—	None	1–4	1–7	16 days/705 km
Landsat-6	October 5, 1993	Failure upon launch	None	None	1–7 plus panchromatic band (ETM)	16 days/705 km
Landsat-7	April 15, 1999	—	None	None	1–7 plus panchromatic band (ETM+)	16 days/705 km

[a]Band 8 (10.4–12.6 μm) failed shortly after launch.

[b]TM data transmission failed in August 1993.

TABLE 6.2 Sensors Used on Landsat-1 to -7 Missions

Sensor	Mission	Sensitivity (μm)	Resolution (m)
RBV	1, 2	0.475–0.575	80
		0.580–0.680	80
		0.690–0.830	80
	3	0.505–0.750	30
MSS	1–5	0.5–0.6	79/82[a]
		0.6–0.7	79/82[a]
		0.7–0.8	79/82[a]
		0.8–1.1	79/82[a]
	3	10.4–12.6[b]	240
TM	4, 5	0.45–0.52	30
		0.52–0.60	30
		0.63–0.69	30
		0.76–0.90	30
		1.55–1.75	30
		10.4–12.5	120
		2.08–2.35	30
ETM[c]	6	Above TM bands plus 0.50–0.90	30 (120 m thermal band) 15
ETM+	7	Above TM bands plus 0.50–0.90	30 (60 m thermal band) 15

[a]79 m for Landsat-1 to -3 and 82 m for Landsat-4 and -5.

[b]Failed shortly after launch (band 8 of Landsat-3).

[c]Landsat-6 launch failure.

Because Landsat-1, -2, and -3 were so similar in their operation, as were Landsat-4 and -5, it is convenient to discuss these systems as two distinct groups, followed by discussion of the Landsat-6 planned mission and Landsat-7.

6.4 LANDSAT-1, -2, AND -3

Figure 6.2 illustrates the basic configuration of Landsat-1, -2, and -3. These butterfly-shaped systems were about 3 m tall and 1.5 m in diameter, with solar panels extending to about 4 m. The satellites weighed about 815 kg and were launched into circular orbits at a nominal altitude of 900 km (the altitude varied between 880 and 940 km) that passed within 9° of the North and South Poles.

Figure 6.3 shows the north-to-south ground traces of the satellite orbits for a single day. Note that they cross the equator at an angle of about 9° from normal, and successive orbits are about 2760 km apart at the equator. Because the sensors aboard the satellite imaged only a 185-km swath, there are

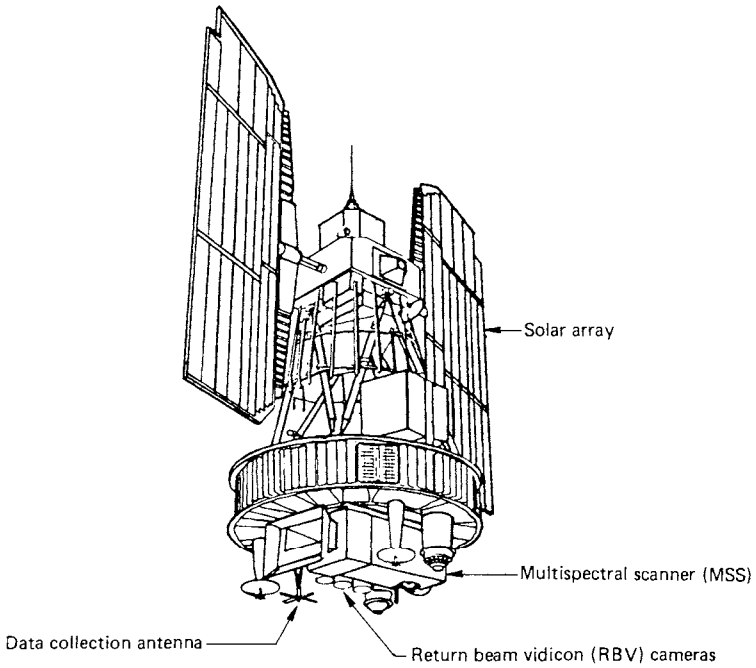

Figure 6.2 Landsat-1, -2, and -3 observatory configuration. (Adapted from NASA diagram.)

large gaps in image coverage between successive orbits on a given day. However, with each new day the satellite orbit progressed slightly westward, just overshooting the orbit pattern of the previous day. (See orbit 15 in Figure 6.3.) This satellite orbit–earth rotation relationship thus yielded images that overlap those of the previous day. The overlap is a maximum at 81° north and south latitudes (about 85 percent) and a minimum (about 14 percent) at the equator. Figure 6.4 shows the set of orbital paths covering the conterminous United States. It took 18 days for the orbit pattern to progress westward to the point of coverage repetition. Thus, the satellites had the capability of covering the globe (except the 82° to 90° polar latitudes) once every 18 days, or about 20 times per year. The satellite orbits were corrected occasionally to compensate for orbital precession caused by atmospheric drag. This ensured that repetitive image centers were maintained to within about 37 km.

At the 103-min orbital period, the 2760-km equatorial spacing between successive orbits caused the satellites to keep precise pace with the sun's westward progress as the earth rotated. As a result, the satellite always crossed the equator at precisely the same local *sun* time (the local clock time varied with location within a time zone). Again, such orbits are referred to as *sun synchronous*.

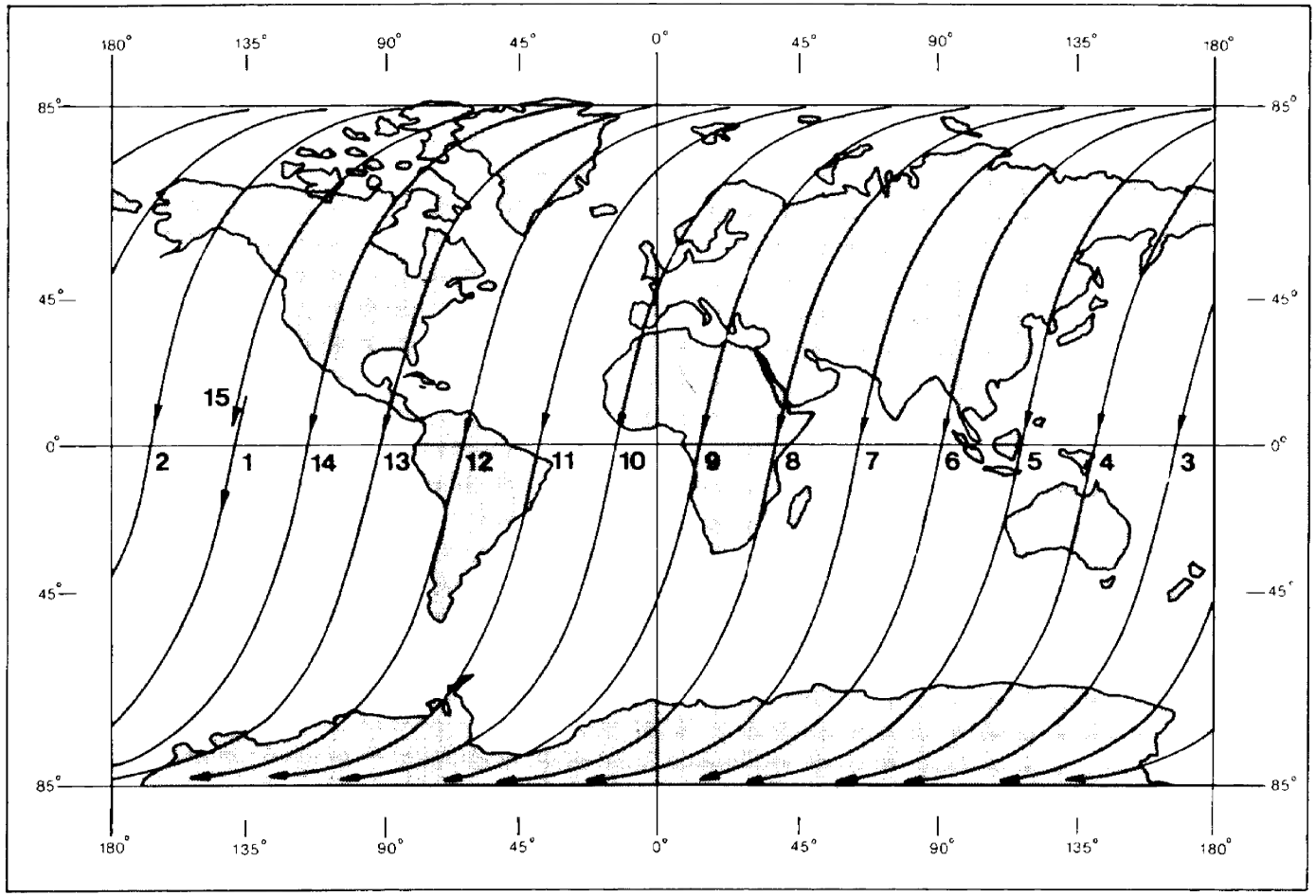

Figure 6.3 Typical Landsat-1, -2, and -3 daily orbit pattern. (Daylight passes only.) (Adapted from NASA diagram.)

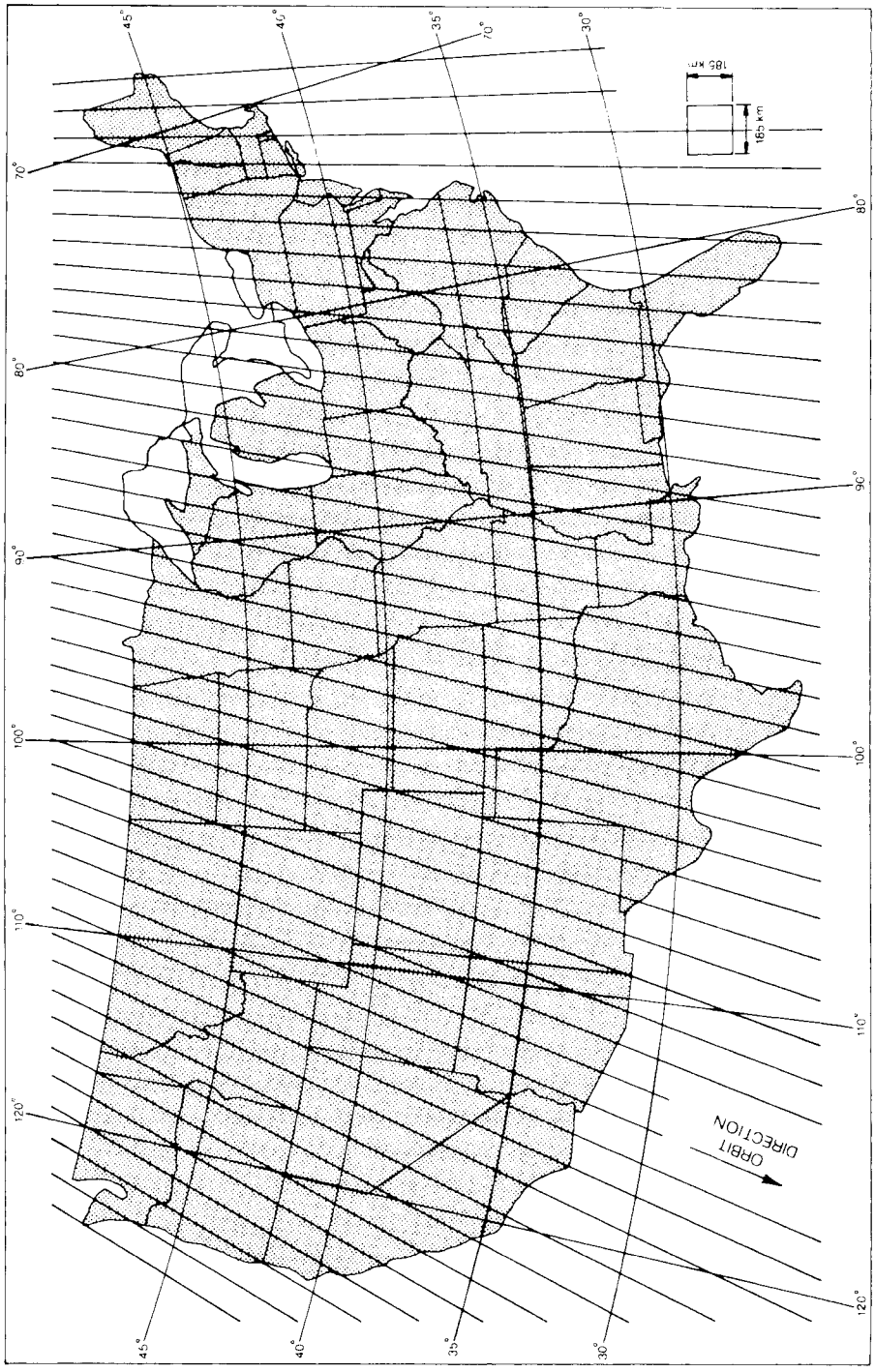

Figure 6.4 Landsat-1, -2, and -3 orbital passes over the conterminous United States. (Adapted from NASA diagram.)

Landsat-1, -2, and -3 were launched into orbits that crossed the equator at 9:42 A.M. local sun time on each pass; however, orbital perturbations caused the crossing times to vary somewhat. This time was selected to take advantage of early morning skies that are generally clearer than later in the day. Because the system's orbital velocity was constant, all other points in its orbit were also passed at a relatively constant local sun time, either slightly after 9:42 A.M. in the Northern Hemisphere or slightly before in the Southern Hemisphere. The important implication of the sun-synchronous orbit is that it ensures repeatable sun illumination conditions during the specific seasons. Repeatable illumination conditions are desirable when mosaicking adjacent tracks of imagery and comparing annual changes in land cover.

Although sun-synchronous orbits ensure repeatable illumination conditions, these conditions vary with location and season. That is, the sun's rays strike the earth at varying solar elevation angles as a function of both latitude and time. For example, the sun's rays strike Sioux Falls, South Dakota, at approximately 20° in December and at 60° in July. Along a single January orbit, the solar elevation changes from 4° in Alaska to 45° near the equator. Likewise, the azimuth direction of solar illumination changes with season and latitude. In short, a sun-synchronous orbit does not compensate for changes in solar altitude, azimuth, or intensity. These factors are always changing and are compounded by variations in atmospheric conditions between scenes.

Landsat-1 and -2 were launched with two identical remote sensing systems onboard: (1) a three-channel RBV system and (2) a four-channel MSS system. The RBV system consisted of three television-like cameras aimed to view the same 185 × 185-km ground area simultaneously. The nominal ground resolution of the cameras was about 80 m, and the spectral sensitivity of each camera was essentially akin to that of a single layer of color IR film: 0.475 to 0.575 μm (green), 0.580 to 0.680 μm (red), and 0.690 to 0.830 μm (near IR). These bands were designated as bands 1, 2, and 3. The RBVs did not contain film, but instead their images were exposed by a shutter device and stored on a photosensitive surface within each camera. This surface was then scanned in raster form by an internal electron beam to produce a video signal just as in a conventional television camera.

Because RBVs image an entire scene instantaneously, in camera fashion, their images have greater inherent cartographic fidelity than those acquired by the Landsat MSS. Also, the RBVs contained a *reseau grid* in their image plane to facilitate geometric correction of the imagery. This resulted in an array of tick marks being precisely placed in each image. By knowing the observed image position versus the theoretical calibration position of these marks, almost all image distortion can be compensated for in the image recording process.

The RBV on Landsat-1 produced only 1690 scenes between July 23 and August 5, 1972, when a tape recorder switching problem (malfunctioning relay switch) forced a system shutdown. The RBV on Landsat-2 was operated

primarily for engineering evaluation purposes and only occasional RBV imagery was obtained, primarily for cartographic uses in remote areas. Two major changes were introduced in the design of the RBV system onboard Landsat-3: The system sensed in a single broad band rather than multispectrally, and the spatial resolution of the system was improved by a factor of about 2.6 compared with the previous RBVs. The spectral sensitivity range of the system was 0.505 to 0.750 μm (green to near IR). The change to 30 m nominal ground resolution was achieved by doubling the focal length of the camera lens system, decreasing the exposure time to reduce image motion during exposure, and maintaining adequate exposure by removing the spectral filters of the previous RBVs. To compensate for the decrease in the ground area covered by doubling the focal length, a two-camera side-by-side configuration was employed. The two cameras were aligned to view adjacent 98-km-square ground scenes with a 13-km sidelap and a 17-km endlap, yielding a 183 $\times$ 98-km scene pair (Figure 6.5). Two successive scene pairs coincided nominally with one MSS scene. The four RBV scenes that filled each MSS scene were designated A, B, C, and D. Figure 6.6 shows one frame of RBV imagery from Landsat-3.

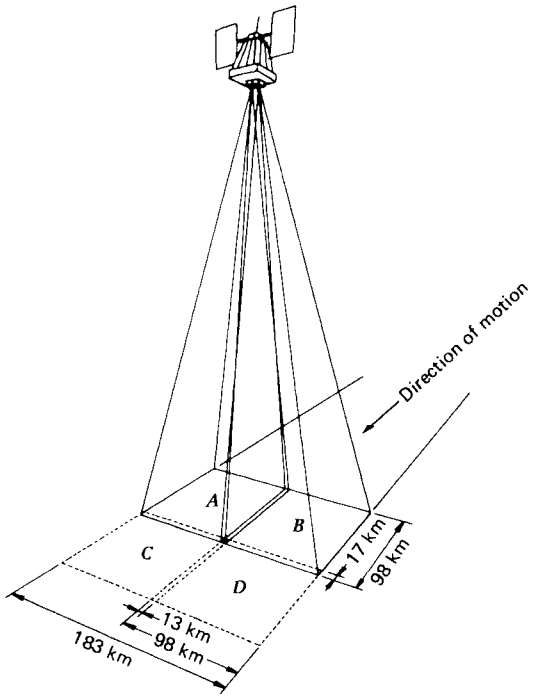

Figure 6.5 Landsat-3 RBV system configuration. (Adapted from NASA diagram.)

Figure 6.6 Landsat-3 RBV image, Cape Canaveral, FL. Scale 1 : 500,000.

While not intended, the RBV systems onboard Landsat-1, -2, and -3 became secondary sources of data in comparison to the MSS systems flown on these satellites. Two factors contributed to this situation. First, RBV operations were plagued with various technical malfunctions. More importantly, the MSS systems were the first global monitoring systems capable of producing multispectral data in a digital format. The advantages in being able to process the MSS data by computer led to their widespread application during the Landsat-1, -2, and -3 era. Several tens of billions of square kilometers of the earth's surface (unique in time but repetitive in area) were imaged by the MSS systems onboard these satellites.

The MSS onboard Landsat-1, -2, and -3 covered a 185-km swath width in four wavelength bands: two in the visible spectrum at 0.5 to 0.6 μm (green) and 0.6 to 0.7 μm (red) and two in the near IR at 0.7 to 0.8 μm and 0.8 to 1.1 μm. These bands were designated as bands 4, 5, 6, and 7. The MSS onboard Landsat-3 also incorporated a thermal band (band 8) operating in the region 10.4 to 12.6 μm. However, operating problems caused this channel to fail shortly after launch. Thus, all three MSS systems effectively produced data in the same four bands. In fact, the identical bands were also used in the MSS systems flown on Landsat-4 and -5 but were designated as bands 1, 2, 3, and 4. In this discussion, we use only the Landsat-1 to -3 MSS band numbers (4, 5, 6, and 7). In Figure 6.7 these bands of operation are compared with the spectral bands associated with color and color IR film.

The MSS operating configuration is shown in Figure 6.8. The instantaneous field of view (IFOV) of the scanner is square and results in a ground resolution cell of approximately 79 m on a side. The total field of view scanned is approximately 11.56°. Because this angle is so small (compared to 90 to 120° in airborne scanners), an oscillating, instead of spinning, scan mirror is employed. The mirror oscillates once every 33 msec. Six contiguous lines are scanned

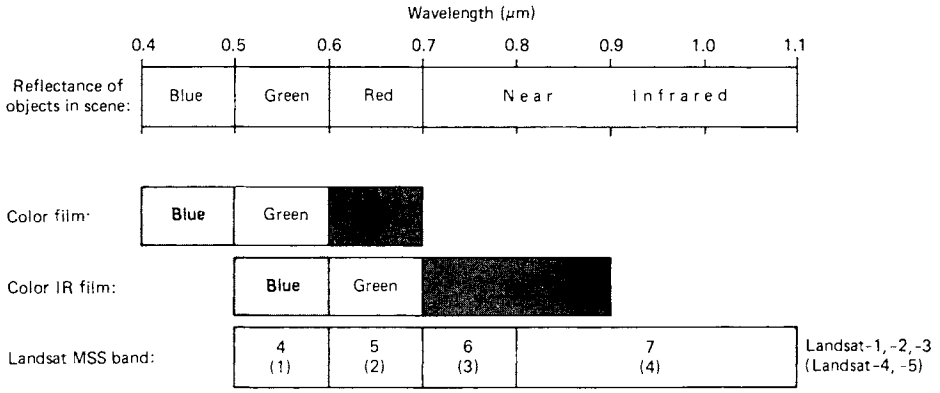

Figure 6.7 Spectral sensitivity of the four Landsat MSS bands compared with the spectral sensitivity of the three emulsion layers used in color and color IR film.

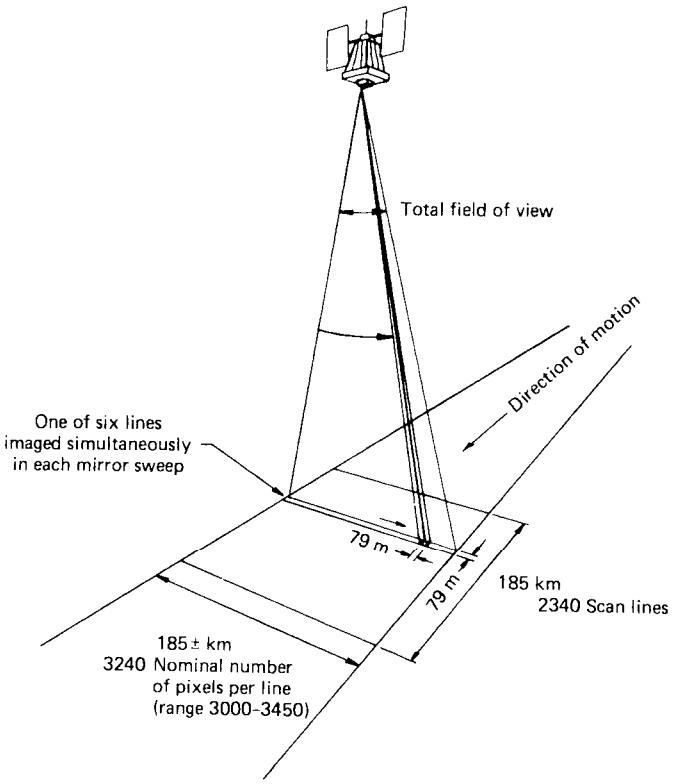

Figure 6.8 Landsat MSS operating configuration. (Adapted from NASA diagram.)

simultaneously with each mirror oscillation. This permits the ground coverage rate to be achieved at one-sixth the single-line scan rate, resulting in improved system response characteristics. This arrangement requires four arrays (one for each band) of six detectors each (one for each line). When not viewing the earth, the detectors are exposed to internal light and sun calibration sources.

The analog signal from each detector is converted to digital form by an onboard A-to-D converter. A digital number range of 0 to 63 (6 bits) is used for this purpose. These data are then scaled to other ranges during subsequent ground-based processing. (Normally, bands 4 to 6 are scaled to a range of 0 to 127 and band 7 is scaled to 0 to 63.)

The A-to-D converter samples the output of the detectors about 100,000 times a second, resulting in a ground sampled distance of 56 m between readings. Because of this spacing, the image values form a matrix of 56 × 79-m cells (as shown in Figure 6.9). Note, however, that the brightness value for each pixel is actually derived from the full 79 × 79-m-ground-resolution cell (shaded area in Figure 6.9).

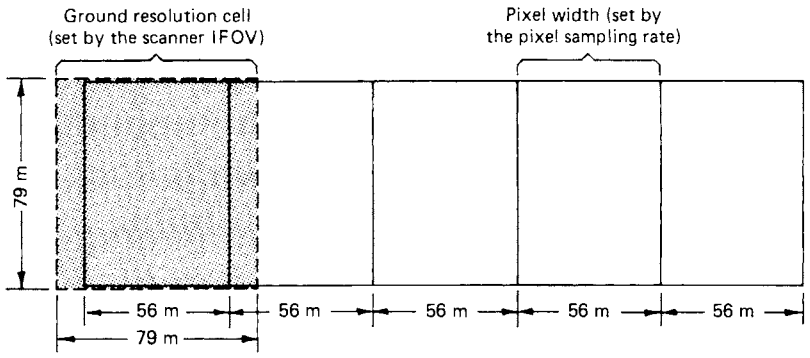

Figure 6.9 Ground resolution cell size versus MSS pixel size. (Adapted from Taranik, 1978.)

The MSS scans each line from west to east with the southward motion of the spacecraft providing the along-track progression of the scan lines. Each Landsat MSS scene is "framed" from the continuous MSS data swath so that it covers approximately a 185 × 185-km area with 10 percent endlap between successive scenes. A nominal scene consists of some 2340 scan lines, with about 3240 pixels per line, or about 7,581,600 pixels per channel. With four spectral observations per pixel, each image data set contains over 30 million observations.

Figure 6.10 is a full-frame, band 5 Landsat MSS scene covering a portion of central New York. Note that the image area is a parallelogram, not a square, because of the earth's rotation during the 25 sec it takes the satellite to travel from the top of the scene to the bottom. The tick marks and numbers around the margins of this image refer to an approximate latitude-and-longitude (degrees and minutes) grid for the image. At the bottom of the image is a step wedge containing 15 steps corresponding to the full potential range of brightness values detected by the MSS. Not all steps are visible on this image because only a limited portion of the full scale was used in printing this scene.

Above the step wedge is an annotation block giving specific information about the acquisition of this image. For Figure 6.10, the block shows, from left to right, the date (10JUN75); the latitude and longitude of the center of the image in degrees and minutes (N43–11/W075–36); the latitude and longitude of the ground point directly beneath the satellite (the nadir) (N43–08/W075–29)—the discrepancy between this location and the center indicates a slight degree of tilt in the image; the sensor and band (MSS 5); the reception mode (D), specifying direct versus recorded; sun elevation and azimuth to the nearest degree (SUN EL57 AZ117); various orbital and processing parameters (191–4668-N-I-N-D-2L); identification as Landsat satellite

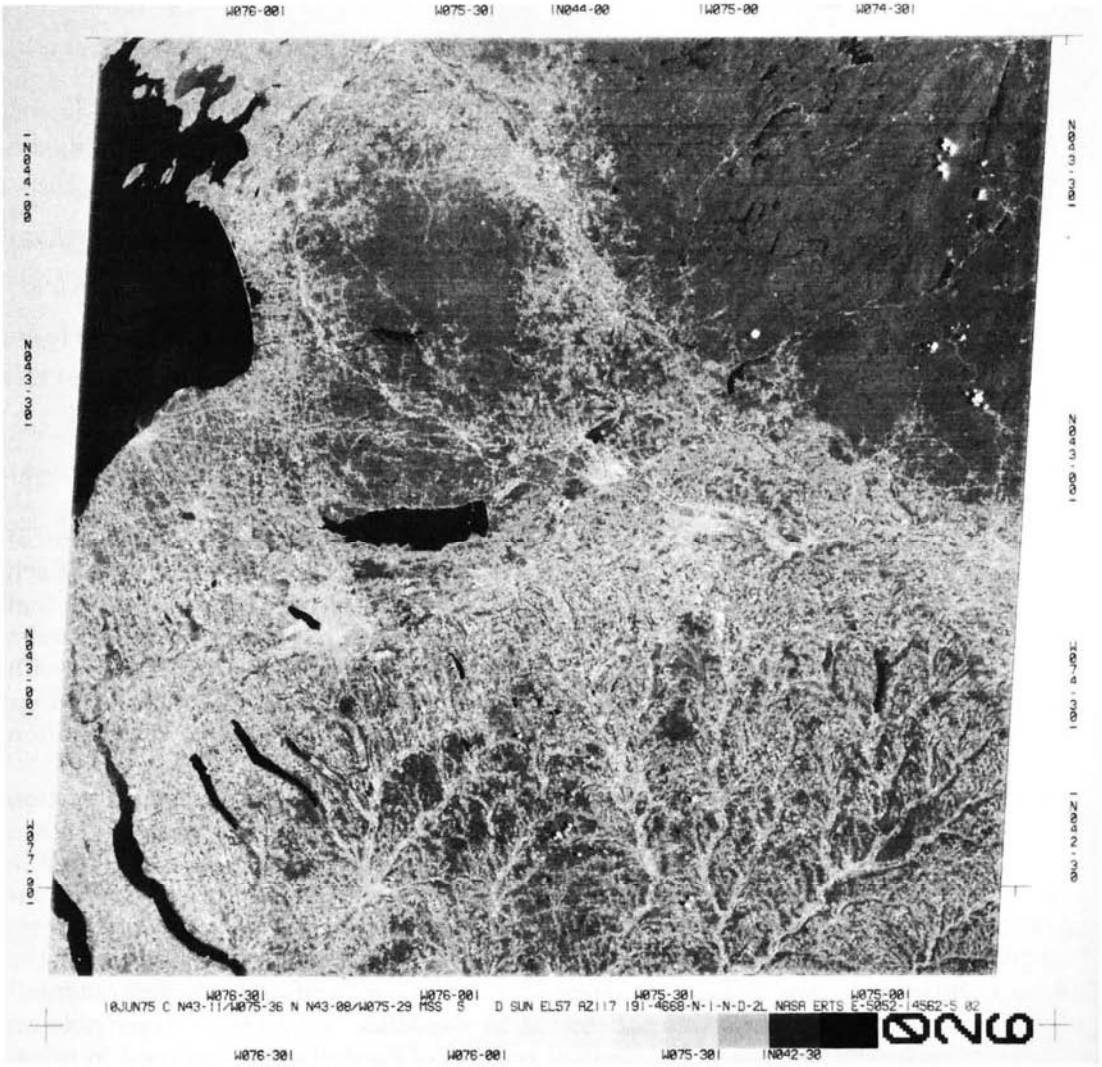

Figure 6.10 Full-frame, band 5 (red), Landsat MSS scene, central New York. 1:1,700,000. Shown are portions of Lake Ontario (upper left), Adirondack Mountains (upper right), and Finger Lakes region (lower left).

(NASA ERTS); and a unique scene identification number (E-5052–14562–5). The exact format of the annotation block has changed periodically through the course of the Landsat program.

In addition to black and white images of single bands, *color composites* can be generated for any MSS data set by printing three MSS bands in registration onto color film or by displaying the three-band data digitally. Generally, band 4 is displayed in blue, band 5 in green, and band 7 in red. This combination simulates the color rendition of color IR film (Figure 6.7).

The distribution of Landsat data in the United States has gone through four distinct phases: experimental, transitional, commercial, and governmental [as part of NASA's Earth Science Enterprise Program (Section 6.18)]. During the experimental phase of Landsat-1, -2, and -3 all imagery and computer-compatible tapes were disseminated by the Earth Resources Observation System (EROS) Data Center at Sioux Falls, South Dakota. The satellites were operated by NASA and the data distribution process was operated by the USGS within the Department of the Interior. Gradually, all operations were assumed by the National Oceanic and Atmospheric Administration (NOAA) within the U.S. Department of Commerce during the transitional period. During this period, the operation of the Landsat program was transferred from the federal government to a commercial firm—the Earth Observation Satellite Company (EOSAT). This transfer was provided for within the Land Remote Sensing Commercialization Act of 1984. With the launch of Landsat-7 on April 15, 1999, operation of the Landsat program reverted to the government (Section 6.7) and the EROS Data Center assumed the role of processing and distributing the data.

As the above changes in the dissemination of Landsat data were being made, several technical improvements were also being made in the manner in which Landsat data were processed prior to distribution. Hence, the precise form of Landsat-1, -2, and -3 data products varied considerably over the course of time. For example, digital MSS data supplied in computer-compatible tape (CCT) format after 1979 were resampled into pixels having a nominal dimension of 57 × 57 m (compared to the 56 × 79-m size used previously).

During the Landsat-1, -2, and -3 era, several countries throughout the world established data-receiving stations. The precise form of data products produced at these facilities likewise varied considerably. Accordingly, prospective users of data from these early missions are advised to closely investigate the exact form of data processing employed to produce the products they may wish to analyze. Also, prospective users of Landsat-3 data obtained between 1979 and 1983 should be aware that the MSS developed a scanning line-start synchronization problem in early 1979. This resulted in loss of all (or portions) of the data from the western 30 percent of each scene. The remaining 70 percent of each scene was normal.

Landsat-1, -2, and -3 images are cataloged according to their location within the *Worldwide Reference System* (*WRS*). In this system each orbit within a cycle is designated as a path. Along these paths, the individual nominal sensor frame centers are designated as rows. Thus, a scene can be uniquely defined by specifying a path, a row, and a date. The WRS for Landsat-1, -2, and -3 has 251 paths corresponding to the number of orbits required to cover the earth in one 18-day cycle. Paths are numbered from 001 to 251, east to west. The rows are numbered so that row 60 coincides with the equator on the orbit's descending node. The U.S. archive of Landsat-1, -2, and -3 data contains 500,000 MSS and RBV scenes. The worldwide database for MSS and RBV data contains some 1.3 million scenes. These data represent an irreplaceable resource for long term global change studies.

6.5 LANDSAT-4 AND -5

Landsat-4 and -5, like their predecessors, were launched into repetitive, circular, sun-synchronous, near-polar orbits. However, these orbits were lowered from 900 to 705 km. These lower orbits were chosen to make the satellites potentially retrievable by the space shuttle and to aid in the improvement of the ground resolution of the sensors onboard.

As was shown in Figure 6.1, Landsat-4 and -5 orbits have an inclination angle of 98.2° (8.2° from normal) with respect to the equator. The satellite crosses the equator on the north-to-south portion of each orbit at 9:45 A.M. local sun time. Each orbit takes approximately 99 min, with just over 14.5 orbits being completed in a day. Due to earth rotation, the distance between ground tracks for consecutive orbits is approximately 2752 km at the equator (Figure 6.11).

The above orbit results in a 16-day repeat cycle for each satellite. The orbits of Landsat-4 and -5 were established 8 days out of phase, such that when both satellites were operational, an 8-day repeat coverage cycle could be maintained with alternating coverage by each satellite. As shown in Figure 6.12, the time interval between adjacent coverage tracks of the same satellite is 7 days. This coverage pattern is quite different from that of the previous three satellites, which had 18-day orbital cycles and a 1-day interval between orbits over adjacent tracks. Consequently, Landsat-4 and -5 images are cataloged according to a set of WRS paths different from those used to reference data from Landsat-1, -2, and -3. The Landsat-4 and -5 WRS is made up of 233 paths numbered 001 to 233, east to west, with path 001 crossing the equator at longitude 64°36′ W. The same number of rows is used as in the previous WRS system. That is, row 60 coincides with the equator at the orbit's descending node. Row 1 of each path starts at 80°47′ N latitude.

Figure 6.13 shows the design of the Landsat-4 and -5 satellites, which include both the MSS and the TM. This spacecraft weighs approximately 2000 kg and includes four 1.5 × 2.3-m solar panels that are mounted to one side. The high gain antenna shown protruding above the spacecraft can be used to relay data through geosynchronous communication satellites included in the *Tracking and Data Relay Satellite System* (*TDRSS*). Direct transmission of MSS and TM data to ground receiving stations is made possible via the X-band and S-band antennas onboard the satellite. The data transmission rates involved are substantial; the MSS transmits 15 megabits per second (Mbps) and the TM transmits 85 Mbps. (The MSS has been flown on these missions primarily to ensure continuity of data for receiving stations unable to receive and process TM data.)

The MSS onboard Landsat-4 and -5 is essentially identical to the MSS sensors on the previous Landsat satellites. The across-track swath of 185 km has been maintained at the lower orbit altitude by increasing the total field of view to 14.92° (from 11.56° on previous systems). The optics of the MSS system have also been modified to yield an 82-m-ground-resolution cell to

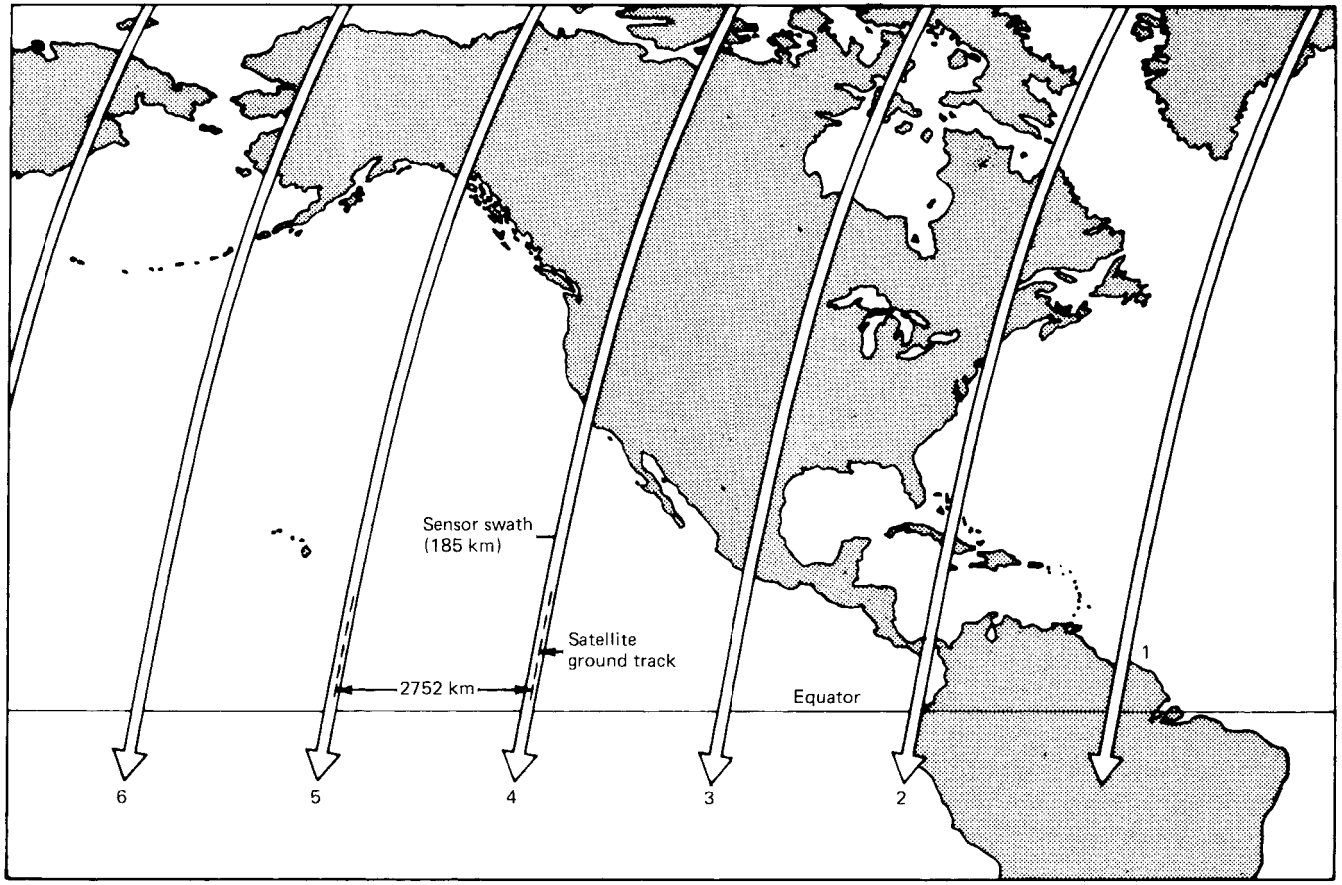

Figure 6.11 Spacing between adjacent Landsat-4 or -5 orbit tracks at the equator. The earth revolves 2752 km to the east at the equator between passes. (Adapted from NASA diagram.)

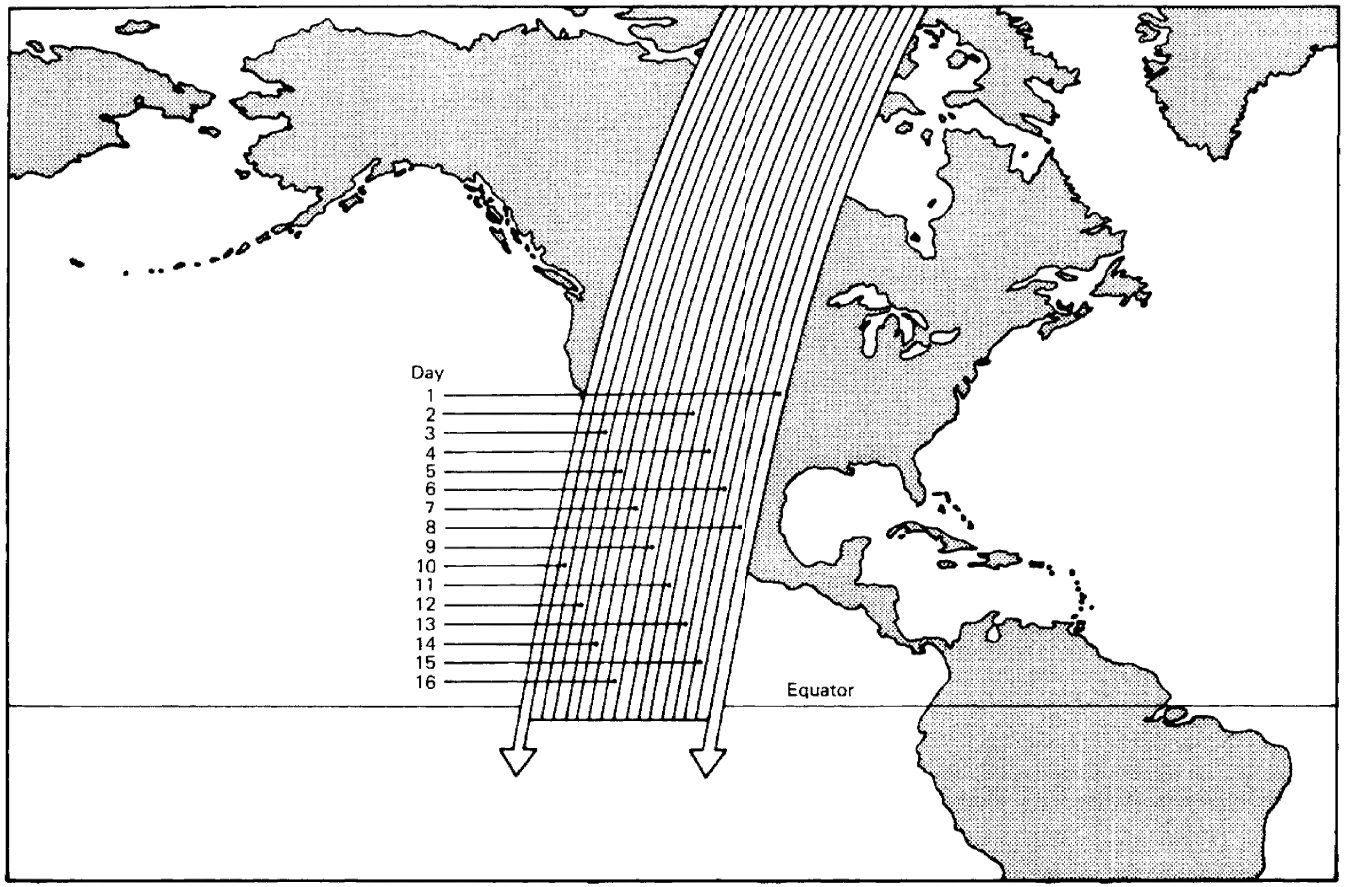

Figure 6.12 Timing of adjacent Landsat-4 or -5 coverage tracks. Adjacent swaths are imaged 7 days apart. (Adapted from NASA diagram.)

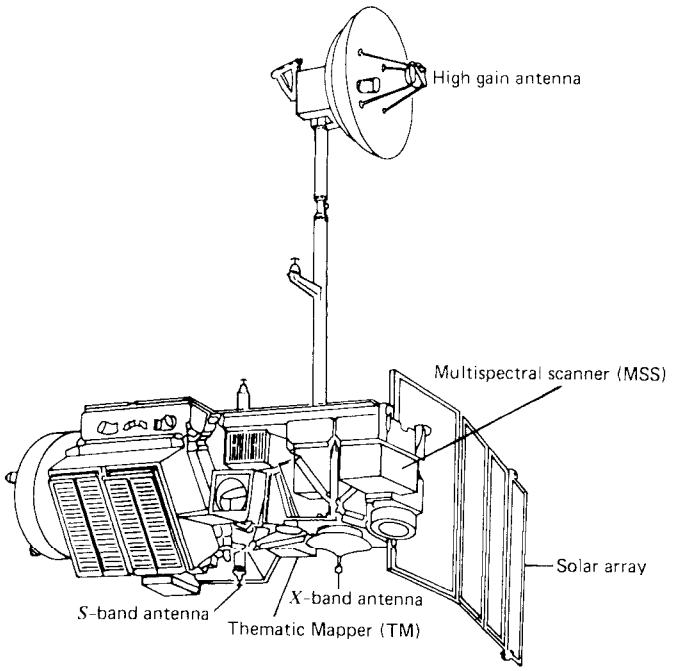

Figure 6.13 Landsat-4 and -5 observatory configuration. (Adapted from NASA diagram.)

approximate the 79-m-ground-resolution cell of the previous systems. The same four spectral bands are used for data collection, but they have been renumbered. That is, bands 1 to 4 of the Landsat-4 and -5 MSS correspond directly to bands 4 to 7 of the previous MSS systems (Figure 6.7).

The TM is a highly advanced sensor incorporating a number of spectral, radiometric, and geometric design improvements relative to the MSS. Spectral improvements include the acquisition of data in seven bands instead of four, with new bands in the visible (blue), mid-IR, and thermal portions of the spectrum. Also, based on experience with MSS data and extensive field radiometer research results, the wavelength range and location of the TM bands have been chosen to improve the spectral differentiability of major earth surface features.

Radiometrically, the TM performs its onboard A-to-D signal conversion over a quantization range of 256 digital numbers (8 bits). This corresponds to a fourfold increase in the gray scale range relative to the 64 digital numbers (6 bits) used by the MSS. This finer radiometric precision permits observation of smaller changes in radiometric magnitudes in a given band and provides greater sensitivity to changes in relationships between bands. Thus, differences in radiometric values that are lost in one digital number in MSS data may now be distinguished.

Geometrically, TM data are collected using a 30-m-ground-resolution cell (for all but the thermal band, which has 120 m resolution). This represents a decrease in the lineal dimensions of the ground resolution cell of approximately 2.6 times, or a reduction in the area of the ground resolution cell of approximately 7 times. At the same time, several design changes have been incorporated within the TM to improve the accuracy of the geodetic positioning of the data. Most geometrically corrected TM data are supplied using a 28.5 × 28.5-m GSD registered to the Space Oblique Mercator (SOM) cartographic projection. The data may also be fit to the Universal Transverse Mercator (UTM) or polar stereographic projections.

Table 6.3 lists the seven spectral bands of the TM along with a brief summary of the intended principal applications of each. The TM bands are more finely tuned for vegetation discrimination than those of the MSS for several reasons. The green and red bands of the TM (bands 2 and 3) are narrower

TABLE 6.3 Thematic Mapper Spectral Bands

Band	Wavelength (μm)	Nominal Spectral Location	Principal Applications
1	0.45–0.52	Blue	Designed for water body penetration, making it useful for coastal water mapping. Also useful for soil/vegetation discrimination, forest-type mapping, and cultural feature identification.
2	0.52–0.60	Green	Designed to measure green reflectance peak of vegetation (Figure 1.10) for vegetation discrimination and vigor assessment. Also useful for cultural feature identification.
3	0.63–0.69	Red	Designed to sense in a chlorophyll absorption region (Figure 1.10) aiding in plant species differentiation. Also useful for cultural feature identification.
4	0.76–0.90	Near IR	Useful for determining vegetation types, vigor, and biomass content, for delineating water bodies, and for soil moisture discrimination.
5	1.55–1.75	Mid IR	Indicative of vegetation moisture content and soil moisture. Also useful for differentiation of snow from clouds.
6[a]	10.4–12.5	Thermal IR	Useful in vegetation stress analysis, soil moisture discrimination, and thermal mapping applications.
7[a]	2.08–2.35	Mid IR	Useful for discrimination of mineral and rock types. Also sensitive to vegetation moisture content.

[a]Bands 6 and 7 are out of wavelength sequence because band 7 was added to the TM late in the original system design process.

than their MSS counterparts. Also, the near-IR TM band (4) is narrower than the combined bands of the MSS in this region and centered in a region of maximum sensitivity to plant vigor. Sensitivity to plant water stress is obtained in both of the TM mid-IR bands (5 and 7). Plant stress discrimination is also aided by data from the TM blue band (1).

In addition to improved discrimination of vegetation, the TM has been designed to afford expanded or improved use of satellite data in a number of other application areas. Among these is the use of TM data (particularly from band 1) in the field of bathymetry. Likewise, the mid-IR bands (5 and 7) have proven to be extremely valuable in discrimination of rock types. Band 5 is also ideal for differentiating between snow- and cloud-covered areas (snow has very low reflectance in this band, while the reflectance of clouds is relatively high). Finally, band 6 makes TM data potentially useful in a range of thermal mapping applications. We treat the visual interpretation of TM data in Section 6.8 and the digital processing of TM data in Chapter 7. In the remainder of this section we discuss the basic differences in the design and operation of the TM and the MSS.

Whereas the MSS collects data only when its IFOV is traversing in the west-to-east direction along a scan line, the TM acquires data during both the forward (west-to-east) and reverse (east-to-west) sweeps of its scan mirror. This bidirectional scanning procedure is employed to reduce the rate of oscillation of the scan mirror and to increase the time an individual detector is able to dwell upon a given portion of the earth within its IFOV. The TM scans through a total field of view of 15.4° (±7.7° from nadir). It completes approximately seven combined forward and reverse scan cycles per second. This relatively slow rate limits the acceleration of the scan mirror, improving the geometric integrity of the data collection process and improving the signal-to-noise performance of the system.

Another major difference between the TM and the MSS is the number of detectors used for the various bands of sensing. Whereas the MSS employs six detectors to record data in each of its four bands of sensing (total of 24 detectors), the TM uses 16 detectors for all nonthermal bands and four detectors for the thermal band (total of 100 detectors). That is, 16 lines of each nonthermal band and four lines of thermal data are acquired with each sweep of the scan mirror. Silicon detectors are used for bands 1 to 4, and these are located within a primary focal plane assembly (Figure 6.14). The detectors for bands 5 to 7 are located in a second focal plane assembly incorporating passive radiation cooling to increase their radiometric sensitivity. Indium antimonide (InSb) detectors are employed for bands 5 and 7, and mercury cadmium telluride (HgCdTe) detectors are used for band 6.

At any instant in time, all 100 detectors view a different area on the ground due to the spatial separation of the individual detectors within the two TM focal planes. Figure 6.14 illustrates the projection of the detector IFOVs onto the ground. Accurate band-to-band data registration requires knowledge of the relative projection of the detectors in both focal planes as a function of time. This information is derived from data concerning the relative position

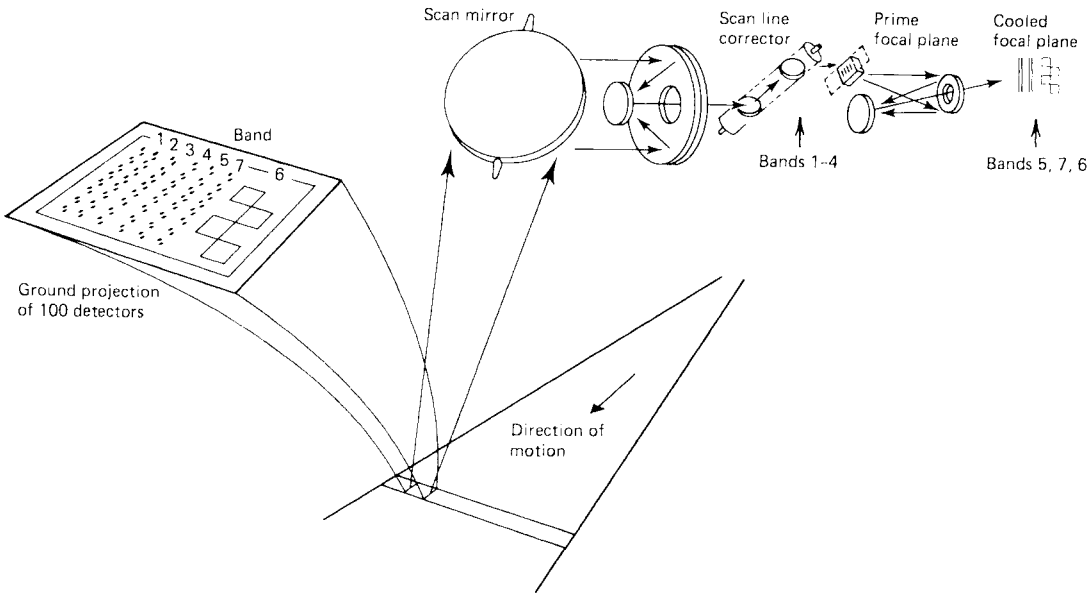

Figure 6.14 Thematic Mapper optical path and projection of detector IFOVs on earth surface. (Adapted from NASA diagram.)

of the individual detector arrays with respect to the optical axis, the spacecraft position and attitude, and the motion of the scan mirror during successive scan cycles. A *scan angle monitor* on the scan mirror generates signals indicating the mirror's angular position as a function of time. These signals are called scan mirror correction data and are transmitted to the ground for incorporation into the geometric processing of TM image data.

Signals from the scan angle monitor are also used to guide the motions of a *scan line corrector* located in front of the primary focal plane (Figure 6.14). The function of the scan line corrector is illustrated in Figure 6.15. During each scan mirror sweep, the scan line corrector rotates the TM line of sight backward along the satellite ground track to compensate for the forward motion of the spacecraft. This prevents the overlap and underlap of scan lines and produces straight scan lines that are perpendicular to the ground track.

The TM also employs an internal radiometric calibration source consisting of three tungsten filament lamps, a blackbody for the thermal band, and a pivot-mounted shutter. The shutter passes through the field of view of the instrument's detectors each time the scan mirror changes directions. The shutter permits light from the lamps to pass into the field of view of the nonthermal bands directly, and a mirror on the shutter directs energy from the thermal calibration source into the field of view of the thermal detectors. These calibration sources are used to monitor the radiometric response of the various detectors over the sensor's service life.

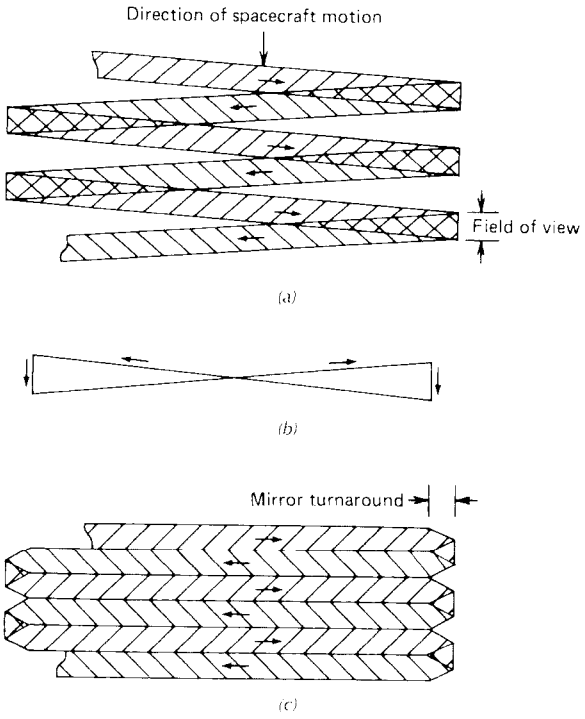

Figure 6.15 Schematic of TM scan line correction process: (*a*) uncompensated scan lines; (*b*) correction for satellite motion; (*c*) compensated scan lines. (Adapted from NASA diagram.)

6.6 LANDSAT-6 PLANNED MISSION

After more than two decades of success, the Landsat program realized its first unsuccessful mission with the October 5, 1993, launch failure of Landsat-6. This satellite was designed to have occupied an orbit identical to that of Landsat-4 and -5. The sensor included on board this ill-fated mission was the Enhanced Thematic Mapper (ETM). To provide data continuity with Landsat-4 and -5, the ETM incorporated the same seven spectral bands and the same spatial resolutions as the TM. The ETM's major improvement over the TM was the addition of an eighth, "panchromatic" band operating in the 0.50- to 0.90-μm range with a spatial resolution of 15 m. The 15-m panchromatic band data could have been merged with various combinations of the 30-m data from ETM bands 1 to 5 and 7 to produce color images with essentially 15 m resolution. (We discuss this "pan sharpening" procedure in Chapter 7). Changes in the design of the detector system for the ETM were to also permit the data for all bands to be automatically coregistered as they were acquired. This capability is referred to as a "monolithic" detector design.

Another improvement made in the design of the ETM was the ability to set the gains for the individual bands from the ground (Section 7.2). The ETM had a 9-bit A-to-D converter that provided either a high or low gain 8-bit setting. The high gain was to be used over areas of low reflectance (such as water) and the low gain was designed to provide reliable readings over very bright regions (such as deserts) without detector saturation.

6.7 LANDSAT-7

The Land Remote Sensing Policy Act of 1992 once again transferred the management responsibility for the Landsat program with the design and operation of Landsat-7. Originally, a joint NASA–U.S. Air Force program was envisioned. This concept was superseded by a 1994 presidential directive and subsequent deliberations that established a joint program between NASA and USGS. The system was also made a part of NASA's Earth Science Enterprise Program.

Landsat-7 was launched on April 15, 1999. The earth-observing instrument onboard this spacecraft is the Enhanced Thematic Mapper Plus (ETM+). The design of the ETM+ stresses the provision of data continuity with Landsat-4 and -5. Similar orbits and repeat patterns are used, as is the 185-km swath width for imaging. As with the ETM planned for Landsat-6, the system is designed to collect 15-m-resolution "panchromatic" data (which actually extend to 0.90 μm in the near IR, well outside the visible spectral range normally associated with panchromatic imagery) and six bands of data in the visible, near-IR, and mid-IR spectral regions at a resolution of 30 m. A seventh, thermal, band is incorporated with a resolution of 60 m (vs. 120 m for the ETM). As with the ETM, high and low gain settings for the individual channels may be controlled from the ground. The system also includes a "dual-mode solar calibrator," in addition to an internal lamp calibrator. This results in onboard absolute radiometric calibration to within an accuracy of 5 percent.

Landsat-7 data can be transmitted to ground either directly or by playback of data stored by an onboard, solid-state, recorder. The primary receiving station for the data is located at the EROS Data Center (EDC) in Sioux Falls, South Dakota. The ground system at the EDC is capable of processing a complete global view of earth's land areas seasonally, or approximately four times per year. In addition, a worldwide network of receiving stations is able to receive real-time direct downlink of image data when and where the satellite is in sight of the receiving station. Landsat-7 data supplied by the EDC can be obtained at the cost of fulfilling user requests.

Figure 6.16 illustrates a portion of the first image acquired by the Landsat-7 ETM+. This is a panchromatic band image depicting Sioux Falls, South Dakota, and vicinity. Features such as the airport (upper center), major roads, and new residential development (especially evident in lower right) are clearly discernible in this 15-m-resolution image. This band can be merged with the

Figure 6.16 The first image acquired by the Landsat-7 ETM+. Panchromatic band (15 m resolution), Sioux Falls, SD, April 18, 1999. Scale 1 : 88,000. (Courtesy EROS Data Center.)

30-m data from ETM+ bands 1 to 5 and 7 to produce "pan-sharpened" color images with essentially 15 m resolution (Section 7.6).

6.8 LANDSAT IMAGE INTERPRETATION

The utility of Landsat image interpretation has been demonstrated in many fields, such as agriculture, botany, cartography, civil engineering, environmental monitoring, forestry, geography, geology, geophysics, land resource analysis, land use planning, oceanography, and water resource analysis.

As shown in Table 6.4, the image scale and area covered per frame are very different for Landsat images than for conventional aerial photographs. For example, more than 1600 aerial photographs at a scale of 1:20,000 with no overlap are required to cover the area of a single Landsat image! Because of scale and resolution differences, Landsat images should be considered as a complementary interpretive tool instead of a replacement for low altitude aerial photographs. For example, the existence and/or significance of certain geologic features trending for tens or hundreds of kilometers, and clearly evident on a Landsat image, might escape notice on low altitude aerial photographs. On the other hand, housing quality studies from aerial imagery would certainly be more effective using low altitude aerial photographs rather than Landsat images, since individual houses cannot be studied on Landsat images. In addition, most Landsat images can only be viewed in two dimensions, whereas most aerial photographs are acquired and viewed in stereo.

The ground resolution cell size of Landsat data is about 79 m for the MSS and about 30 m for the TM. However, linear features as narrow as a few meters, having a reflectance that contrasts sharply with that of their surroundings, can often be seen on such images (e.g., two-lane roads, concrete bridges crossing water bodies). On the other hand, objects much larger than the ground resolution cell size may not be apparent if they have a very low reflectance contrast with their surroundings, and features visible in one band may not be visible in another.

TABLE 6.4 Comparison of Image Characteristics

Image Format	Image Scale	Area Covered per Frame (km^2)
Low altitude USDA–ASCS aerial photographs (230 × 230 mm)	1:20,000	21
High altitude NASA aerial photographs (RB-57 or ER-2) (230 × 230 mm)	1:120,000	760
Landsat scene (185 × 185 mm)	1:1,000,000	34,000

Because the Landsat MSS and TM are across-track scanning systems, they produce images having one-dimensional relief displacement. Because there is displacement only in the scan direction and not in the flight track direction, Landsat images can be viewed in stereo only in areas of sidelap on adjacent orbit passes. This sidelap varies from about 85 percent near the poles to about 14 percent at the equator. Consequently, only a limited area of the globe may be viewed in stereo. Also, the vertical exaggeration when viewing Landsat images in stereo is quite small compared to conventional airphotos. This stems from the high platform altitude (ranging from 705 to 900 km) of the Landsat satellites compared to the base distance between images. Whereas stereo airphotos may have a 4× vertical exaggeration, stereo Landsat vertical exaggeration ranges from about 1.3× at the equator to less than 0.4× at latitudes above about 70°. Subtle as this stereo effect is, geologists in particular have found stereoviewing in Landsat overlap areas quite valuable in studying topographic expression. However, most interpretations of Landsat imagery are made monoscopically, either because sidelapping imagery does not exist or because the relief displacement needed for stereoviewing is small.

Figure 6.17, a small portion of a Landsat scene, illustrates the comparative appearance of the seven Landsat TM bands. Here, the blue-green water of the lake, river, and ponds in the scene has moderate reflection in bands 1 and 2 (blue and green), a small amount of reflection in band 3 (red), and virtually no reflection in bands 4, 5, and 7 (near and mid IR). Reflection from roads and urban streets is highest in bands 1, 2, and 3 and least in band 4 (other cultural features such as new subdivisions, gravel pits, and quarries would have similar reflectances). Overall reflection from agricultural crops is highest in band 4 (near IR). Note also the high band 4 reflectance of the golf courses appearing to the right of the river and the lake. The distinct tonal lineations from upper right (northeast) to lower left (southwest) in these images are a legacy from the most recent glaciation of Wisconsin. Glacial ice movement from northeast to southwest left a terrain characterized by many drumlins and scoured bedrock hills. Present-day crop and soil moisture patterns reflect the alignment of this grooved terrain. The thermal band (band 6) has a less distinct appearance than the other bands because the ground resolution cell of this band is 120 m. It has an indistinct, rather than blocky, appearance because the data have been resampled into the 30-m format of the other bands. As would be expected on a summertime thermal image recorded during the daytime, the roads and urban areas have the highest radiant temperature, and the water bodies have the lowest radiant temperature.

Plate 17 shows six color composite images of the same area shown in Figure 6.17. Table 6.5 shows the color combinations used to generate each of these composites. Note that (*a*) is a "normal color" composite, (*b*) is a "color infrared" composite, and (*c*) to (*f*) are some of the many other "false color" combinations that can be produced. A study at the USGS EDC (NOAA, 1984) showed an interpreter preference for several specific band–color combinations

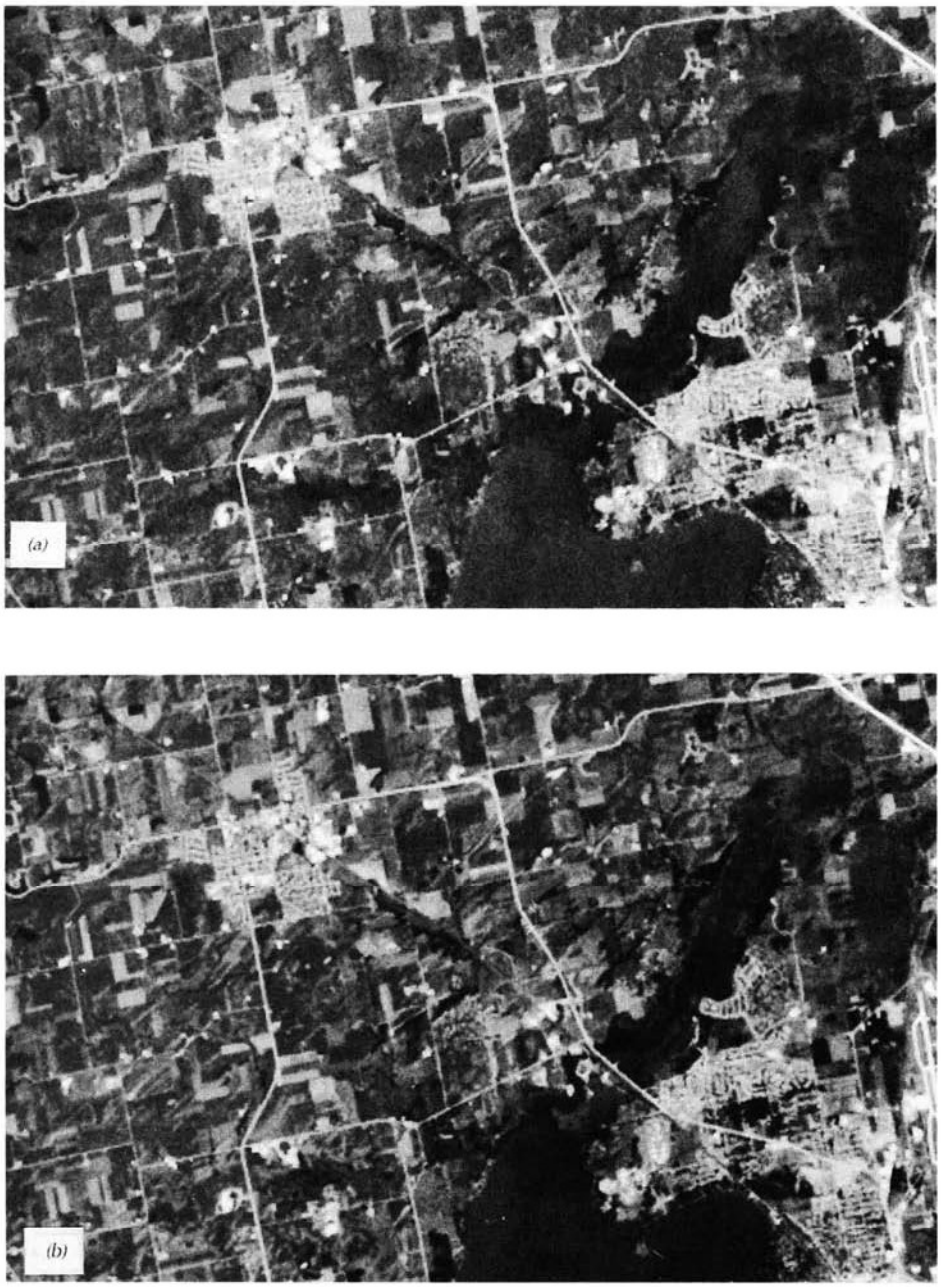

Figure 6.17 Individual Landsat TM bands, suburban Madison, WI, late August (scale 1:115,000): (*a*) band 1, 0.45 to 0.52 μm (blue); (*b*) band 2, 0.52 to 0.60 μm (green); (*c*) band 3, 0.63 to 0.69 μm (red); (*d*) band 4, 0.76 to 0.90 μm (near IR); (*e*) band 5, 1.55 to 1.75 μm (mid IR); (*f*) band 7, 2.08 to 2.35 μm (mid IR); (*g*) band 6, 10.4 to 12.5 μm (thermal IR).

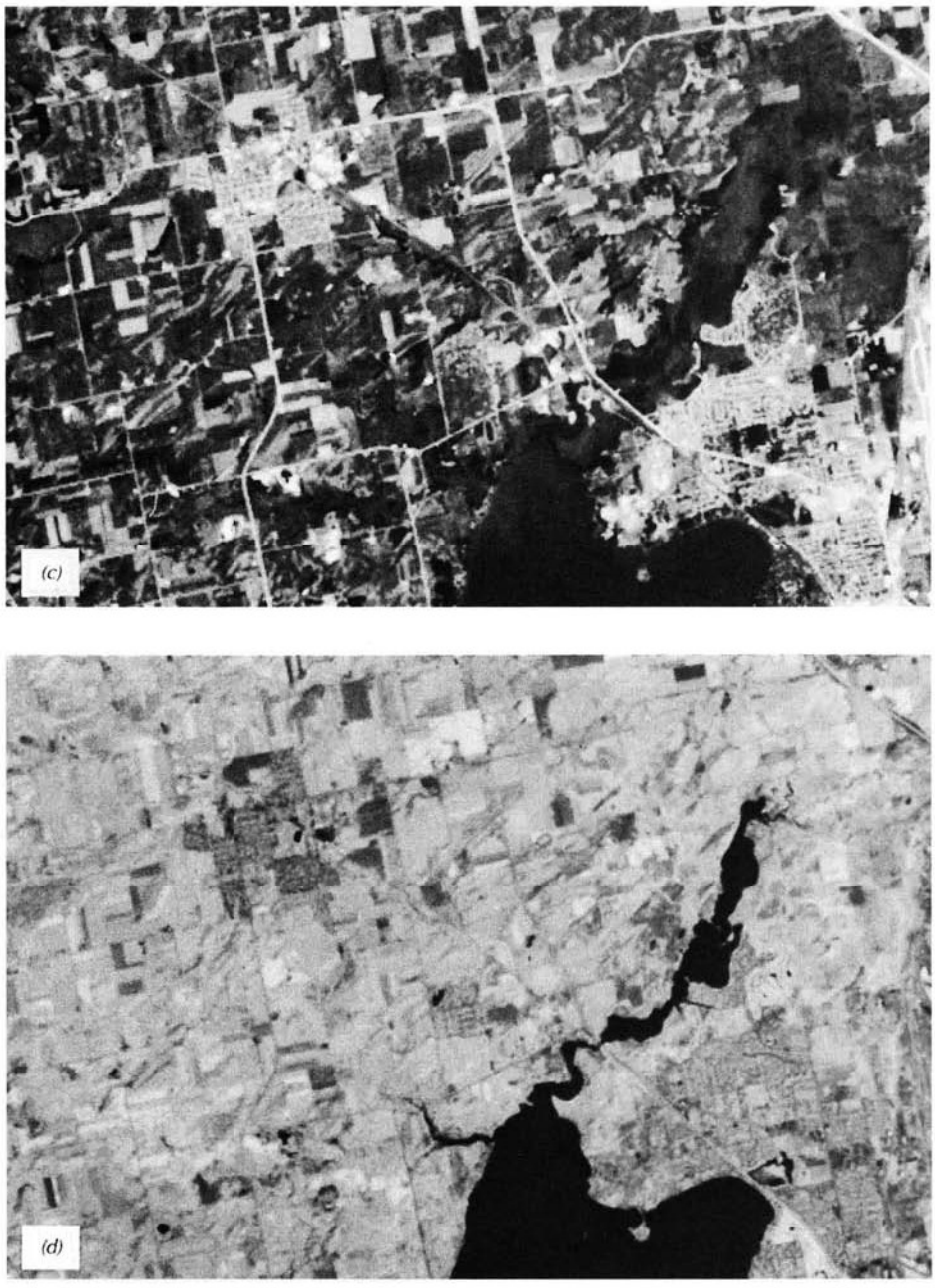

Figure 6.17 *(Continued)*

Figure 6.17 *(Continued)*

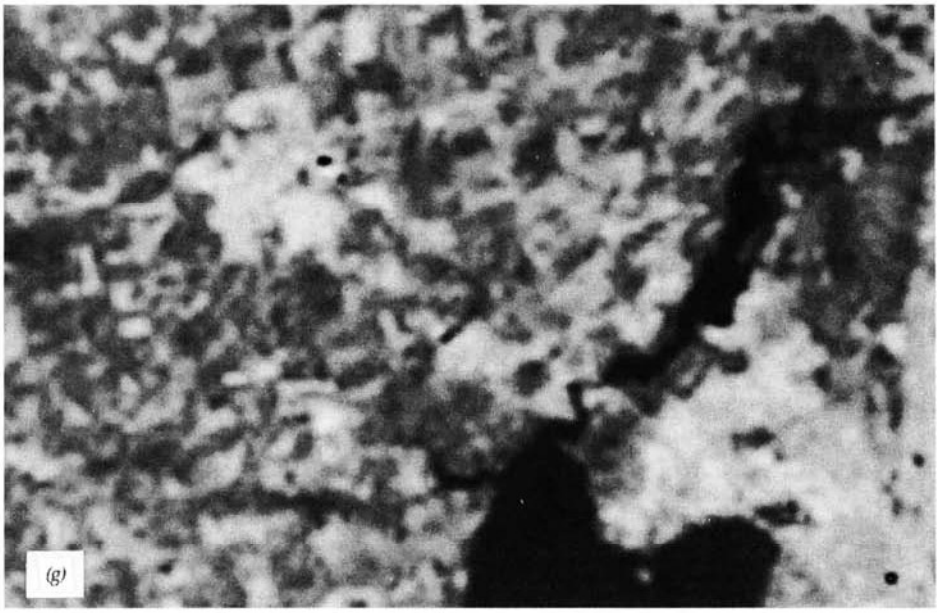

Figure 6.17 *(Continued)*

for various features. For the mapping of water sediment patterns, a normal color composite of bands 1, 2, and 3 (displayed as blue, green, and red) was preferred. For most other applications, such as mapping urban features and vegetation types, the combinations of (1) bands 2, 3, and 4 (color IR composite), (2) bands 3, 4, and 7, and (3) bands 3, 4, and 5 (all in the order blue, green, and red) were preferred. In general, vegetation discrimination is enhanced through the incorporation of data from one of the mid-IR bands (5 or 7). Combinations of any one visible (bands 1 to 3), the near-IR (band 4), and one mid-IR (band 5 or 7) band are also very useful. However, a great deal of

TABLE 6.5 TM Band–Color Combination Shown in Plate 17

	TM Band-Color Assignment in Composite		
Plate 17	Blue	Green	Red
(*a*)	1	2	3
(*b*)	2	3	4
(*c*)	3	4	5
(*d*)	3	4	7
(*e*)	3	5	7
(*f*)	4	5	7

Figure 6.18 Landsat TM band 6 (thermal IR) image, Green Bay and Lake Michigan, Wisconsin–Michigan, mid-July. Scale 1 : 225,000.

personal preference is involved in band–color combinations for interpretive purposes, and for specific applications, other combinations could be optimum.

Figure 6.18 shows a Landsat TM band 6 (thermal) image of Green Bay and Lake Michigan (between the states of Wisconsin and Michigan). In this image, the land area has been masked out and is shown as black (using techniques described in Chapter 7). Based on a correlation with field observations of water surface temperature, the image data were "sliced" into six gray levels, with the darkest tones having a temperature less than 12°C, the brightest tones having a temperature greater than 20°C, and each of the four intermediate levels representing a 2°C range between 12 and 20°C.

Each Landsat satellite passes over the same area on the earth's surface during daylight hours about 20 times per year. The actual number of times per year a given ground area is imaged depends on amount of cloud cover, sun angle, and whether or not the satellite is in operation on any specific pass. This provides the opportunity for many areas to have Landsat images available for several dates per year. Because the appearance of the ground in many areas with climatic change is dramatically different in different seasons, the image interpretation process is often improved by utilizing images from two or more dates.

Figure 6.19 shows MSS band 5 (red) images of a portion of Wisconsin as imaged in September and December. The ground is snow covered (about 200 mm deep) in the December image and all water bodies are frozen, except for a small stretch of the Wisconsin River. The physiography of the area can be better appreciated by viewing the December image, due in part to the low solar elevation angle in winter that accentuates subtle relief. A series of stream valleys cuts into the horizontally bedded sedimentary rock in the upper left portion of this scene. The snow-covered upland areas and valley floors have a very light tone, whereas the steep, tree-covered valley sides have a darker tone. The identification of urban, agricultural, and water areas can better be accomplished using the September image. The identification of forested areas can be more positively done using the December image.

The synoptic view afforded by space platforms can be particularly useful for observing short-lived phenomena. However, the use of Landsat images to capture such ephemeral events as floods, forest fires, and volcanic activity is, to some degree, a hit-or-miss proposition. If a satellite passes over such an event on a clear day when the imaging system is in operation, excellent images of such events can be obtained. On the other hand, such events can easily be missed if there are no images obtained within the duration of the event or, as is often true during floods, extensive cloud cover obscures the earth's surface. However, some of these events do leave lingering traces. For example, soil is typically wet in a flooded area for at least several days after the flood waters have receded, and this condition may be imaged even if the flood waters are not. Thematic Mapper images of the Missouri River in preflood and flooding conditions were shown in Figure 4.25.

Figure 6.20 is a black and white copy of a band 3, 4, and 5 color composite Landsat TM image showing extensive deforestation near Rondônia, Brazil.

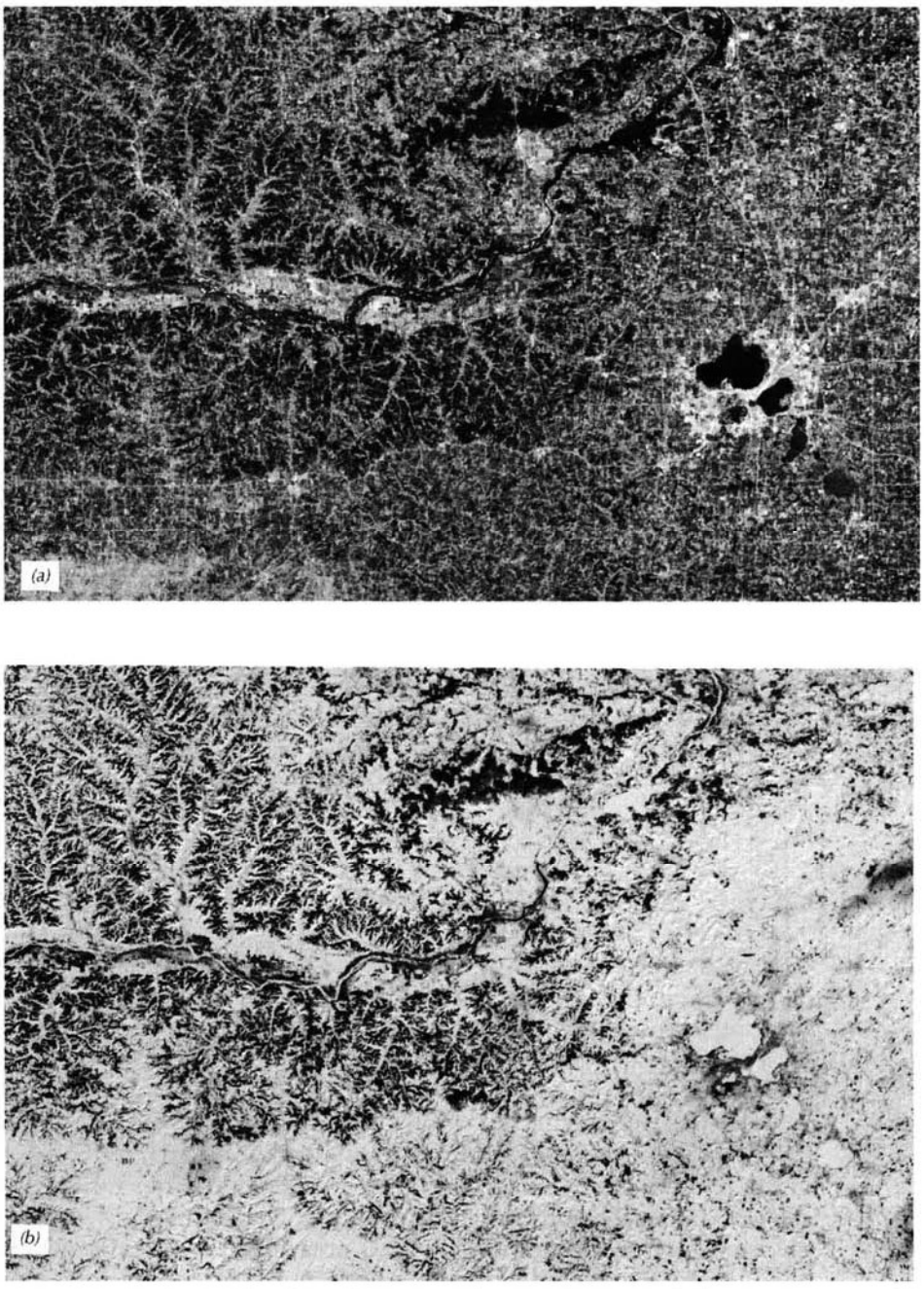

Figure 6.19 Landsat MSS band 5 (red) images, southwestern Wisconsin. Scale 1:1,000,000: (*a*) mid-September; (*b*) mid-December.

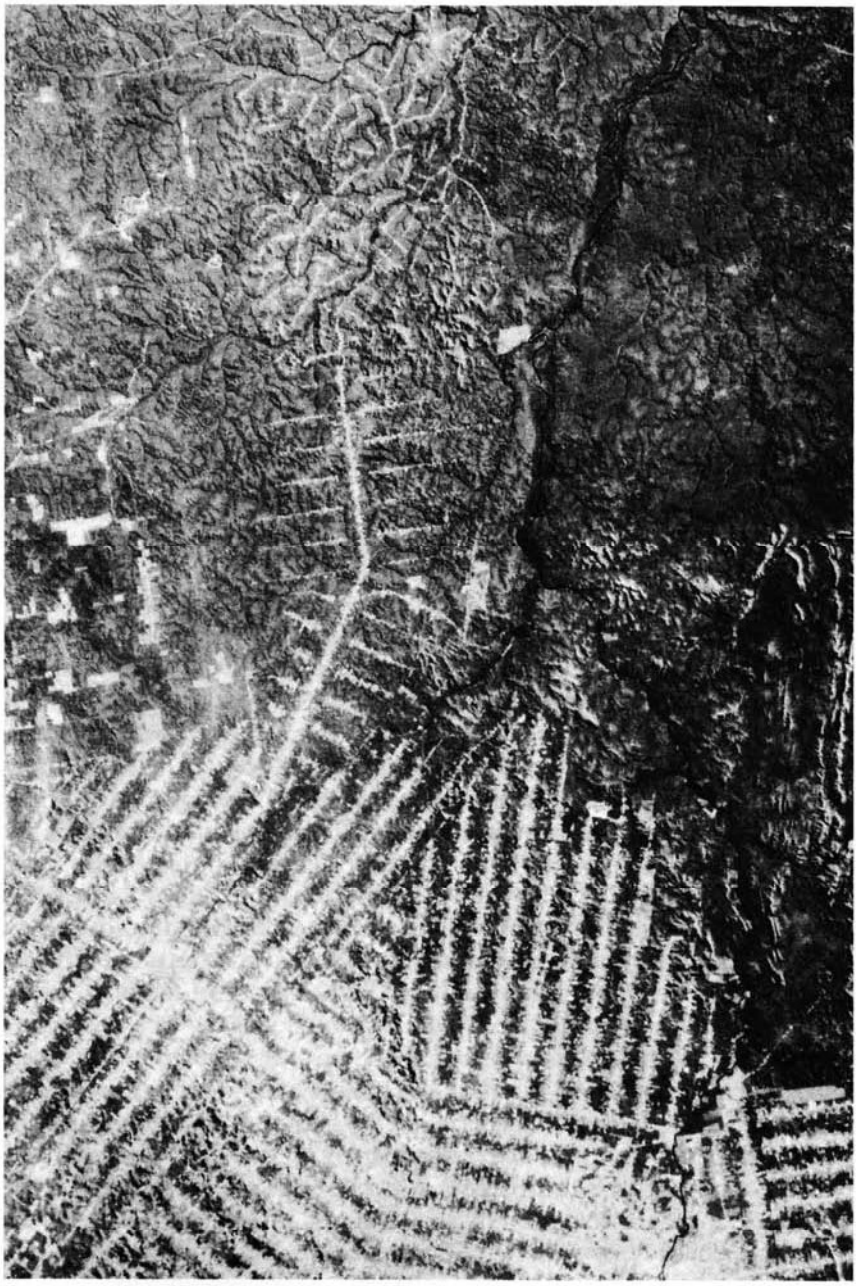

Figure 6.20 Landsat TM image, Rondônia, Brazil, and vicinity, mid-August. Black and white copy of band 3–4–5 color composite image. Scale 1:1,000,000. (Courtesy EOSAT.)

This band combination has been found to be effective for monitoring deforestation in the Amazon region during the dry season. The light-toned "fishbonelike" pattern in this image represents clearings for small farm settlements in the Brazilian jungle.

Thematic Mapper data have been used extensively to prepare image maps over a range of mapping scales. Such maps have proven to be useful tools for resource assessment in that they depict the terrain in actual detail, rather than in the line-and-symbol format of conventional maps. Image maps are often used as map supplements to augment conventional map coverage and to provide coverage of unmapped areas.

As we will see in Chapter 7, there are several digital image processing procedures that may be applied to the image mapping process. These include large-area digital mosaicking, image enhancement procedures, merging of image data with conventional cartographic information, and streamlining the map production and printing process using highly automated cartographic systems. Extensive research continues in the area of image mapping, with numerous sources of image data.

6.9 LANDSAT DATA CONTINUITY MISSION

The Land Remote Sensing Policy Act (1992) instructed the USGS and NASA to examine options for the Landsat program beyond the operational life of Landsat-7. The *Landsat Data Continuity Mission* (*LDCM*) is a joint effort of the USGS and NASA to plan for the continued collection of "Landsat-like" imagery in the future. Major elements of the LDCM program include maintaining data continuity, serving a variety of public interests, incorporating improved technology, providing data at low cost, and relying on private sector organizations for a significant portion of LDCM development and operations. The latter goal may be achieved by a privately operated system that would acquire more valuable (e.g., higher resolution) data for commercial distribution in combination with the acquisition of moderate resolution "Landsat continuity" data on behalf of the U.S. government.

The current (2002) plan for the LDCM calls for a privately developed and operated system that would provide an average of 250 images per day for the USGS archive, about half the number of scenes now provided by Landsat-7. In the words of the draft Request for Proposals, these data would be "sufficiently consistent in terms of acquisition geometry, coverage characteristics, spectral characteristics, output product quality, and data availability to ensure continuity of the Landsat mission." More specifically, the proposed system would have a set of nine spectral bands, including six that correspond to the 30-m bands on the Landsat-7 ETM+, an additional band in the blue portion of the spectrum (0.43 to 0.45 μm), one "Sharpening" band analogous to the panchromatic band on SPOT and Landsat-7, and a "Cirrus" band for high

altitude cloud detection in the mid IR. (At the present time, the LDCM plans do not necessarily call for inclusion of a thermal-IR band.) The Sharpening band would have a spatial resolution of 15 m or better, the Cirrus band 120 m or better, and the remaining bands 30 m or better. The swath width would be at least as wide as that of the ETM+ (185 km), and the orbit would correspond to the World Wide Reference System used for Landsat-4 through -7.

It is expected that LDCM data would begin to be collected during 2006, slightly after the end of the minimum expected lifetime of Landsat-7. Whether Landsat-7 will continue operating long enough to ensure true "continuity" from the LDCM thus remains to be seen.

6.10 SPOT SATELLITE PROGRAM

In early 1978 the French government decided to undertake the development of the *Système Pour l'Observation de la Terre*, or *SPOT*, program. Shortly thereafter Sweden and Belgium agreed to participate in the program with the aim of launching the first of a series of SPOT earth observation satellites. From its inception, SPOT was designed as a commercially oriented program that was to be operational, rather than experimental, in character.

Conceived and designed by the French Centre National d'Etudes Spatiales (CNES), SPOT has developed into a large-scale international program with ground receiving stations and data distribution outlets located in more than 20 countries. The first satellite in the program, SPOT-1, was launched from the Kourou Launch Range in French Guiana on February 21, 1986, onboard an Ariane launch vehicle. This satellite began a new era in space remote sensing, for it is the first earth resource satellite system to include a linear array sensor and employ pushbroom scanning techniques. It is also the first system to have pointable optics. This enables side-to-side off-nadir viewing capabilities, and it affords full-scene stereoscopic imaging from two different satellite tracks permitting coverage of the same area.

SPOT-1 was retired from full-time service on December 31, 1990 (it was used in a backup mode thereafter). The SPOT-2 satellite was launched on January 21, 1990; SPOT-3 was launched on September 25, 1993; and SPOT-4 was launched on March 23, 1998. In that SPOT-1, -2, and -3 have identical orbits and sensor systems, we describe them together in the following section. Section 6.12 treats SPOT-4.

6.11 SPOT-1, -2, AND -3

Like the Landsat satellites, SPOT-1, -2, and -3 have a circular, near-polar, sun-synchronous orbit. The nominal orbit of SPOT-1, -2, and -3 has an altitude of 832 km and an inclination of 98.7°. They descend across the equator

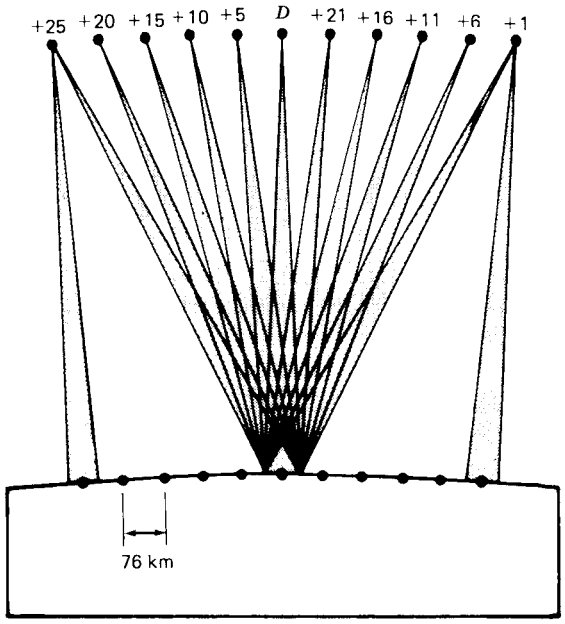

(a)

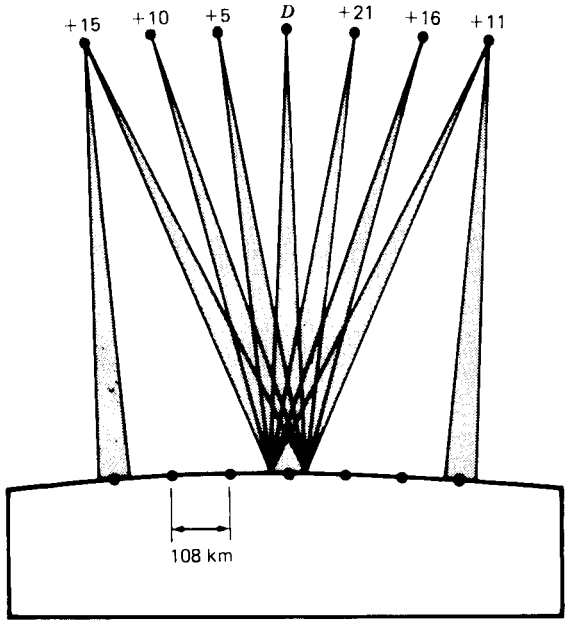

(b)

Figure 6.21 SPOT revisit pattern: (*a*) latitude 45°; (*b*) latitude 0°. (Adapted from CNES diagram.)

at 10:30 A.M. local solar time, with somewhat later crossings in northern latitudes and somewhat earlier crossings in southern latitudes. For example, SPOT crosses areas at a latitude of 40° N at approximately 11:00 A.M. and areas at a latitude of 40° S at 10:00 A.M.

The orbit pattern for SPOT-1, -2, and -3 repeats every 26 days. This means any given point on the earth can be imaged using the same viewing angle at this frequency. However, the pointable optics of the system enable off-nadir viewing during satellite passes separated alternatively by 1 and 4 (and occasionally 5) days, depending on the latitude of the area viewed (Figure 6.21). For example, during the 26-day period separating two successive satellite passes directly over a point located at the equator, seven viewing opportunities exist (day D and days $D + 5$, $+10$, $+11$, $+15$, $+16$, and $+21$). For a point located at a latitude of 45° a total of 11 viewing opportunities exist (day D and days $D + 1$, $+5$, $+6$, $+10$, $+11$, $+15$, $+16$, $+20$, $+21$, and $+25$). This "revisit" capability is important in two respects. First, it increases the potential frequency of coverage of areas where cloud cover is a problem. Second, it provides an opportunity for viewing a given area at frequencies ranging from successive days to several days to a few weeks. Several application areas, particularly within agriculture and forestry, require repeated observations over these types of time frames.

Figure 6.22 is a schematic of the SPOT-1, -2, and -3 satellites. The systems weigh approximately 1750 kg and the main body of the satellites is approximately $2 \times 2 \times 3.5$ m. The solar panel has an overall length of approximately 15.6 m. The SPOT platform is of modular design such that it is compatible with a variety of sensor payloads. Thus, in subsequent SPOT missions, changes in sensor design can be implemented without significant modification of the platform.

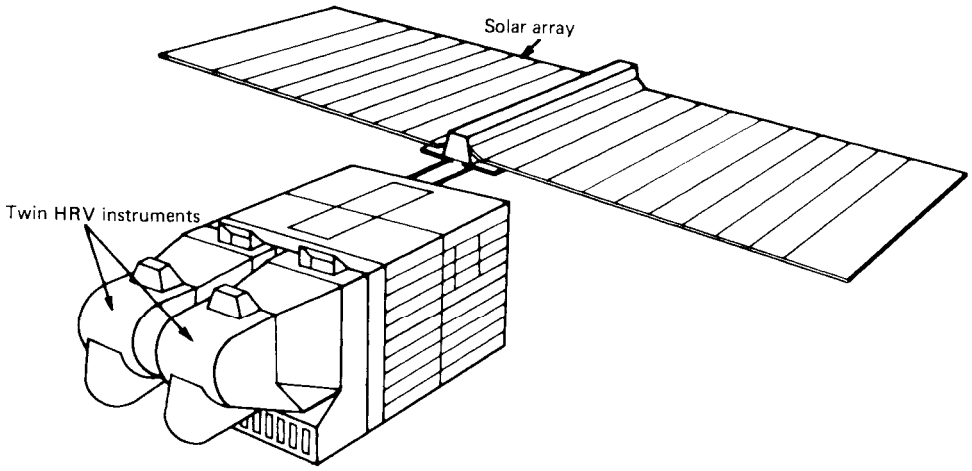

Figure 6.22 SPOT observatory configuration. (Adapted from CNES diagram.)

The sensor payload for SPOT-1, -2, and -3 consists of two identical *high resolution visible* (HRV) imaging systems and auxiliary magnetic tape recorders. Each HRV is designed to operate in either of two modes of sensing: (1) a 10-m-resolution 'panchromatic' (black and white) mode over the range 0.51 to 0.73 μm or (2) a 20-m-resolution multispectral (color IR) mode over the ranges 0.50 to 0.59 μm, 0.61 to 0.68 μm, and 0.79 to 0.89 μm.

The HRV employs along-track, or pushbroom, scanning, as described in Section 5.3. Each HRV actually contains four CCD subarrays. A 6000-element subarray is used in the panchromatic mode to record data at 10 m resolution. Three 3000-element subarrays are employed in the multispectral mode at 20 m resolution. Data are effectively encoded over a 256-digital-number range and are transmitted at a rate of 25 Mbps. Each instrument's field of view is 4.13°, such that the ground swath of each HRV scene is 60 km wide under nadir viewing conditions.

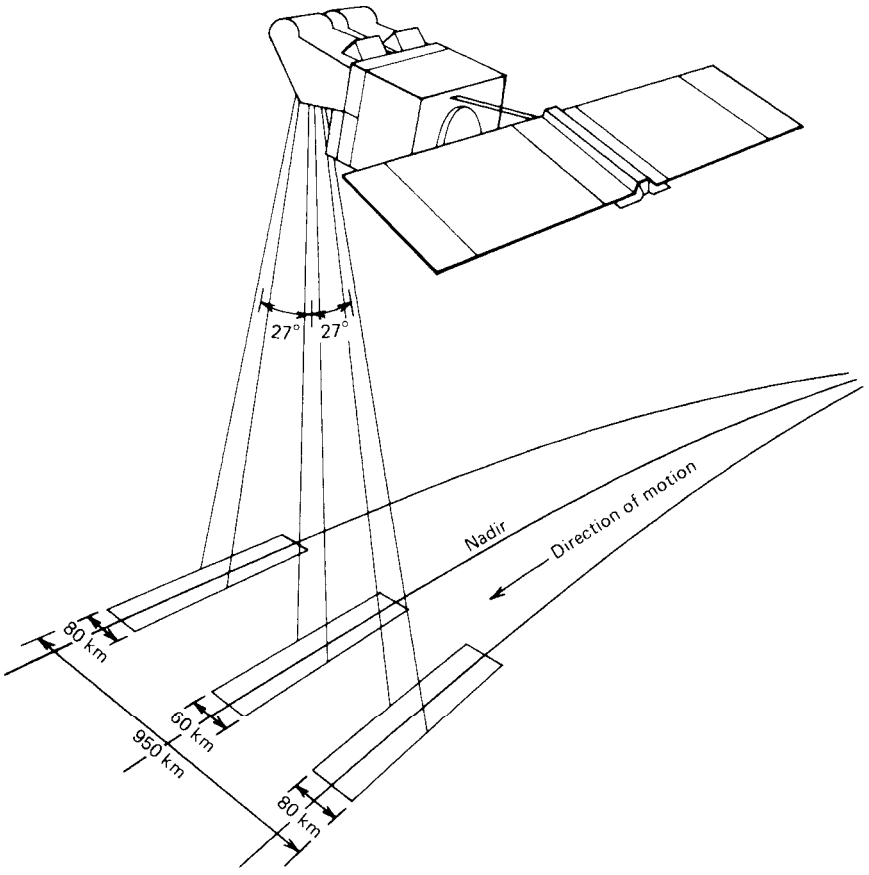

Figure 6.23 SPOT off-nadir viewing range. (Adapted from CNES diagram.)

The first element in the optical system for each HRV is a plane mirror that can be rotated to either side by ground command through an angle of ±27° (in 45 steps of 0.6° each). This allows each instrument to image any point within a strip extending 475 km to either side of the satellite ground track (Figure 6.23). The size of the actual ground swath covered naturally varies with the pointing angle employed. At the 27° maximum value, the swath width for each instrument is 80 km. When the two instruments are pointed so as to cover adjacent image fields at nadir, the total swath width is 117 km and the two fields overlap by 3 km (Figure 6.24). While each HRV instrument is capable of collecting panchromatic and multispectral data simultaneously, resulting in four data streams, only two data streams can be transmitted at one time. Thus, either panchromatic or multispectral data can be transmitted over a 117-km-wide swath, but not both simultaneously.

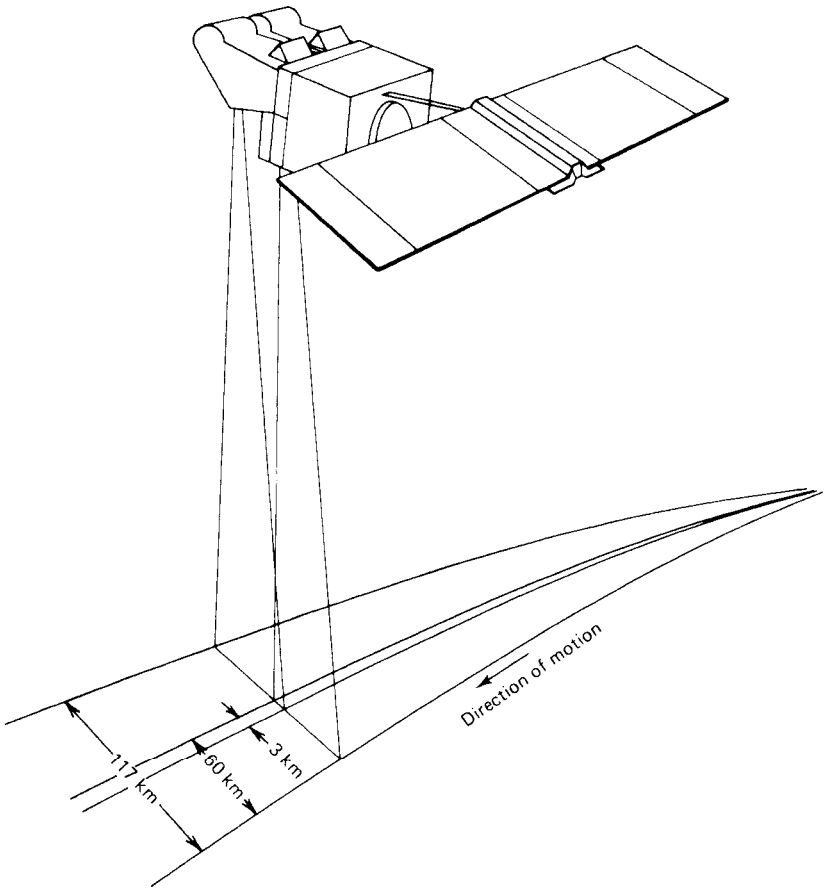

Figure 6.24 SPOT ground coverage with HRVs recording adjacent swaths. (Adapted from CNES diagram.)

Stereoscopic imaging is also possible due to the off-nadir viewing capability of the HRV. That is, images of an area recorded on different satellite tracks can be viewed in stereo (Figure 6.25). The frequency with which stereoscopic coverage can be obtained, being tied directly to the revisit schedule for the satellite, varies with latitude. At a latitude of 45° (Figure 6.21*a*), there are six possible occasions during the 26-day orbit cycle on which *successive-day* stereo coverage may be obtained (day D with $D + 1$, $D + 5$ with $D + 6$, $D + 10$ with $D + 11$, $D + 15$ with $D + 16$, $D + 20$ with $D + 21$, and $D + 25$ with day D of the next orbit cycle). At the equator (Figure 6.21*b*), only two stereoviewing opportunities on successive days are possible ($D + 10$ with $D + 11$ and $D + 15$ with $D + 16$). The base–height ratio also varies with latitude, from approximately 0.50 at 45° to approximately 0.75 at the equator. (If stereoscopic coverage need not be acquired on a successive-day basis, the range of possible viewing opportunities and viewing geometries greatly increases.)

It should now be clear that the SPOT-1, -2, and -3 system affords a broad range of viewing conditions and spectral modes of operation. The particular observation sequence for a given day of satellite operation is loaded into the system's onboard computer by the Toulouse, France, ground control station

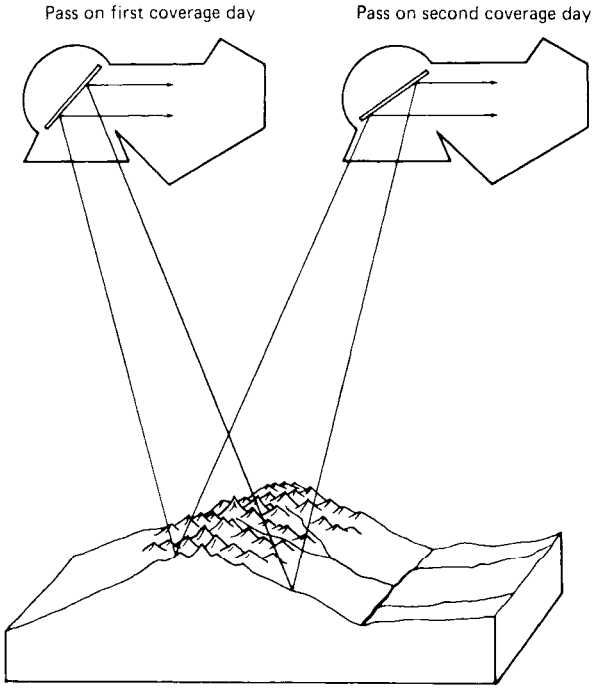

Figure 6.25 SPOT stereoscopic imaging capability. (Adapted from CNES diagram.)

while the satellite is within its range. The day's operating sequence for each HRV is controlled entirely independently. This includes the viewing angles of the two instruments, the spectral mode of operation (panchromatic or multispectral), timing of image acquisition, and modes of data transmission. Data are normally transmitted directly when the satellite is within range of a ground receiving station (approximately a 2600-km-radius around the station). The onboard tape recorders are used when images are acquired over areas outside the range of a ground receiving station. In such cases, the recorded image data are subsequently transmitted to the Toulouse or Kiruna, Sweden, station when the satellite reenters its range.

6.12 SPOT-4

Like its Landsat counterpart, the SPOT program has been designed to provide long term continuity of data collection but with successive improvements in the technical capability and performance of the sensing systems involved. SPOT-4, launched on March 23, 1998, reflects this continuity with improved performance design philosophy. The primary imaging systems on board this satellite are the *high resolution visible and infrared* (*HRVIR*) sensors and the *Vegetation* instrument.

HRVIR

Similar to the HRV system incorporated in SPOT-1 to -3, the *HRVIR* system includes two identical sensors capable of imaging a total nadir swath width of 120 km. Among the major improvements in the system is the addition of a 20-m-resolution band in the mid-IR portion of the spectrum (between 1.58 and 1.75 μm). This band improves the vegetation monitoring, mineral discriminating, and soil moisture mapping capability of the data. Furthermore, mixed 20- and 10-m data sets are coregistered onboard instead of during ground processing. This has been accomplished by replacing the panchromatic band of SPOT-1, -2, and -3 (0.49 to 0.73 μm) with the "red" band from these systems (0.61 to 0.68 μm). This band is used to produce both 10-m black and white images and 20-m multispectral data.

Vegetation

Another major addition to SPOT-4's payload is the Vegetation instrument. While designed primarily for vegetation monitoring, this system is useful in a range of applications where frequent, large-area coverage is important. (We illustrate several of these applications in our discussion of meteorological and

TABLE 6.6 Comparison of Spectral Bands Used by the SPOT-4 HRVIRs and the Vegetation Instrument

Spectral Band (μm)	Nominal Spectral Location	HRVIR	Vegetation Instrument
0.43–0.47	Blue	—	Yes
0.50–0.59	Green	Yes	—
0.61–0.68	Red	Yes	Yes
0.79–0.89	Near IR	Yes	Yes
1.58–1.75	Mid IR	Yes	Yes

ocean-monitoring satellites.) The instrument uses linear-array technology to provide a very wide angle image swath 2250 km wide with a spatial resolution at nadir of approximately 1 km and global coverage on a daily basis. (A few zones near the equator are covered every other day.)

As shown in Table 6.6, the Vegetation instrument uses three of the same spectral bands as the HRVIR system, namely the red, near-IR, and mid-IR bands, but it also incorporates a blue band (0.43 to 0.47 μm) for oceanographic applications.

Flown in combination, the Vegetation instrument and the HRVIR system afford the opportunity for coincident sampling of comparable large-area, coarse-resolution data and small-area, fine-resolution data. Intercomparison of the data from both systems is facilitated by the use of the same geometric reference system for both instruments and the spectral bands common to the two systems (Table 6.6). Given the flexibility of the combined system, data users can tailor sampling strategies to combine the benefits of Vegetation's revisit capability and the HRVIR system's high spatial resolution to validate the lower resolution data. Applications of the combined data sets range from regional forecasting of crop yield to monitoring forest cover and observing long term environmental change.

6.13 SPOT-5

On May 3, 2002, the SPOT program entered a new era with the successful launch of SPOT-5. The satellite carries two *high resolution geometric* (*HRG*) instruments, a single *high resolution stereoscopic* (*HRS*) instrument, and a Vegetation instrument similar to that on SPOT-4. The HRG systems are designed to provide high spatial resolution, with either 2.5- or 5-m-resolution panchromatic imagery, 10 m resolution in the green, red, and near-IR multispectral bands, and 20 m resolution in the mid-IR band. The panchromatic band has a spectral range similar to that of the HRV on SPOT-1, -2, and -3 (0.48 to 0.71 μm), rather than the high resolution red band that was adopted

TABLE 6.7 Sensors Carried on SPOT-5

Sensor	Spectral Band (μm)	Spatial Resolution (m)	Swath Width (km)	Stereoscopic Coverage
HRG	Pan: 0.48–0.71	2.5 or 5[a]	60–80	Cross-track pointing to ±31.06°
	B1: 0.50–0.59	10		
	B2: 0.61–0.68	10		
	B3: 0.78–0.89	10		
	B4: 1.58–1.75	20		
HRS	Pan: 0.49–0.69	5–10[b]	120	Along-track stereo coverage
Vegetation 2[c]	B0: 0.45–0.52	1000	2250	
	B2: 0.61–0.68	1000		
	B3: 0.78–0.89	1000		
	B4: 1.58–1.75	1000		

[a]The HRG panchromatic band has two linear arrays with 5 m spatial resolution that can be combined to yield 2.5 m resolution.

[b]The HRS panchromatic band has a spatial resolution of 10 m in the along-track direction and 5 m in the across-track direction.

[c]For consistency with the band numbering on other SPOT sensors, the Vegetation instrument's blue band is numbered 0 and the red band is numbered 2; there is no band 1.

for the SPOT-4 HRVIR. The high resolution mode in the panchromatic band is achieved by using two linear arrays of CCDs, offset horizontally within the focal plane by one-half the width of a CCD. Each linear array has a nominal ground sampling distance of 5 m. During processing at the ground station, data from the two linear arrays are interlaced and interpolated, resulting in a single panchromatic image with 2.5 m resolution.

The HRS instrument incorporates fore-and-aft stereo collection of panchromatic imagery, to facilitate the preparation of digital elevation models (DEMs) at a resolution of 10 m. It is also possible to acquire across-track stereoscopic imagery from the twin HRG instruments, which are pointable to ±31° off nadir. Table 6.7 summarizes the spatial and spectral characteristics of the HRG and HRS instruments on SPOT-5.

6.14 SPOT IMAGE INTERPRETATION

The use of SPOT HRV and HRVIR data for various interpretive purposes is facilitated by the system's combination of multispectral sensing with moderate spatial resolution, high geometric fidelity, and the provision for multidate and stereo imaging.

The spatial resolution of SPOT-1, -2, and -3 panchromatic imagery is illustrated in Figure 6.26, which shows Baltimore's Inner Harbor. Many individual

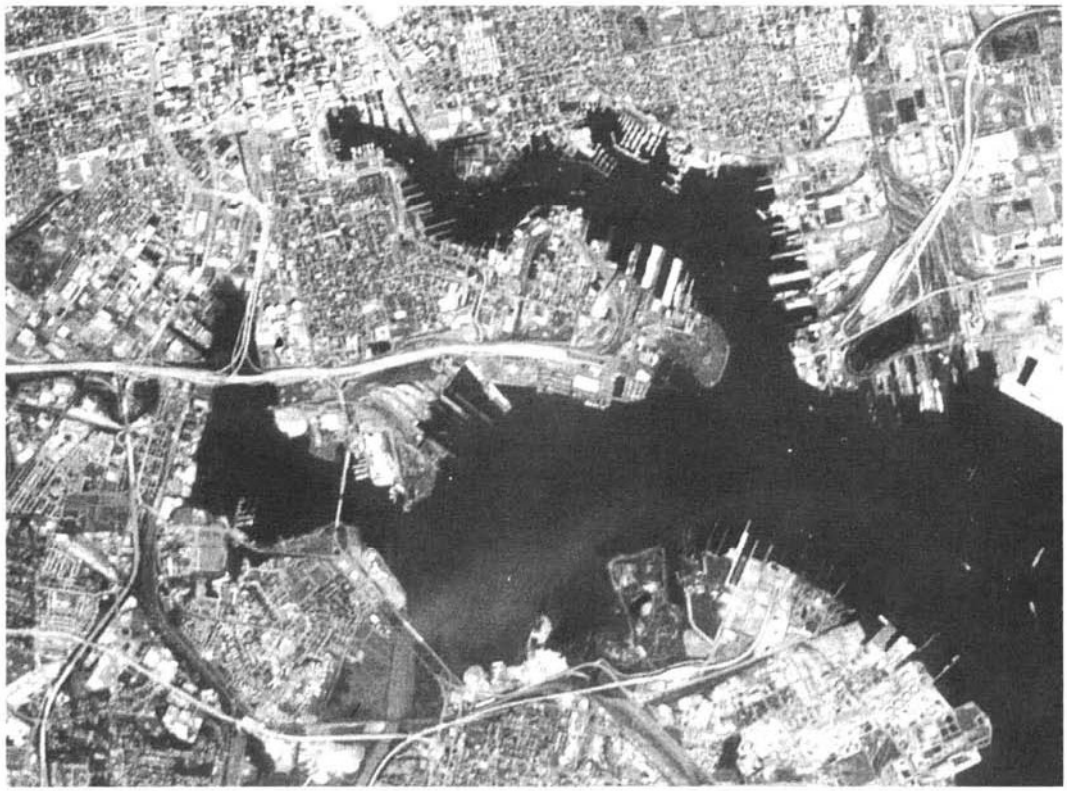

Figure 6.26 SPOT-1 panchromatic image, Baltimore, MD, Inner Harbor, late August. Scale 1:70,000. (Copyright © 1986 CNES. Courtesy SPOT Image Corp.)

buildings, industrial and harbor facilities, and the transportation network are clearly visible.

The stereoscopic imaging capability of the SPOT satellites is illustrated in Figure 6.27, a stereopair acquired on the third and fourth days after the launch of SPOT-1. In these images of Libya, an eroded plateau is seen at the top and center, and alluvial fans are shown at the bottom. Some vertical streaking can be seen, especially in the left-hand image. This artifact is present in this early image from the system because the scene was processed using preflight calibration parameters to record this "engineering data set" and the individual detectors of the CCDs were not fully calibrated at that time.

Using the parallax resulting when SPOT data are acquired from two different orbit tracks, perspective views of a scene can be calculated and displayed. Figure 6.28 shows a perspective view of the Albertville area in the French Alps generated entirely from SPOT data acquired from two different

Figure 6.27 SPOT-1 panchromatic image, stereopair, February 24 and 25, 1986, Libya. (Copyright © 1986 CNES. Courtesy SPOT Image Corp.)

orbit tracks. Perspective views can also be produced by processing data from a single image with digital elevation data of the same scene (as discussed in Chapter 7).

Figure 6.29 shows SPOT panchromatic images of an area in the Mojave Desert located approximately 60 km southeast of Barstow, California. These images were acquired before and after a major earthquake (magnitude 7.5), the Landers earthquake of June 28, 1992. The Emerson fault, which runs

Figure 6.28 Perspective view of the Albertville area in the French Alps, generated entirely from SPOT data, on successive days in late July. (Produced by ISTAR. Copyright © 1993 CNES. Provided by SPOT Image Corp.)

from upper left to lower right in these images, cracked extensively during the earthquake with motion across the fault of about 4 m. The trace of ground cracks created during the earthquake is clearly evident in the postearthquake images (*b*) and (*d*). Although individual cracks are not visible, they are so numerous within the fault zone that collectively they appear darkened in the postearthquake images. The preearthquake images (*a*) and (*c*) do not show any fault cracks.

Figure 6.30 shows a portion of a SPOT-5 image collected over Stockholm, Sweden. This image was among the first acquired after SPOT-5's launch in May, 2002. The 10-m red band is shown in (*a*), and 2.5-m panchromatic imagery for the central city is shown in (*b*). As discussed in Section 6.13, this 2.5 m resolution is achieved through interpolation of the data collected by two separate 5 m resolution linear array sensors. Stockholm is situated along a waterway between Lake Mälaren, on the left side of (*a*), and an inlet of the

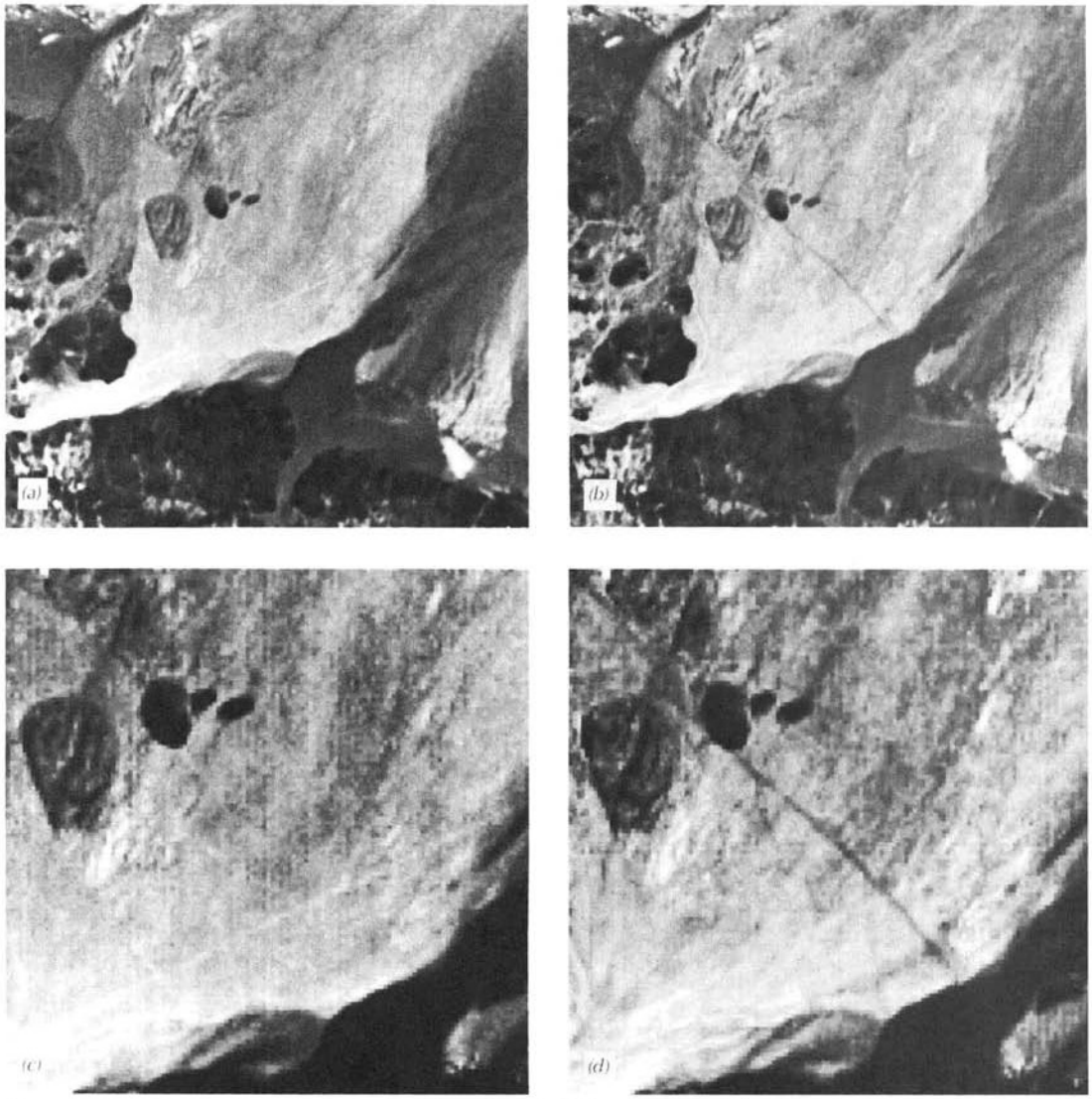

Figure 6.29 SPOT panchromatic images, Mohave Desert, 60 km southeast of Barstow, CA, before and after a major earthquake: (*a*, *c*) July 27, 1991; (*b*, *d*) July 25, 1992, 27 days after the earthquake. Scale 1 : 36,000 for (*a*) and (*b*); scale 1 : 18,000 for (*c*) and (*d*). (Copyright © 1992 CNES. Courtesy NASA Jet Propulsion Laboratory.)

Baltic Sea. Between the city and the sea lies an archipelago of some 24,000 islands, only some of which are visible at the right side of this image. The Old City area includes the royal palace, located near the north end of the island of Stadsholmen, in the center of image (*b*). At 2.5 m resolution, numerous bridges, docks, and boats can be seen along the waterways of the city.

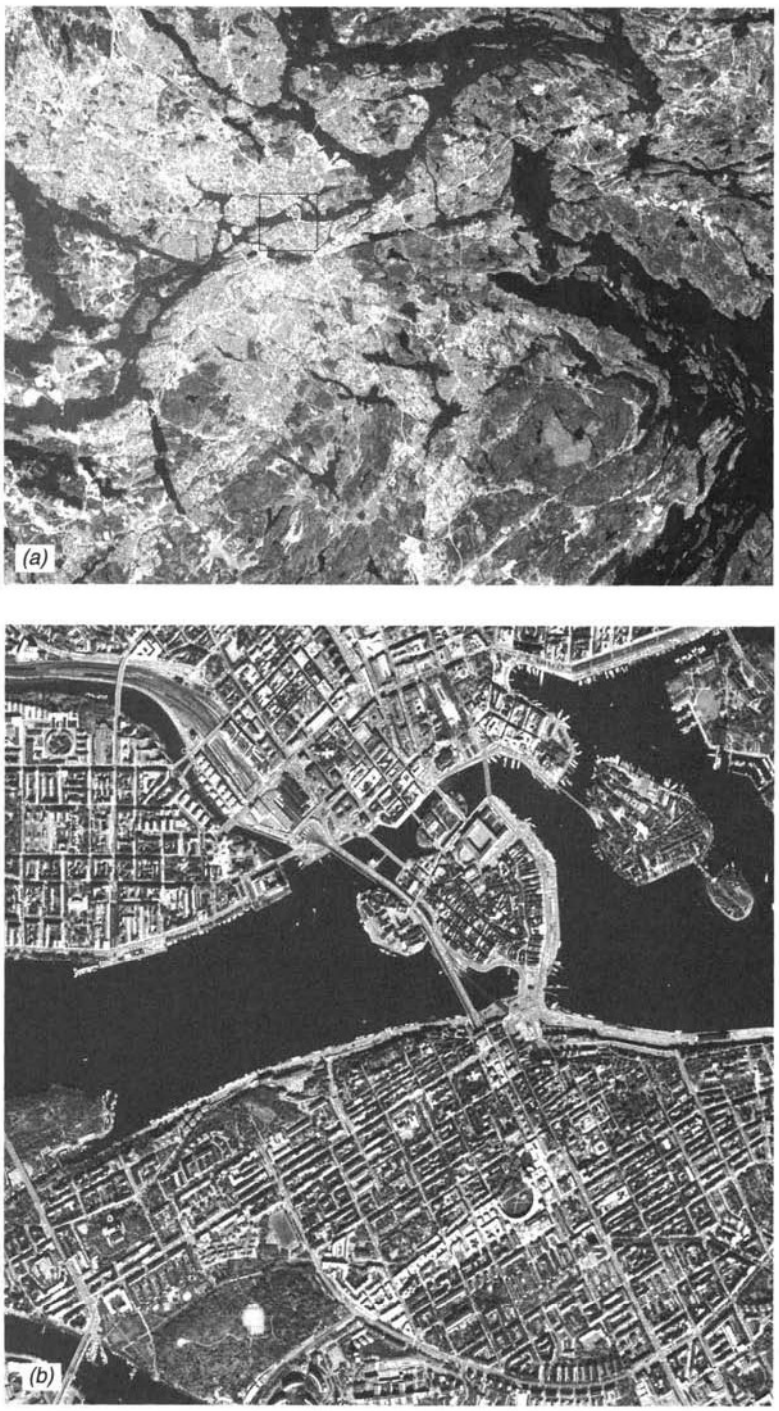

Figure 6.30 SPOT-5 HRG imagery of Stockholm, Sweden, May, 2002: (*a*) Band 2, 10 m resolution (red); (*b*) panchromatic band, 2.5 m resolution. (Courtesy CNES and SPOT Image, Inc.)

Plate 18 shows four images obtained with the SPOT Vegetation instrument. In (*a*), the red tones associated with the healthy green vegetation in western Europe contrast sharply with the yellow-brown colors of the North African desert. Snow cover in the Alps is also readily apparent in this image. In (*b*), most of the area around the Red Sea does not support much vegetation, but the Nile River floodplain and delta stand out in red tones near the upper left of the image. In (*c*) much of the land area in this portion of Southeast Asia is a bright red color associated with lush tropical vegetation. Plate 18*d* is a combination of red, near-IR, and mid-IR bands, in contrast to the blue, red, and near-IR combination used for (*a*), (*b*), and (*c*). Here the resulting colors are quite different than seen in the previous color band combinations. This image covers portions of the U.S. Pacific Northwest and western Canada. Mountainous areas with significant snow cover and bare rock are a distinct pink color. The areas with the most lush vegetation are depicted in brown tones in areas of Washington and Oregon west of the Cascade Mountains and on Vancouver Island, British Columbia. (The brown colors result from high reflection in the near-IR and mid-IR bands.) The white streaks over the ocean area at upper left are aircraft contrails. The bright white area in the lower left part of the image is coastal fog.

6.15 OTHER EARTH RESOURCE SATELLITES

Due to their historical long term use and widespread availability, Landsat and SPOT data have been emphasized in this discussion. However, it should be pointed out that many other earth observation satellite systems have been operated or are planned for launch in the not too distant future. These can be generally classified into the categories of moderate resolution systems, high resolution systems, and hyperspectral systems. Representative examples of each of these categories are discussed in this section.

Moderate Resolution Systems

The Republic of India has successfully developed, launched, and operated several moderate resolution *Indian Remote Sensing* (*IRS*) satellite systems, beginning with IRS-1A in 1988 and continuing with three additional IRS-series satellites in the 1990s. IRS-1A and -B included the *Linear Imaging Self-scanning Sensor* (*LISS*)-*I and -II*, multispectral sensors roughly equivalent to the MSS and TM systems from the Landsat program. IRS-1C and IRS-1D carry three sensors: the *LISS-III*, a panchromatic sensor, and a *Wide Field Sensor* (*WiFS*). Figure 6.31 is a portion of a LISS-III panchromatic image that includes the Denver International Airport and illustrates the level of detail

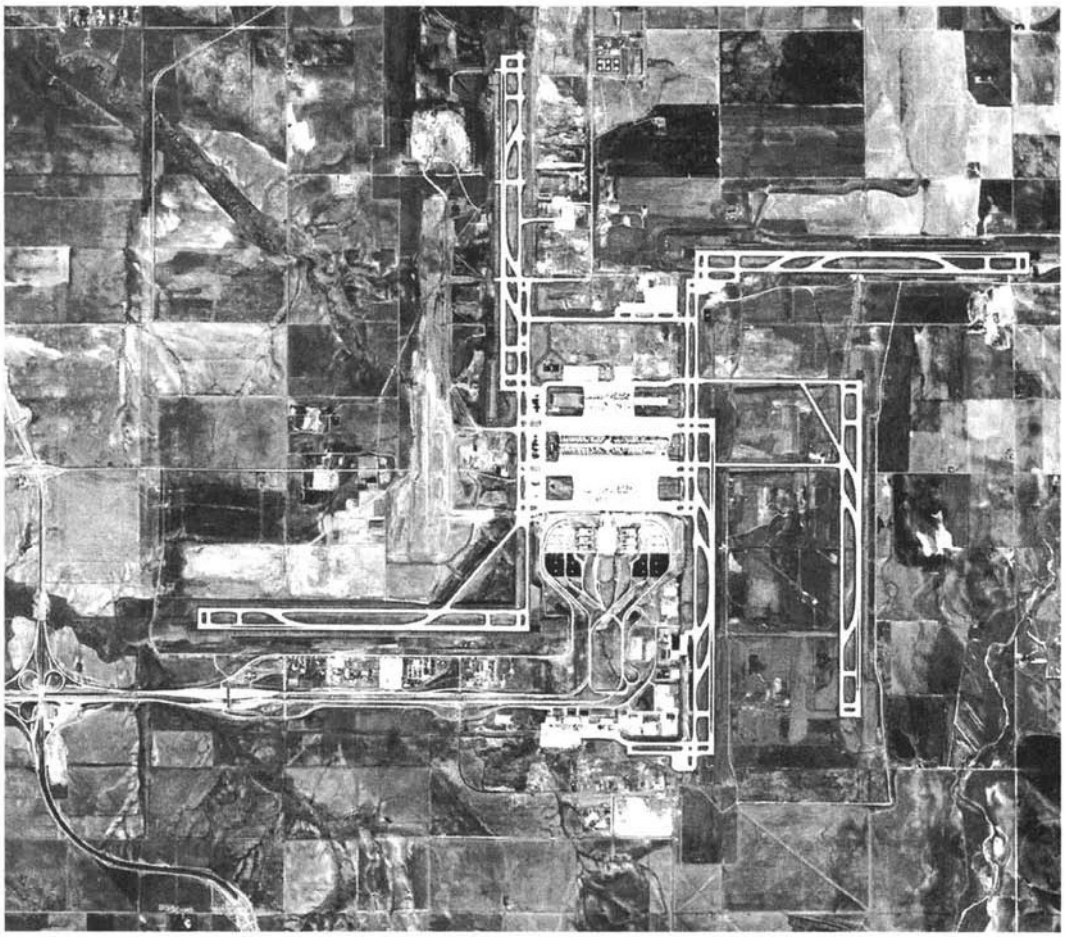

Figure 6.31 IRS panchromatic image (5.8 m resolution), Denver International Airport. Scale 1 : 85,000. (Image courtesy of Space Imaging, Thornton, CO.)

available with the 5.8-m data. Table 6.8 summarizes the characteristics of IRS-1A through IRS-1D.

The former Soviet Union launched two *RESURS-O1* satellites in 1985 and 1988. The RESURS program was then continued by Russia, with launches of RESURS-O1-3 in 1994 and RESURS-O1-4 in 1998. The latter two were the first in the series from which data were readily available outside the former Soviet Union; these data are now distributed by Eurimage. The orbital altitude, spatial resolution, and swath width for the RESURS-O1 satellites have changed significantly over the duration of the program. The characteristics of RESURS-O1-3 and RESURS-O1-4 are summarized in Table 6.9.

TABLE 6.8 Summary of IRS-1A through IRS-1D Satellite Characteristics

Satellite	Launch Year	Sensor	Spatial Resolution (m)	Spectral Band (μm)	Swath Width (km)
IRS-1A	1988	LISS-I	72.5	0.45–0.52 0.52–0.59 0.62–0.68 0.77–0.86	148
		LISS-II	36.25	0.45–0.52 0.52–0.59 0.62–0.68 0.77–0.86	146
IRS-1B	1991	Same as IRS-1A			
IRS-1C	1995	Pan	5.8	0.50–0.75	70
		LISS-III	23	0.52–0.59 0.62–0.68 0.77–0.86	142
			70	1.55–1.70	148
		WiFS	188	0.62–0.68	774
			188	0.77–0.86	774
IRS-1D	1997	Same as IRS-1C			

TABLE 6.9 Summary of RESURS-O1-3 and RESURS-O1-4 Satellite Characteristics

Satellite	Launch Year	Sensor	Spatial Resolution (m)		Spectral Band (μm)	Swath Width (km)
			Along Track	Across Track		
RESURS-O1-3	1994	MSU-E	35	45	0.5–0.6 0.6–0.7 0.8–0.9	45
		MSU-SK	140	185	0.5–0.6 0.6–0.7 0.7–0.8 0.8–1.0	600
			560	740	10.4–12.6	
RESURS-O1-4	1998	MSU-E	33	29	0.5–0.6 0.6–0.7 0.8–0.9	58
		MSU-SK	130	170	0.5–0.6 0.6–0.7 0.7–0.8 0.8–1.0	710
			520	680	10.4–12.6	

The RESURS-O1 satellites carry the *MSU-E* and *MSU-SK* multispectral scanners. The MSU-E is a linear array system that can be pointed up to 30° off nadir. In contrast, the MSU-SK employs a conical scanning procedure. In this approach to data acquisition, the IFOV of the system is aimed obliquely forward and the scan lines become a successive series of circular segments where the conical path of the field of view intersects the surface of the earth below. This procedure yields a constant resolution and viewing angle for all pixels, resulting in high radiometric accuracy. The unusual geometry of the MSU-SK image data is accounted for in the system correction of the image data during ground processing.

Launched by Japan on August 17, 1996, the *Advanced Earth Observing Satellite* (*ADEOS*) carried two primary sensing systems: the *Advanced Visible and Near Infrared Radiometer* (*AVNIR*) and the *Ocean Color and Temperature Sensor* (*OCTS*). The ADEOS acquired global earth observation data for approximately 7 months, prior to structural damage to its solar array. The AVNIR instrument is summarized in Table 6.10, while OCTS is discussed with other ocean-monitoring systems in Section 6.17.

While designed primarily as a radar remote sensing mission (see Chapter 8), Japan's *JERS-1* satellite (launched February 11, 1992) also carried the Optical Sensor (OPS), an along-track multispectral sensor. The OPS system included along-track stereoscopic coverage in one band, for topographic mapping purposes. Table 6.11 characterizes the JERS-1 OPS.

China and Brazil pursued joint development of *CBERS-1*, launched on October 14, 1999. CBERS-1 carried three sensors, including a CCD camera, a moderate resolution multispectral scanner, and a coarse resolution wide-field imaging system (Table 6.12). The CCD camera was designed to provide across-track stereoscopic coverage.

The *New Millennium Program* (*NMP*), managed by NASA's Jet Propulsion Laboratory, is aimed at developing and testing new technology in space missions. The NMP's first *Earth Orbiter* (*EO-1*) mission, launched on November 21, 2000, focused on validating a range of new developments in lightweight materials, detector arrays, spectrometers, communication, power generation, propulsion, and data storage. The EO-1 mission includes three land-imaging

TABLE 6.10 Summary of the AVNIR Sensor on ADEOS

Spectral Band (μm)	Spatial Resolution (m)	Swath Width (km)	Stereoscopic Coverage
0.52–0.69	8	80	Cross-track pointing to ±40°
0.42–0.50	16	80	Cross-track pointing to ±40°
0.52–0.60	16		
0.61–0.69	16		
0.76–0.89	16		

TABLE 6.11 Summary of the OPS Sensor on JERS-1

Spectral Band (μm)	Spatial Resolution (m)	Swath Width (km)	Stereoscopic Coverage
0.52–0.60	18 × 24	75	None
0.63–0.69			None
0.76–0.86			Along-track
1.60–1.71			None
2.01–2.12			None
2.13–2.25			None
2.27–2.40			None

instruments: the *Atmospheric Corrector* (*AC*) and *Hyperion*, both of which are discussed below in the context of hyperspectral satellite systems, and the *Advanced Land Imager* (*ALI*).

The ALI represents a technology verification project designed to demonstrate comparable or improved Landsat ETM+ spatial and spectral resolution with substantial reduction in sensor mass, volume, and cost. For example, the ALI consists of only 25 percent of the mass, requires only 20 percent of the electric power, and involves only approximately 40 percent of the overall mission cost of launching the ETM+. The ALI employs pushbroom scanning and features 10-m-resolution panchromatic and 30-m-resolution multispectral image acquisition. Table 6.13 provides a comparison of the spectral bands and resolutions for the ETM+ and the ALI. The ALI bands have been designed to mimic several of the ETM+ bands as well as to test the utility of bands covering 0.433 to 0.453 μm, 0.845 to 0.890 μm, and 1.20 to 1.30 μm. Finally, in order to facilitate the comparison of ALI and ETM+ imagery, the

TABLE 6.12 Sensors Carried on CBERS-1

Sensor	Spectral Band (μm)	Spatial Resolution (m)	Swath Width (km)	Stereoscopic Coverage
CCD camera	0.51–0.73	20	113	Cross-track pointing to ±32°
	0.45–0.52			
	0.52–0.59			
	0.63–0.69			
	0.77–0.89			
IR-MSS	0.50–1.10	80	120	None
	1.55–1.75			
	2.08–2.35			
	10.40–12.50	160	120	None
WFI	0.63–0.69	260	890	None
	0.76–0.90			

TABLE 6.13 Comparison of Landsat-7 ETM+ and ALI Spectral Bands and Spatial Resolutions

ETM+		ALI	
Band (μm)	Resolution (m)	Band (μm)	Resolution (m)
0.450–0.515	30	0.433–0.453	30
0.525–0.605	30	0.450–0.510	30
0.630–0.690	30	0.525–0.605	30
0.750–0.900	30	0.630–0.690	30
1.55–1.75	30	0.775–0.805	30
10.40–12.50	60	0.845–0.890	30
2.09–2.35	30	1.20–1.30	30
0.520–0.900 (pan)	15	1.55–1.75	30
		2.08–2.35	30
		0.480–0.680 (pan)	10

EO-1 satellite was maneuvered into an orbit that matched that of Landsat-7 to within 1 min.

A partial list of those countries (or agencies) operating, planning, or developing various remote sensing satellites has been provided by Glackin (1998). The list includes Argentina, Australia, Brazil, Canada, China, European Space Agency (ESA), France, Germany, India, Israel, Italy, Japan, Korea, Malaysia, Russia, South Africa, Spain, Taiwan, Thailand, United Kingdom, Ukraine, and the United States. Space limits our description of these satellites, and many of the details of the launch and operation of these satellites are subject to change.

High Resolution Systems

Numerous systems have been launched, or are in the development phase, that achieve much higher spatial resolution than those described earlier in this discussion. Following are descriptions of some of the most widely available sources of high resolution data. These systems are summarized in Table 6.14.

The first successful launch of a commercially developed high resolution earth observation satellite occurred on September 24, 1999, with the launch of Space Imaging's *IKONOS* system. IKONOS occupies a 682-km sun-synchronous orbit with an equatorial crossing time of 10:30 A.M. The ground track of the system repeats every 11 days, but the revisit time for

TABLE 6.14 High Resolution Earth Observation Satellite Systems

Satellite	Launch Date	Spatial Resolution (m)	Spectral Bands (μm)	Swath Width (km)	Altitude (km)
IKONOS	Sept. 24, 1999	1 4	Pan: 0.45–0.90 1: 0.45–0.52 2: 0.52–0.60 3: 0.63–0.69 4: 0.76–0.90	11	681
EROS-A	Dec. 5, 2000	1.8	Pan: 0.50–0.90	13.5	480
QuickBird	Oct. 18, 2001	0.61 2.40	Pan: 0.45–0.90 1: 0.45–0.52 2: 0.52–0.60 3: 0.63–0.69 4: 0.76–0.90	16.5	450
OrbView-3	2003 (planned)	1 4	Pan: 0.45–0.90 1: 0.45–0.52 2: 0.52–0.60 3: 0.63–0.69 4: 0.76–0.90	8	470
EROS-B1	2004 (planned)	0.82 3.48	Pan: 0.50–0.90 Four multispectral bands planned	13	600

imaging is less than 11 days, based on latitude and the angular orientation of the system selected to acquire any given image. The system includes the capability to collect data at angles of up to 45° from vertical both in the across-track and along-track directions. This not only provides the opportunity for frequently covering a given area but also enables the collection of both side-by-side (cross-track) and fore-and-aft (along-track) stereoscopic imagery. At nadir, the system has a swath width of 11 km. A typical image is 11 × 11 km in size, but user-specified image strips and mosaics can also be collected.

IKONOS employs linear array technology and collects data in four multispectral bands at a nominal ground resolution of 4 m, as well as a 1-m-resolution panchromatic band. The panchromatic band and the multispectral bands can be combined to produce "pan-sharpened" multispectral imagery (with an effective resolution of 1 m). As noted in Table 6.14, the spectral ranges for these bands are essentially identical to their counterparts on the Landsat-7 ETM+. Data are collected over 2048 gray levels (11 bits).

The IKONOS satellite is designed to be highly maneuverable. The system is capable of pointing to a new target and stabilizing itself within a few seconds. This enables the system to be programmed to follow meandering

features or power lines and similar features. The entire spacecraft, not just the optical system, is pointed in the direction of data collection.

The first IKONOS image, collected on September 30, 1999, is shown in Figure 6.32*a*. Enlargements of selected portions of the image, including a runway at National Airport (*b*) and the Washington Monument (*c*), illustrate the level of detail that can be seen in 1-m-resolution panchromatic imagery. At the time this image was acquired, the Washington Monument was undergoing renovation, and scaffolding can be seen on the side facing the sensor. The monument also shows the effects of relief displacement in this image.

Plate 19 shows a small portion of an IKONOS image acquired during early summer over an agricultural area in eastern Wisconsin. Included are a false-color composite of IKONOS multispectral bands 2, 3, and 4 at original 4 m resolution; the panchromatic band at 1 m resolution; and a merged image

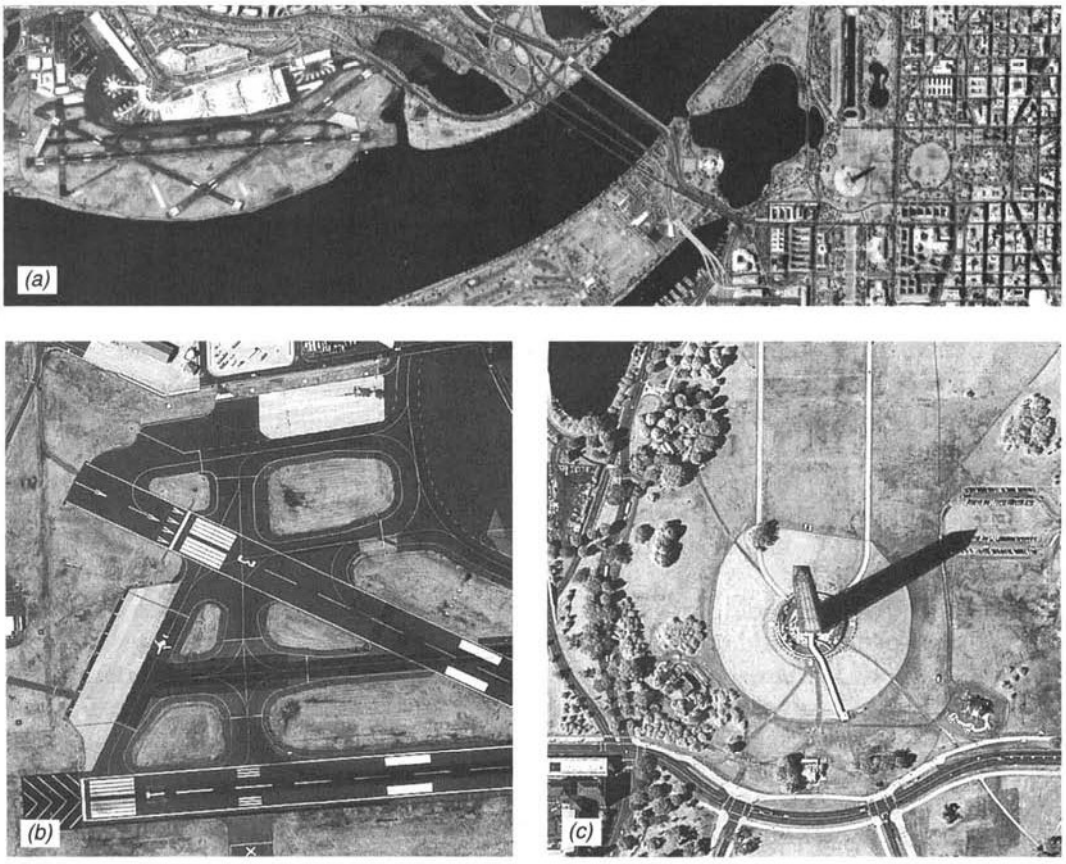

Figure 6.32 First IKONOS image, acquired on September 30, 1999, over Washington, DC: (*a*) Panchromatic image; (*b*) enlargement showing runway at National Airport; (*c*) enlargement showing Washington Monument (with scaffolding present during renovation activity). (Courtesy Space Imaging, Inc.)

showing the results of the pan-sharpening process (Section 7.6). The sharpened image has the spectral information present in the original multispectral data, but with an effective spatial resolution of 1 m.

ImageSat International launched *EROS-A* on December 5, 2000. The first of a planned series of several high resolution satellites, EROS-A has a single pushbroom panchromatic sensor with 1.8 m resolution. Off-nadir pointing (up to 45°) in any direction is possible, by changing the angular orientation of the satellite. Current plans call for a second system, *EROS-B1*, to be launched in 2004, with a 0.82-m-resolution panchromatic band and four 3.48-m-resolution multispectral bands. If the proposed constellation of six EROS satellites is successfully brought into operation, it will permit at least daily, if not more frequent, imaging of any point within a ground station's coverage area. Currently, EROS-A data are distributed through ImageNet, a service of Core Software Technology.

The highest resolution satellite imagery currently available to the public is provided by *QuickBird*, launched on October 18, 2001, and operated by DigitalGlobe, Inc. The system is in a sun-synchronous, relatively low orbit, at an altitude of 450 km. The average revisit time is 1 to 3.5 days, depending on latitude and image collection angle. QuickBird features a 0.61-m-resolution panchromatic sensor and a four-band multispectral sensor having a resolution of 2.40 m. As shown in Table 6.14, the spectral ranges of these linear array sensors are essentially equivalent to those of the IKONOS system. Similarly, 11-bit data recording is employed.

Figure 6.33 shows a panchromatic image (61 cm resolution) of the Taj Mahal of India, collected by QuickBird on February 15, 2002. The complex was built by the Muslim Emperor Shah Jahan as a mausoleum for his wife, queen Mumtaz Mahal. The height of the minarets at the four corners of the main structure is indicated by the length of their shadows. In addition, the peaks of the domes appear to be offset from the centers of the domes, due to relief displacement in this image.

Plate 20 illustrates the use of pan-sharpening techniques to produce color QuickBird images with an effective 61 cm resolution. The image shows a true-color composite derived from the merger of data from the QuickBird panchromatic band and multispectral bands 1, 2, and 3 shown as blue, green, and red, respectively. It was acquired on May 10, 2002, over the Burchardkai Container Terminal at the Port of Hamburg. The outlines and colors of individual cargo containers can be readily differentiated at the resolution of this image.

ORBIMAGE's *OrbView-3* system is currently scheduled for launch in 2003. The satellite is to be operated at an altitude of 470 km in a sun-synchronous orbit having a 10:30 A.M. equatorial crossing time. The system orbit does not repeat exactly, but approximate repetition is accomplished in less than 3 days depending on latitude. The sensing system on board will include a panchromatic band (with 1 m resolution) and four multispectral bands (with 4 m resolution).

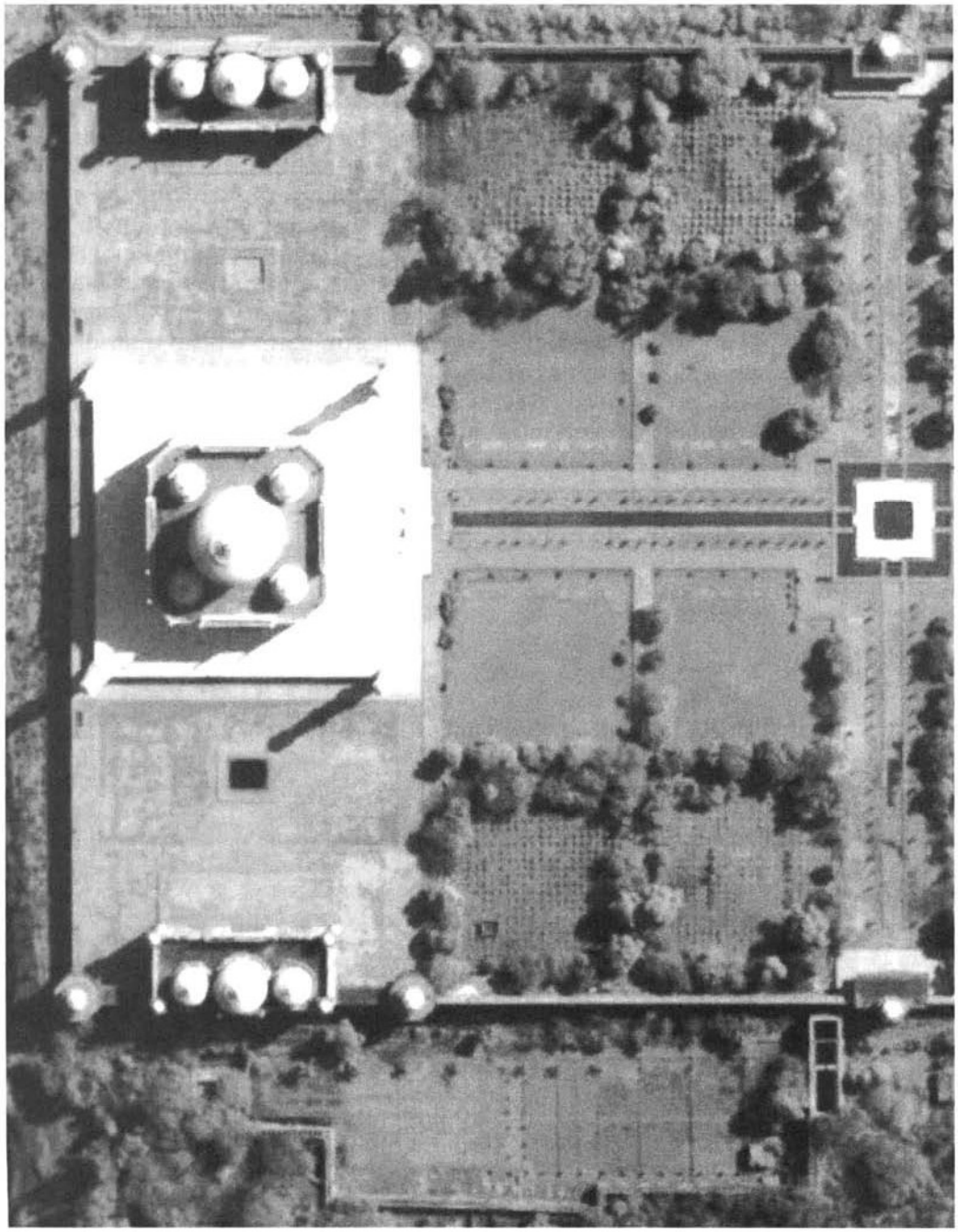

Figure 6.33 QuickBird panchromatic image of the Taj Mahal, India, 61 cm resolution. (Courtesy DigitalGlobe.)

The swath width of the instrument is 8 km at nadir, and the sensor can be tilted up to 45° cross-track. The spectral bands of the system are functionally equivalent to those of the IKONOS and QuickBird instruments.

While this discussion has focused on electro-optical systems, high resolution photographic satellite imagery has been available for several years from a series of formerly classified Russian military satellite systems, known as *Space Information-2 Meter* (*SPIN-2*). SPIN-2 data are produced by digitizing panchromatic (0.51 to 0.76 μm) photographs taken by the KUR-1000 camera, a panoramic camera system employing a 1-m-focal-length lens. Operated from an altitude of 220 km, the camera acquires photographs at an average scale of 1:220,000 with individual scenes covering an area of 40 × 160 km, with a GRD of approximately 1 m at nadir. The average ground cell size for the digitized data is 1.56 m per pixel. Both photographic and digital data derived from the system are available through TerraServer on the Internet (www.terraserver.com).

SPIN-2 image data are rectified by operating the KUR-1000 camera in conjunction with a 10-m-resolution "topographic camera," the TK-350. The TK-350 has a 350-mm focal length and produces photographs at a scale of 1:660,000 with ground coverage of 200 × 300 km. These photographs are acquired with 80 percent overlap and are used to prepare DEMs to rectify the KUR-1000 images. The exterior orientation parameters for the camera are determined by two onboard systems that base their calculations on a combination of celestial readings and laser altimeter data. The quoted geometric accuracy of the 2-m data is 10 m without the use of supplemental ground control and 3 to 4 m with supplemental control. The quoted vertical accuracy of the DEMs produced from the 10-m data is 10 m without ground control and 5 m when ground control is used.

Hyperspectral Satellite Systems

In Chapter 5, we discussed the concept of airborne hyperspectral scanning. This involves collecting data in numerous, narrow, contiguous spectral bands. At the time of this writing (2002), there was only one operating spaceborne hyperspectral scanning system, the Hyperion instrument carried on the previously mentioned EO-1 spacecraft. Several other attempts to launch hyperspectral satellite systems have ended in failure. With other such systems currently in development, it is expected that spaceborne hyperspectral imaging will experience a period of significant growth over the coming decade.

The EO-1 Hyperion instrument nominally provides 242 spectral bands of data over the 0.36- to 2.6-μm range, each of which has a width of 0.010 to 0.011 μm. Some of the bands, particularly those at the lower and upper ends of the range, exhibit a poor signal-to-noise ratio. As a result, during Level 1 processing, only 198 of the 242 bands are calibrated; radiometric values in

the remaining bands are set to 0 for most data products. Hyperion consists of two distinct linear array sensors, one with 70 bands in the UV, visible, and near IR, and the other with 172 bands in the near IR and mid IR (with some overlap in the spectral sensitivity of the two arrays). The spatial resolution of this experimental sensor is 30 m, and the swath width is 7.5 km. Data from the Hyperion system are distributed by the USGS.

The EO-1 AC (also referred to as the *LEISA AC or LAC*) is a hyperspectral imager of coarse spatial resolution covering the 0.85- to 1.5-μm-wavelength range. It was designed to correct imagery from other sensors for atmospheric variability due primarily to water vapor and aerosols. The AC has a spatial resolution of 250 m at nadir. Acquisition of AC data was ended after the first year of the EO-1 mission, though Hyperion and ALI data continue to be collected as of the time of this writing (2002).

Several additional hyperspectral systems have been proposed or are in development. The U.S. Navy's Office of Naval Research has sponsored the development of a hyperspectral imaging system to be launched on the proposed *Naval EarthMap Observer* (*NEMO*) satellite. This hyperspectral instrument on NEMO would acquire data in 200 spectral bands over the range of 0.4 to 2.5 μm. It would permit data acquisition at resolutions of either 30 or 60 m over a 30-km-wide swath, with cross-track pointing capability. The satellite would be launched into a 605-km, sun-synchronous orbit with a 10:30 A.M. ascending equatorial crossing time. A 5-m-resolution *Panchromatic Imaging Camera* (*PIC*) would be flown in combination with the hyperspectral instrument, covering the same 30-km swath.

The NEMO program features many design characteristics that are directly responsive to the Navy's needs for data collection in the coastal zone of the world's oceans. Among these needs are information on shallow water bathymetry, bottom-type composition, currents, oil slicks, underwater hazards, water clarity, atmospheric visibility, beach characterization, and near-shore soil and vegetation. Several of these requirements dictate that the system have a very high signal-to-noise ratio for maximum water penetration over the very low reflectance range typical of ocean water. Because of this, along-track pointing is used to increase the integration time over which data are collected in the 30-m mode. This technique is called *ground motion compensation* (*GMC*). At the beginning of a scene the spacecraft is pointed forward and continues to stare at the same ground position as the satellite moves forward. This mode of operation results in a fivefold increase in the dwell time over which the system views the scene elements below and a corresponding increase in signal-to-noise performance.

Another unique aspect of the NEMO system is onboard feature recognition and data compression based on the *Optical Real-Time Adaptive Spectral Identification System* (*ORASIS*) data processing algorithm. This computationally intensive process is implemented using an *Imagery On-Board Processor* (*IOBP*). The basic approach employed by the ORASIS system is to analyze the spectrum from each pixel in a scene sequentially, discarding duplicate spec-

tra, and subsequently analyzing only the unique spectra using such procedures as subpixel spectral demixing and feature extraction (Chapter 7).

Another proposed hyperspectral satellite system is the *Australian Resource Information and Environmental Satellite* (*ARIES*). Its nominal specifications include a hyperspectral imager with up to 105 bands located between 0.4 and 2.5 μm, 30 m resolution, a 15-km swath, up to 30° cross-track pointing, and a 7-day revisit period. The system also would include a 10-m panchromatic imager. While designed primarily for mineral exploration, ARIES would have substantial utility in applications ranging from agriculture and forestry to wetland mapping and environmental monitoring. Indeed, the future for this and similar hyperspectral satellite systems is an extremely bright one.

.16 METEOROLOGICAL SATELLITES FREQUENTLY APPLIED TO EARTH SURFACE FEATURE OBSERVATION

Designed specifically to assist in weather prediction and monitoring, *meteorological satellites*, or *metsats*, generally incorporate sensors that have very coarse spatial resolution compared to land-oriented systems. On the other hand, metsats afford the advantages of global coverage at very high temporal resolution. Accordingly, metsat data have been shown to be useful in natural resource applications where frequent, large-area mapping is required and fine detail is not. Apart from the advantage of depicting large areas at high temporal resolution, the coarse spatial resolution of metsats also greatly reduces the volume of data to be processed for a particular application.

Numerous countries have launched various types of metsats with a range of orbit and sensing system designs. In the remainder of this section we treat only three representative series of metsats that are operated by the United States. The first is the *NOAA* series named after the *National Oceanic and Atmospheric Administration*. These satellites are in near-polar, sun-synchronous orbits similar to those of Landsat and SPOT. In contrast, the *GOES* series of satellites are geostationary, remaining in a constant relative position over the equator. Solving Eq. 6.1 for an orbital period of 24 hr yields an orbital altitude of about 36,000 km above the earth's surface for geostationary satellites. GOES is an acronym for *Geostationary Operational Environmental Satellite*. The final systems we discuss are part of the *Defense Meteorological Satellite Program* (*DMSP*). All three of these satellite series carry a range of meteorological sensors. We treat only the salient characteristics of those sensors used most often in land remote sensing applications.

NOAA Satellites

Several generations of satellites have been flown in the NOAA series. Germane to this discussion are the NOAA-6 through NOAA-17 missions that contained

the *Advanced Very High Resolution Radiometer* (*AVHRR*). NOAA-6, -8, -10, -12, -15, and -17 have daytime (7:30 A.M., or 10:00 A.M. for NOAA-17) north-to-south equatorial crossing times while NOAA-7, -9, -11, -14, and -16 have nighttime (1:30 to 2:30 A.M.) north-to-south equatorial crossing times. Table 6.15 lists the basic characteristics of these missions and the AVHRR instrument. Figure 6.34 shows the 2400-km swath width characteristic of the system. Coverage is acquired at a ground resolution of 1.1 km at nadir. This

TABLE 6.15 Characteristics of NOAA-6 to -17 Missions

Parameter	NOAA-6, -8, -10, -12, -15, and -17	NOAA-7, -9, -11, -14, and -16[a]
Launch	6/27/79, 3/28/83, 9/17/86, 5/14/91, 5/13/98, 6/24/02	6/23/81, 12/12/84, 9/24/88, 12/30/94, 9/21/00
Altitude, km	833	870
Period of orbit, min	101	102
Orbit inclination	98.7°	98.9°
Orbits per day	14.2	14.1
Distance between orbits	25.6°	25.6°
Day-to-day orbital shift[b]	5.5° E	3.0° E
Orbit repeat period (days)[c]	4–5	8–9
Scan angle from nadir	±55.4°	±55.4°
Optical field of view, mrad	1.3	1.3
IFOV at nadir, km	1.1	1.1
IFOV off-nadir maximum, km		
Along track	2.4	2.4
Across track	6.9	6.9
Swath width, km	2400	2400
Coverage	Every 12 hr	Every 12 hr
Northbound equatorial crossing[d]	7:30 P.M.	1:30–2:30 P.M.
Southbound equatorial crossing[d]	7:30 A.M.	1:30–2:30 A.M.
AVHRR spectral channels, μm		
1	0.58–0.68	0.58–0.68
2	0.72–1.10	0.72–1.10
3	3.55–3.93[e]	3.55–3.93
4	10.5–11.50	10.3–11.30
5	Channel 4 repeat[f]	11.5–12.50

[a]NOAA-13 failed due to a short circuit in its solar array.

[b]Satellite differences due to differing orbital alignments.

[c]Caused by orbits per day not being integers.

[d]NOAA-17 has equatorial crossing times of 10:00 P.M. (northbound) and 10:00 A.M. (southbound).

[e]NOAA-15, -16, and -17 include two separate channels: 3A (1.58–1.64 μm) and 3B (3.55–3.93 μm).

[f]NOAA-12, -15, and -17 include a separate channel 5.

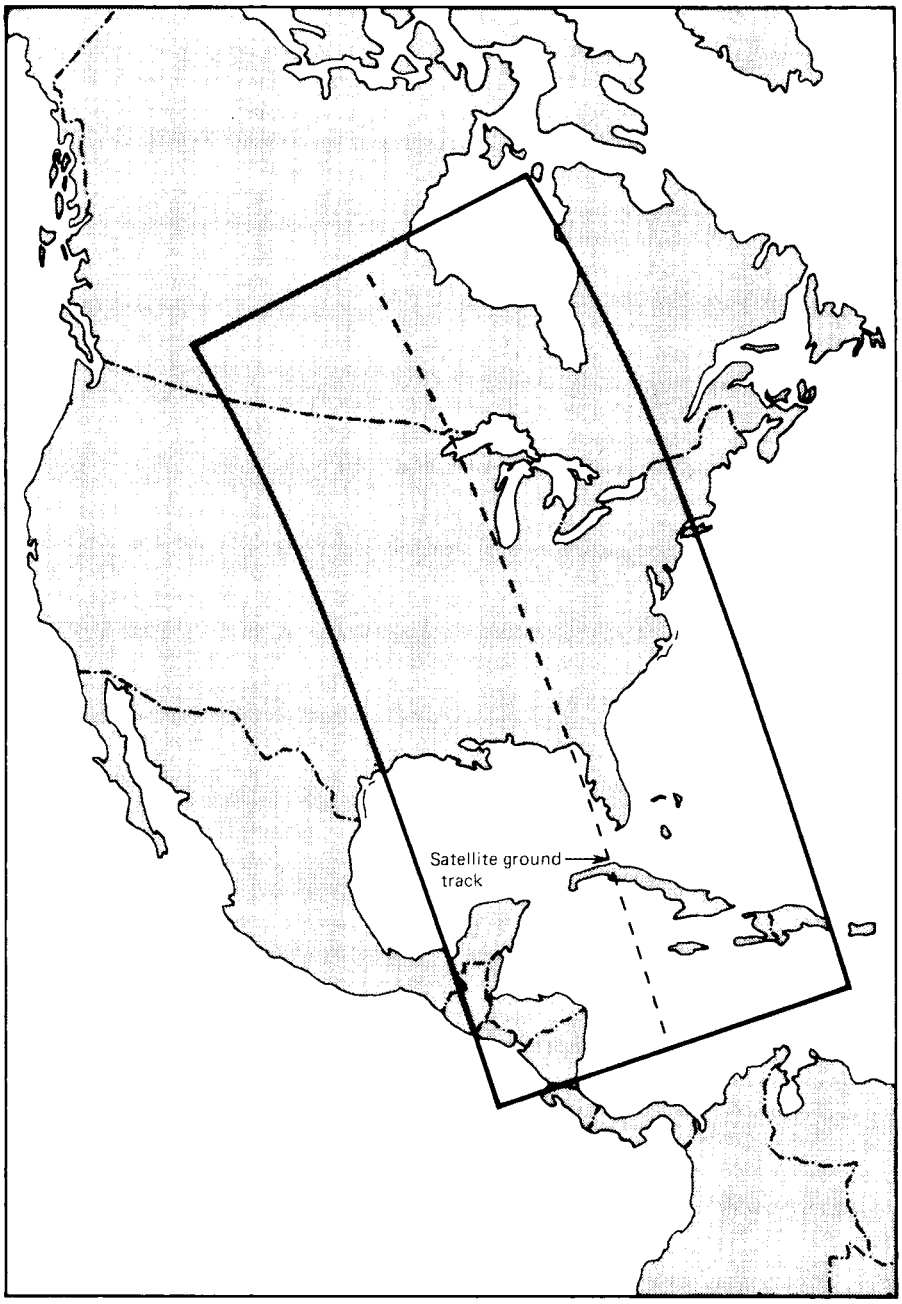

Figure 6.34 Example coverage of the NOAA AVHRR.

resolution naturally becomes coarser with increases in the viewing angle off nadir. NOAA receives AVHRR data at full resolution and archives them in two different forms. Selected data are recorded at full resolution, referred to as local area coverage (LAC) data. All of the data are sampled down to a nominal resolution of 4 km, referred to as global area coverage (GAC) data. Figure 6.35 summarizes the spectral sensitivity of the AVHRR relative to the Landsat MSS, the Landsat TM, the Landsat ETM+, the SPOT HRV, SPOT HRVIR, and the SPOT Vegetation sensor.

NOAA satellites provide daily (visible) and twice-daily (thermal IR) coverage. Images and digital tapes are used operationally in a host of applications requiring timely data. For example, Plate 21 illustrates the use of NOAA AVHRR thermal data for water temperature mapping. Here, the AVHRR data provide a synoptic view of water surface temperatures in all five of the Laurentian Great Lakes simultaneously.

In addition to surface water temperature mapping, AVHRR data have been used extensively in applications as varied as snow cover mapping, flood monitoring, vegetation mapping, regional soil moisture analysis, wildfire fuel mapping, fire detection, dust and sandstorm monitoring, and various geologic applications including observation of volcanic eruptions and mapping of regional drainage and physiographic features. Both AVHRR and GOES data (described below) have also been used in regional climate change studies. For example, Wynne et al. (1998) have used 14 years of such data to monitor the phenology of lake ice formation and breakup as a potential climate change indicator in the U.S. Upper Midwest and portions of Canada.

AVHRR data have been used extensively for large-area vegetation monitoring. Typically, the spectral bands used for this purpose have been the channel 1 visible band (0.58 to 0.68 μm) and the channel 2 near-IR band (0.73 to 1.10 μm). Various mathematical combinations of the AVHRR channel 1 and 2 data have been found to be sensitive indicators of the presence and condition of green vegetation. These mathematical quantities are thus referred to as *vegetation indices*. Two such indices have been routinely calculated from AVHRR data—a simple vegetation index (VI) and a normalized difference vegetation index (NDVI). These indices are computed from the equations

$$\mathrm{VI} = \mathrm{Ch}_2 - \mathrm{Ch}_1 \tag{6.2}$$

and

$$\mathrm{NDVI} = \frac{\mathrm{Ch}_2 - \mathrm{Ch}_1}{\mathrm{Ch}_2 + \mathrm{Ch}_1} \tag{6.3}$$

where Ch_1 and Ch_2 represent data from AVHRR channels 1 and 2, preferably expressed in terms of radiance or reflectance (see Chapter 7).

Vegetated areas will generally yield high values for either index because of their relatively high near-IR reflectance and low visible reflectance. In contrast, clouds, water, and snow have larger visible reflectance than near-IR reflectance.

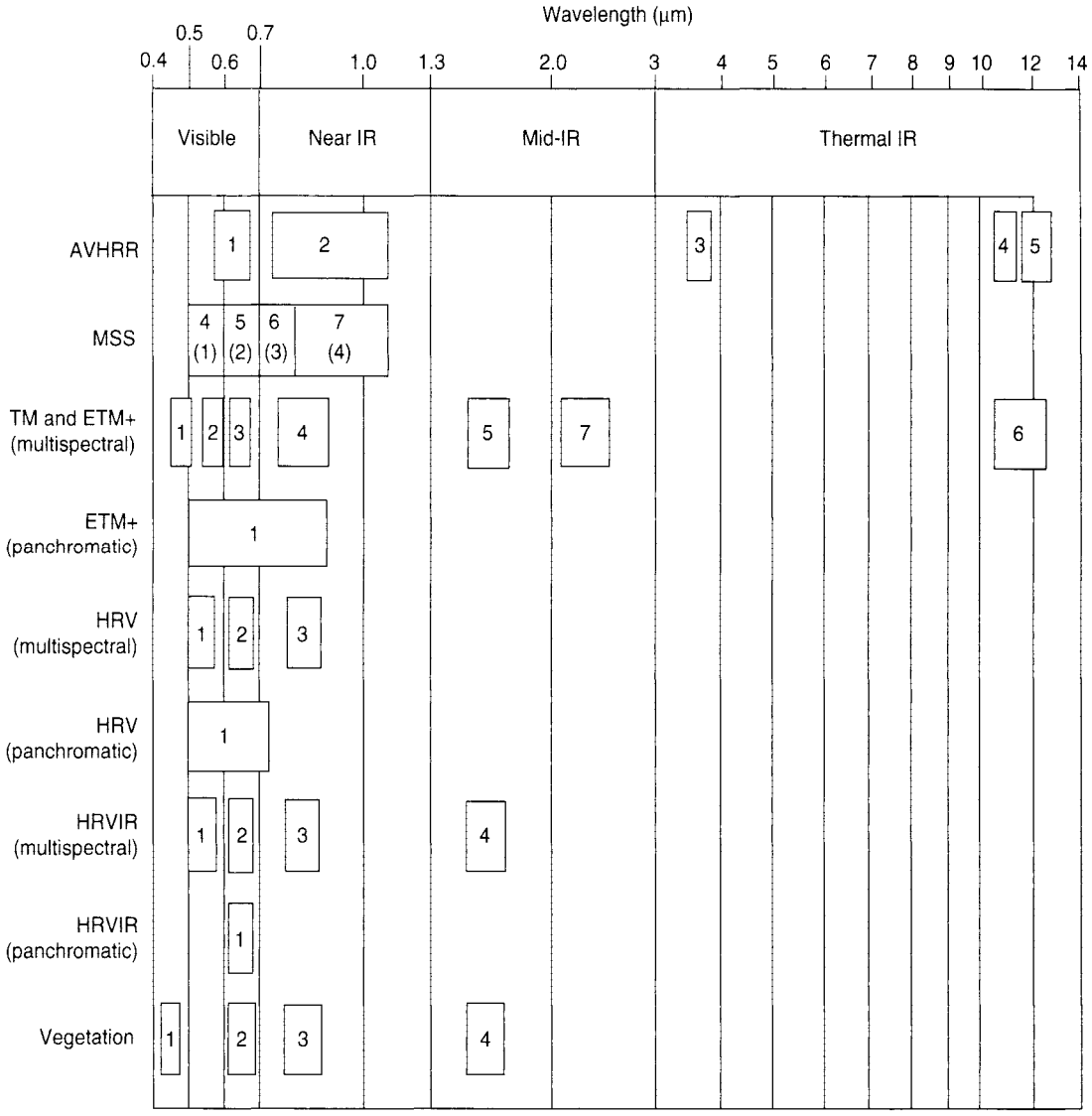

Figure 6.35 Summary of spectral sensitivity of NOAA AVHRR, Landsat MSS, TM, ETM+, and SPOT HRV, HRVIR, and Vegetation Instrument. Shown are the band numbers and associated bandwidths for each sensing system.

Thus, these features yield negative index values. Rock and bare soil areas have similar reflectances in the two bands and result in vegetation indices near zero.

The normalized difference vegetation index is preferred to the simple index for global vegetation monitoring because the NDVI helps compensate for changing illumination conditions, surface slope, aspect, and other extraneous factors.

Plate 22 shows NDVI maps of the conterminous United States for six 2-week periods during 1998 prepared from AVHRR data. The NDVI values for vegetation range from a low of 0.05 to a high of 0.66+ in these maps and are displayed in various colors (see key at bottom of plate). Clouds, snow, and bright nonvegetated surfaces have NDVI values of less than zero. The NDVI selected for each pixel is the greatest value on any day during the 14-day period (the highest NDVI value is assumed to represent the maximum vegetation "greenness" during the period). This process eliminates clouds from the composite (except in areas that are cloudy for all 14 days).

Scientists associated with the EDC have also produced numerous global NDVI composites to meet the needs of the international community. In these efforts, data collected at 29 international receiving stations, in addition to that recorded by NOAA, were acquired (starting April 1, 1992) on a daily global basis. Several tens of thousands of AVHRR images have been archived for this program and numerous 10-day maximum NDVI composites have been produced (Eidenshink and Faundeen, 1994).

Numerous investigators have related the NDVI to several vegetation phenomena. These phenomena have ranged from vegetation seasonal dynamics at global and continental scales to tropical forest clearance, leaf area index measurement, biomass estimation, percentage ground cover determination, and photosynthetically active radiation estimation. In turn, these vegetation attributes are used in various models to study photosynthesis, carbon budgets, water balance, and related processes.

Notwithstanding the widespread use of the AVHRR NDVI, it should be pointed out that a number of factors can influence NDVI observations that are unrelated to vegetation conditions. Among these factors are variability in incident solar radiation, radiometric response characteristics of the sensor, atmospheric effects (including the influence of aerosols), and off-nadir viewing effects. Recall that the AVHRR scans over $\pm 55°$ off nadir (compared to $\pm 7.7°$ for Landsat and $\pm 2.06°$ within a SPOT scene). This causes a substantial change not only in the size of the ground resolution cell along an AVHRR scan line but also in the angles and distances over which the atmosphere and earth surface features are viewed. Normalizing for such effects is the subject of continuing research. (We further discuss vegetation indices in Chapter 7.)

GOES Satellites

The Geostationary Operational Environmental Satellites (GOES) are part of a network of meteorological satellites located in geostationary orbit around the globe. The United States normally operates two such systems, typically located at 75° W longitude (and the equator) and at 135° W longitude (and the equator). These systems are referred to as GOES-EAST and GOES-WEST, respectively. Similar systems have been placed in operation by several other

countries as part of a corporate venture within the World Meteorological Organization.

From its vantage point, GOES can see an entire hemispherical disk (Figure 6.36). The repeat frequency is therefore limited only by the time it takes to scan and relay an image. The current generation of GOES imagers (GOES-8 and -10) are five-band systems having one visible band (0.55 to 0.75 μm) and four thermal bands (3.80 to 4.00 μm, 6.50 to 7.00 μm, 10.20 to 11.20 μm, and 11.50 to 12.50 μm). The spatial resolution at nadir of the visible band is 1 km, and the thermal bands have resolutions of 4, 8, 4, and 4 km, respectively. The IFOVs for all bands are simultaneously swept east

Figure 6.36 GOES-2 visible band (0.55 to 0.7 μm) image of hemispherical disk including North and South America, early September. A hurricane is clearly discernible in the Gulf of Mexico. (Courtesy NOAA/National Environmental Satellite, Data, and Information Service.)

to west and west to east along a north-to-south path by mirrors of a two-axis mirror scan system. The instrument can produce scans of the full hemispherical disks of the earth, "sector" images that contain the edges of the earth, or images of local regions. (Prior to GOES-8, only hemispherical disk images were produced in a visible and a single thermal band.) GOES-1 was launched in 1975; GOES-8 and -10 were launched in 1994 and 1997, respectively.

GOES images are by now very familiar to us all. They are distributed in near real time for use in local weather forecasting. They have also been used in numerous other large-area analyses, such as regional snow and ice cover mapping, when higher resolution data are not required.

Defense Meteorological Satellite Program

NOAA also coordinates the Defense Meteorological Satellite Program (DMSP), which was originally administered by the U.S. Air Force. Some of the data produced from the satellites in this program have been available to civilian users on an unclassified basis since April 1973. The DMSP satellites carry a range of meteorological sensors. Scanners onboard the satellites produce images in the 0.4- to 1.1-μm (visible and near-IR) band and the 8- to 13-μm (thermal IR) band. System resolution is on the order of 3 km and sun-synchronous polar orbits permit day and night global coverage. A unique capability of the DMSP scanner is nighttime visible band imaging. This comes about through the ability to "tune" the amplifiers of the system to obtain images under low illumination conditions. The system produces vivid images of phenomena such as the urban light patterns that were shown in Figures 4.28 and 4.29. Auroral displays, volcanoes, oil and gas fields, and forest fires have also been detected with the low light sensor. Both the thermal and daytime visible images of the DMSP have been used for such civilian applications as snow extent mapping.

6.17 OCEAN MONITORING SATELLITES

The oceans, which cover more than two-thirds of the earth's surface, have important influences on global weather and climate; yet they represent a natural resource about which comparatively little is known. Satellite imaging can provide synoptic views of the oceans over large areas and extended time periods. This task is virtually impossible to accomplish with traditional oceanographic measurement techniques.

Seasat (Section 8.11) carried several instruments dedicated to ocean monitoring that operated in the microwave portion of the spectrum. Another satellite carrying ocean-monitoring sensors was the Nimbus-7 satellite, launched in Oc-

TABLE 6.16 Spectral Bands of the Coastal Zone Color Scanner

Channel	Wavelength (μm)	Principal Parameter Measured
1	0.43–0.45	Chlorophyll absorption
2	0.51–0.53	Chlorophyll absorption
3	0.54–0.56	*Gelbstoffe* (yellow substance)
4	0.66–0.68	Chlorophyll concentration
5	0.70–0.80	Surface vegetation
6	10.50–12.50	Surface temperature

tober 1978. This satellite carried the *Coastal Zone Color Scanner* (*CZCS*), which was employed on a limited-coverage "proof-of-concept" mission. The CZCS was designed specifically to measure the color and temperature of the coastal zones of the oceans. Table 6.16 lists the six bands in which the CZCS operated. These included bands in the visible, near-IR, and thermal regions of the spectrum. The system had a 1566-km swath width and an 825-m-resolution cell at nadir.

The first four (visible) bands of the CZCS were very narrow (0.02 μm wide) and centered to enhance the discrimination of very subtle water reflectance differences. Data from these bands were used to successfully map phytoplankton concentrations and inorganic suspended matter such as silt. The near-IR channel was used to map surface vegetation and to aid in separating water from land areas prior to processing data in the other bands. The thermal IR channel was used to measure sea surface temperatures. In short, the CZCS was used to successfully detect chlorophyll, temperature, suspended solids, and *gelbstoffe* (yellow substance) in the combinations and concentrations typical of near-shore and coastal waters. The CZCS ceased operation in mid-1986.

Seasat and the CZCS vividly demonstrated the capability to measure important ocean properties from space. Based on this experience, various other ocean-monitoring systems have been launched and several others are in the design phase. For example, Japan launched its first *Marine Observations Satellite* (*MOS-1*) on February 19, 1987, and a successor to this system (MOS-1b) on February 7, 1990. These satellites employed the three instruments included in Table 6.17, namely a four-channel *Multispectral Electronic Self-Scanning Radiometer* (*MESSR*), a four-channel *Visible and Thermal Infrared Radiometer* (*VTIR*), and a two-channel *Microwave Scanning Radiometer* (*MSR*). (We describe passive microwave radiometers in Section 8.20.)

MOS-1 and MOS-1b operated from an orbit height of 909 km and had a revisit period of 17 days. The design life for each system was 2 years. Note that the MESSR's spectral bands were very similar to those of the Landsat MSS, making MESSR data applicable to many land as well as marine applications.

TABLE 6.17 Instruments Included in MOS-1 and MOS-1b Missions

	Instrument		
	MESSR	VTIR	MSR
Spectral bands	0.51–0.59 μm 0.61–0.69 μm 0.72–0.80 μm 0.80–1.10 μm	0.50–0.70 μm 6.0–7.0 μm 10.5–11.5 μm 11.5–12.5 μm	1.26 cm 0.96 cm
Ground resolution	50 m	900 m (visible) 2700 m (thermal)	32 km (λ = 1.26 cm) 23 km (λ = 0.96 cm)
Swath width	100 km	1500 km	317 km

Another major source of ocean-oriented remote sensing data has been the *Sea-viewing Wide-Field-of-View Sensor* (*SeaWiFS*). SeaWiFS incorporates an eight-channel across-track scanner operating over the range of 0.402 to 0.885 μm (See Table 6.18). This system is designed primarily for the study of ocean biogeochemistry and is a joint venture between NASA and private industry.

Under a procurement arrangement known as a "data buy," NASA contracted with Orbital Sciences Corporation (OSC) to build, launch, and operate SeaWiFS on the OSC OrbView-2 satellite to meet NASA's science requirements for ocean-monitoring data. Orbital Sciences retains the rights to market the resulting data for commercial applications. This is the first time that industry has led the development of an entire mission. The system was launched on August 1, 1997, and has produced data since September 18, 1997.

From a scientific perspective, SeaWiFS data have been used for the study of such phenomena as ocean primary production and phytoplankton processes; cycles of carbon, sulfur, and nitrogen; and ocean influences on

TABLE 6.18 Major Characteristics of the SeaWiFS System

Spectral bands	402–422 nm 433–453 nm 480–500 nm 500–520 nm 545–565 nm 660–680 nm 745–785 nm 845–885 nm
Ground resolution	1.1 km
Swath width	2800 km

physical climate, including heat storage in the upper ocean and marine aerosol formation. Commercial applications have ranged from fishing to navigation, weather prediction, and agriculture.

SeaWiFS produces two major types of data. *Local Area Coverage* (*LAC*) data with 1.13 km nadir resolution are broadcast directly to receiving stations and *Global Area Coverage* (*GAC*) data (subsampled onboard every fourth line, every fourth pixel) are recorded on board the OrbView-2 spacecraft for subsequent transmission. The system was designed to obtain full global coverage (GAC) data every 2 days. The LAC data are collected less frequently on a research priority basis. A 705-km orbit, with a southbound equatorial crossing time of 12:00 noon and a $\pm 58.3°$ scan angle, characterize the system. This provides a scan swath width of approximately 2800 km.

Although originally designed for ocean observation, SeaWiFS has provided a unique opportunity to study land and atmospheric processes as well. In its first year of operation alone, SeaWiFS provided new scientific insights into a number of phenomena. Among others, these include the El Niño and La Niña climate processes; a range of natural disasters, including fires in Florida, Canada, Indonesia, Mexico, and Russia; floods in China; dust storms in the Sahara and Gobi Deserts; hurricanes in numerous locations; and unprecedented phytoplankton blooms. More than 800 scientists representing 35 countries accessed the data in the first year of system operation and more than 50 ground stations throughout the world began receiving the data. In a sense, with its ability to observe ocean, land, and atmospheric processes simultaneously, SeaWIFS has acted as a precursor to the series of instruments comprising the EOS.

Plate 23 is a composite of SeaWiFS GAC data for an 11-month time period showing chlorophyll *a* concentrations in the ocean areas and normalized difference vegetation index values over the land areas.

As part of its Envisat-1 payload, the European Space Agency will operate the *Medium Resolution Imaging Spectrometer* (*MERIS*). This system is also primarily aimed at addressing the needs of oceanographic observations (with additional utility in atmospheric and land observations on a secondary basis).

The MERIS is a pushbroom instrument having a 1150-km-wide swath that is divided into five segments for data acquisition. Five identical sensor arrays collect data side by side with a slight overlap between adjacent swaths. Data are collected at 300 m nadir resolution over coastal zones and land areas. Open-ocean data can also be collected at a reduced resolution of 1200 m through onboard combinations of 4×4 adjacent pixels across and along track.

The MERIS has the ability to record data in as many as 15 bands. This system is programmable by ground command such that the number, location, and width of each spectral band can be varied within the 0.4- to 1.05-μm range.

6.18 EARTH OBSERVING SYSTEM

The *Earth Observing System* (*EOS*) is one of the primary components of a NASA-initiated concept originally referred to as *Mission to Planet Earth* (*MTPE*), which was renamed the *Earth Science Enterprise* (*ESE*) during 1998. The ESE is an international earth science program aimed at providing the observations, understanding, and modeling capabilities needed to assess the impacts of natural events and human-induced activities on the earth's environment. The program incorporates both space- and ground-based measurement systems to provide the basis for documenting and understanding global change with an initial emphasis on climate change. The program also focuses on the necessary data and information systems to acquire, archive, and distribute the data and information collected about the earth. The intent is to further international understanding of the earth as a system.

The EOS component of the ESE includes the currently operational observing systems (beginning with Landsat-7), new programs under development, and planned programs for the future. Clearly, programs of this magnitude, cost, and complexity are subject to change. Also, the EOS program includes numerous platforms and sensors that are outside the realm of land-oriented remote sensing. We make no attempt to describe the overall program. Rather, we limit our attention to the first two EOS-dedicated platforms, the *Terra* and *Aqua* spacecrafts. Sometimes described as the "flagship" of EOS, Terra was launched on December 18, 1999. It was followed on May 4, 2002, by Aqua. Both of these platforms are complex systems with multiple remote sensing instruments. Five sensors are included on Terra:

ASTER:	Advanced Spaceborne Thermal Emission and Reflection Radiometer
CERES:	Clouds and the Earth's Radiant Energy System
MISR:	Multi-Angle Imaging Spectro-Radiometer
MODIS:	Moderate Resolution Imaging Spectro-Radiometer
MOPITT:	Measurements of Pollution in the Troposphere

Aqua carries six instruments, two of which (MODIS and CERES) are also present on Terra. The remaining four instruments on Aqua include:

AMSR/E:	Advanced Microwave Scanning Radiometer-EOS
AMSU:	Advanced Microwave Sounding Unit
AIRS:	Atmospheric Infrared Sounder
HSB:	Humidity Sounder for Brazil

Table 6.19 summarizes the salient characteristics and applications associated with each of the instruments on Terra and Aqua.

TABLE 6.19 Sensors Carried on Terra and Aqua

Sensor	Terra/ Aqua	General Characteristics	Primary Applications
ASTER	Terra	Three scanners operating in the visible and near, mid, and thermal IR, 15–90 m resolution, along-track stereo	Study vegetation, rock types, clouds, volcanoes; produce DEMs; provide high resolution data for overall mission requirements
MISR	Terra	Four-channel CCD arrays providing nine separate view angles	Provide multiangle views of earth surface features, data on clouds and atmospheric aerosols, and correction for atmospheric effects to data from ASTER and MODIS
MOPITT	Terra	Three channel near-IR scanner	Measure carbon monoxide and methane in the atmospheric column
CERES	Both	Two broadband scanners	Measure radiant flux at top of the atmosphere to monitor earth's total radiation energy balance
MODIS	Both	Thirty-six-channel imaging spectrometer; 250 m to 1 km resolution	Useful for multiple land and ocean applications, cloud cover, cloud properties
AIRS	Aqua	Hyperspectral sensor with 2378 channels, 2 to 14 km spatial resolution	Measure atmospheric temperature and humidity, cloud properties, and radiative energy flux
AMSR/E	Aqua	Twelve-channel microwave radiometer, 6.9 to 89 GHz	Measure precipitation, land surface wetness and snow cover, sea surface characteristics, cloud properties
AMSU	Aqua	Fifteen-channel microwave radiometer, 50 to 89 GHz	Measure atmospheric temperature and humidity
HSB	Aqua	Five-channel microwave radiometer, 150 to 183 MHz	Measure atmospheric humidity

The intent in the design of Terra and Aqua is to provide a suite of highly synergistic instruments on each platform. For example, four of the five instruments on Terra are used in a complementary manner to obtain data about cloud properties. Similarly, measurements made by one instrument (e.g., MISR) can be used to atmospherically correct the data for another (e.g., MODIS). In composite, each spacecraft provides detailed measurements contributing to a number of interrelated scientific objectives. Figure 6.37 illustrates the basic relationships among the science objectives, measurements, and instruments included in the Terra mission.

Both Terra and Aqua are quite massive for earth-observing satellites. Terra is approximately 6.8 m long and 3.5 m in diameter and weighs 5190 kg, while Aqua is 16.7 × 8.0 × 4.8 m and weighs 2934 kg. The satellites are in near-polar, sun-synchronous orbits at 705 km altitude, and their orbits fit those of the WRS-2 numbering system developed for Landsat-4, -5, and -7.

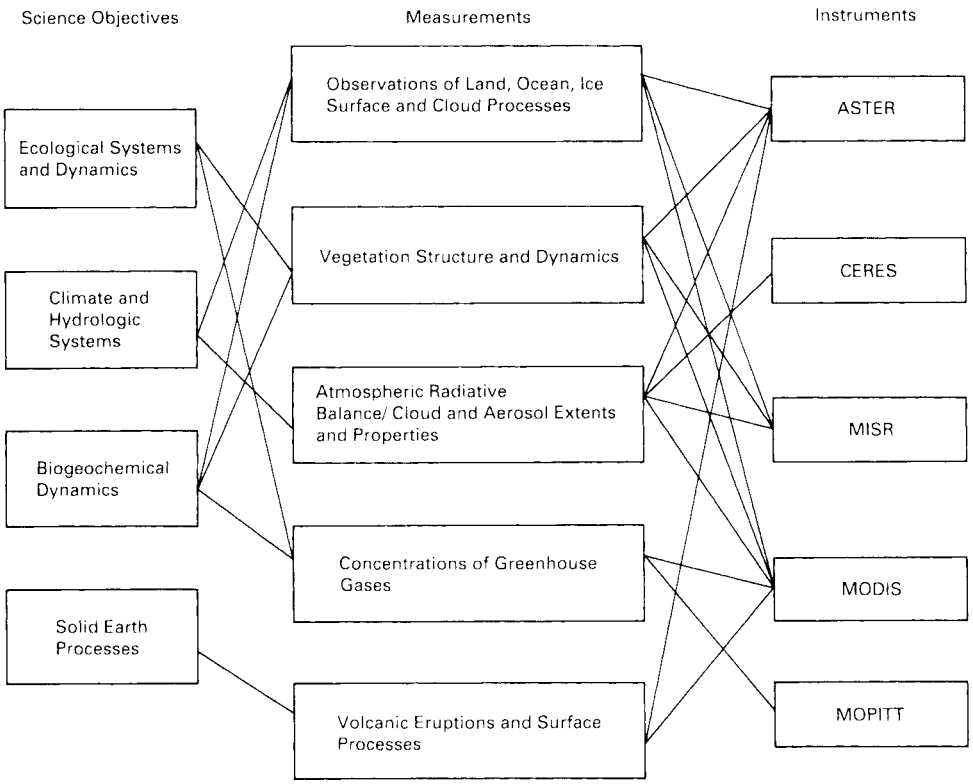

Figure 6.37 Principal relationships among the science objectives, measurements, and instruments involved in the Terra mission. (After NASA diagram.)

Terra has a 10:30 A.M. equatorial crossing time (descending), a time chosen to minimize cloud cover. Aqua has a 1:30 P.M. equatorial crossing time (ascending). Among the instruments carried on Terra and Aqua, the three of greatest interest to the readership of this book are the MODIS, ASTER, and MISR instruments.

MODIS

Flown on both the Terra and Aqua satellites, MODIS is a sensor that is intended to provide comprehensive data about land, ocean, and atmospheric processes simultaneously. Its design is rooted in various earlier sensors, or "heritage instruments," such as the AVHRR and CZCS. However, MODIS is a highly improved successor to these earlier systems. MODIS not only provides 2-day repeat global coverage with greater spatial resolution (250, 500, or 1000 m, depending on wavelength) than the AVHRR, but it also collects data in 36 carefully chosen spectral bands (Table 6.20), with 12-bit radiometric sensitivity. In addition,

TABLE 6.20 MODIS Spectral Bands

Primary Use	Band	Bandwidth	Resolution (m)
Land/cloud boundaries	1	620–670 nm	250
	2	841–876 nm	250
Land/cloud properties	3	459–479 nm	500
	4	545–565 nm	500
	5	1230–1250 nm	500
	6	1628–1652 nm	500
	7	2105–2155 nm	500
Ocean color/ phytoplankton/ biogeochemistry	8	405–420 nm	1000
	9	438–448 nm	1000
	10	483–493 nm	1000
	11	526–536 nm	1000
	12	546–556 nm	1000
	13	662–672 nm	1000
	14	673–683 nm	1000
	15	743–753 nm	1000
	16	862–877 nm	1000
Atmospheric water vapor	17	890–920 nm	1000
	18	931–941 nm	1000
	19	915–965 nm	1000
Surface/cloud temperature	20	3.660–3.840 μm	1000
	21[a]	3.929–3.989 μm	1000
	22	3.929–3.989 μm	1000
	23	4.020–4.080 μm	1000
Atmospheric temperature	24	4.433–4.498 μm	1000
	25	4.482–4.549 μm	1000
Cirrus clouds	26[b]	1.360–1.390 μm	1000
Water vapor	27	6.538–6.895 μm	1000
	28	7.175–7.475 μm	1000
	29	8.400–8.700 μm	1000
Ozone	30	9.580–9.880 μm	1000
Surface/cloud temperature	31	10.780–11.280 μm	1000
	32	11.770–12.270 μm	1000
Cloud top altitude	33	13.185–13.485 μm	1000
	34	13.485–13.758 μm	1000
	35	13.785–14.085 μm	1000
	36	14.085–14.385 μm	1000

[a]Band 21 and 22 are similar, but band 21 saturates at 500 K versus 328 K.

[b]Wavelength out of sequence due to change in sensor design.

MODIS data are characterized by improved geometric rectification and radiometric calibration. Band-to-band registration for all 36 MODIS channels is specified to be 0.1 pixel or better. The 20 reflected solar bands are absolutely calibrated radiometrically with an accuracy of 5 percent or better. The calibrated accuracy of the 16 thermal bands is specified to be 1 percent or better.

These stringent calibration standards are a consequence of the EOS/ESE requirement for a long term continuous series of observations aimed at documenting subtle changes in global climate. This data set must not be sensor dependent; hence, the emphasis on sensor calibration.

The total field of view of MODIS is $\pm 55°$, providing a swath width of 2330 km. A large variety of data products can be derived from MODIS data. Among the principal data products available are the following:

Cloud mask at 250 m and 1000 m resolution during the day and 1000 m resolution at night.

Aerosol concentration and optical properties at 5 km resolution over oceans and 10 km over land during the day.

Cloud properties (optical thickness, effective particle radius, thermodynamic phase, cloud top altitude, cloud top temperature) at 1 to 5 km resolution during the day and 5 km resolution at night.

Vegetation and land surface cover, conditions, and productivity, defined as vegetation indices corrected for atmospheric effects, soil, polarization, and directional effects; surface reflectance; land cover type; and net primary productivity, leaf area index, and intercepted photosynthetically active radiation.

Snow and sea-ice cover and reflectance.

Surface temperature with 1 km resolution, day and night, with absolute accuracy goals of 0.3 to 0.5°C over oceans and 1°C over land.

Ocean color (ocean-leaving spectral radiance measured to 5 percent), based on data acquired from the MODIS visible and near-IR channels.

Concentration of chlorophyll *a* (within 35 percent) from 0.05 to 50 mg/m^3 for case 1 waters.

Chlorophyll fluorescence (within 50 percent) at surface water concentration of 0.5 mg/m^3 of chlorophyll *a*.

Plates 24 and 25 show examples of high-level products derived from MODIS imagery. Plate 24 shows a global rendition of land surface reflectance and sea surface temperature. Both data sets were developed from composites of multiple dates of MODIS imagery in March and April 2000, with 7 dates being used for the sea surface temperature data and 20 dates for the land surface reflectance. Plate 25 shows a MODIS-based sea surface temperature map of the western Atlantic, including a portion of the Gulf Stream. Land areas and clouds have been masked out. Cold water, approximately 7°C, is shown in purple, with blue, green, yellow, and red representing increasingly warm water, up to approximately 22°C. The warm current of the Gulf Stream stands out clearly in deep red colors.

ASTER

The ASTER is an imaging instrument that is a cooperative effort between NASA and Japan's Ministry of International Trade and Industry. In a sense, ASTER serves as a "zoom lens" for the other instruments aboard Terra in that it has the highest spatial resolution of any of them. ASTER consists of three separate instrument subsystems, each operating in a different spectral region, using a separate optical system, and built by a different Japanese company. These subsystems are the *Visible and Near Infrared* (*VNIR*), the *Short Wave Infrared* (*SWIR*), and the *Thermal Infrared* (*TIR*), respectively. Table 6.21 indicates the basic characteristics of each of these subsystems.

The VNIR subsystem incorporates three spectral bands that have 15 m ground resolution. The instrument consists of two telescopes—one nadir looking with a three-band CCD detector and the other backward looking (27.7° off nadir) with a single-band (band 3) detector. This configuration enables

TABLE 6.21 ASTER Instrument Characteristics

Characteristic	VNIR	SWIR	TIR
Spectral range	Band 1: 0.52–0.60 μm, nadir looking	Band 4: 1.600–1.700 μm	Band 10: 8.125–8.475 μm
	Band 2: 0.63–0.69 μm, nadir looking	Band 5: 2.145–2.185 μm	Band 11: 8.475–8.825 μm
	Band 3: 0.76–0.86[a] μm, nadir looking	Band 6: 2.185–2.225 μm	Band 12: 8.925–9.275 μm
	Band 3: 0.76–0.86[a] μm, backward looking	Band 7: 2.235–2.285 μm	Band 13: 10.25–10.95 μm
		Band 8: 2.295–2.365 μm	Band 14: 10.95–11.65 μm
		Band 9: 2.360–2.430 μm	
Ground resolution (m)	15	30	90
Cross-track pointing (deg)	±24	±8.55	±8.55
Cross-track Pointing (km)	±318	±116	±116
Swath width (km)	60	60	60
Quantization (bits)	8	8	12

[a]Stereoscopic imaging subsystem.

along-track stereoscopic image acquisition in band 3 with a base-height ratio of 0.6. This permits the construction of DEMs from the stereo data with a vertical accuracy of approximately 7 to 50 m. Cross-track pointing to 24° on either side of the orbit path is accomplished by rotating the entire telescope assembly.

The SWIR subsystem operates in six spectral bands through a single, nadir-pointing telescope that provides 30 m resolution. Cross-track pointing to 8.55° is accomplished through the use of a pointing mirror.

The TIR subsystem operates in 5 bands in the thermal IR region with a resolution of 90 m. Unlike the other instrument subsystems, it incorporates a whiskbroom scanning mirror. Each band uses 10 detectors, and the scanning mirror functions both for scanning and cross-track pointing to 8.55°.

All ASTER bands cover the same 60-km imaging swath with a pointing capability in the cross-track direction to cover ±116 km from nadir. This means that any point on the globe is accessible at least once every 16 days with full 14-band spectral coverage from the VNIR, SWIR, and TIR. In that the VNIR subsystem has a larger pointing capability, it can collect data up to ±318 km from nadir, with an average revisit period of 4 days at the equator.

Plate 26 shows examples of ASTER imagery for the San Francisco Bay region in California, acquired on March 3, 2000. The color infrared composite (*a*) uses ASTER bands 1, 2, and 3, from the visible and near IR. Vegetation appears red, urban areas are gray, and sediment in the bays shows up as lighter shades of blue. At the spatial resolution of 15 m, shadows of the towers along the Bay Bridge can be seen (but not at the scale shown in this plate). In Plate 26*b*, a composite of bands in the mid IR displays differences in soils and rocks in the mountainous areas. Even though these regions appear entirely vegetated in the visible and near IR, there are enough openings in the vegetation to allow the ground to be imaged. Plate 26*c* shows a composite of three ASTER thermal bands, revealing differences in urban materials in varying colors. Separation of materials is due to differences in thermal emission properties. Where the thermal emissivity is known (e.g., for the water of San Francisco Bay), the ASTER thermal bands can be used to calculate kinetic temperature, as shown in Plate 26*d*. This is a color-coded temperature image of water temperature, with warm waters in white and yellow and colder waters in blue. Suisun Bay in the upper right is fed directly from the cold Sacramento River. As the water flows through San Pablo and San Francisco Bays on the way to the Pacific, the waters warm up.

Three individual bands of an ASTER data set for a 13.3 × 54.8-km area in Death Valley, California, are shown as Figure 6.38. Note that this area represents only a portion of the full ASTER swath width. Plate 27 shows three color composites of ASTER data for the same area as shown in Figure 6.38. Plate 27*a* is a color composite of three VNIR (visible and near-IR) bands, part (*b*) shows three SWIR (mid-IR) bands, and part (*c*) shows three TIR (thermal IR) bands. Various geological and vegetation differences are displayed in the

three parts of this plate. For example, the bright red areas in (*a*) are patches of vegetation on the Furnace Creek alluvial fan that reflect more highly in the near-IR than in the green or red parts of the spectrum. These are seen as blue in (*b*), but are difficult to discern in (*c*), which shows thermal bands with 90 m resolution as contrasted with the 15 m resolution of (*a*) and the 30 m resolution of (*b*). A striking difference in geological materials is seen in (*c*), where surfaces containing materials high in the mineral quartz have a red color.

Because the nadir-looking and backward-looking band 3 sensors can obtain data of the same area from two different angles, stereo ASTER data can be used to produce DEMs. Various bands of ASTER image data can then be "draped" over the DEMs to produce perspective views of an area, as illustrated in Figure 6.39. (The area shown in Figure 6.39 roughly corresponds with that in Figure 6.38 and Plate 27.) Such perspective views can help image analysts to obtain an overview of the area under study. For example, in this figure, bedrock mountains are located at left (west) and right (east). The broad, very light toned area through the center of the image is the floor of Death Valley. Between the mountains and the valley floor, many alluvial fans (essentially continuous on the west side of the valley floor) can be seen.

MISR

The MISR instrument differs from most other remote sensing systems in that it has nine sensors viewing the earth simultaneously at different angles. Each sensor consists of a set of linear arrays providing coverage in four spectral bands (blue, green, red, and near IR). One sensor is oriented toward nadir (0°); four sensors are viewing forward at angles of 26.1°, 45.6°, 60.0°, and 70.5°; and four are viewing backward at similar angles. The system has a swath width of 360 km, and a spatial resolution of 250 m in the nadir-viewing sensor and 275 m in the off-nadir sensors.

The MISR viewing angles were selected to address several different objectives. The nadir-viewing sensor provides imagery with the minimum interference from the atmosphere. The two sensors at 26.1° off nadir were selected to provide stereoscopic coverage for measurement of cloud-top altitudes, among other purposes. The 45.6° sensors provide information about aerosols in the atmosphere, which are of great importance for studies of global change and the earth's radiation budget. The 60.0° sensors minimize the effects of directional differences in the scattering of light from clouds and can be used to estimate the hemispherical reflectance of land surface features. Finally, the 70.5° sensors were chosen to provide the most oblique angle that could be achieved within practical limitations, in order to maximize the impact of off-nadir scattering phenomena.

Analysis of MISR imagery contributes to studies of the earth's climate and helps monitor the global distribution of particulate pollution and different

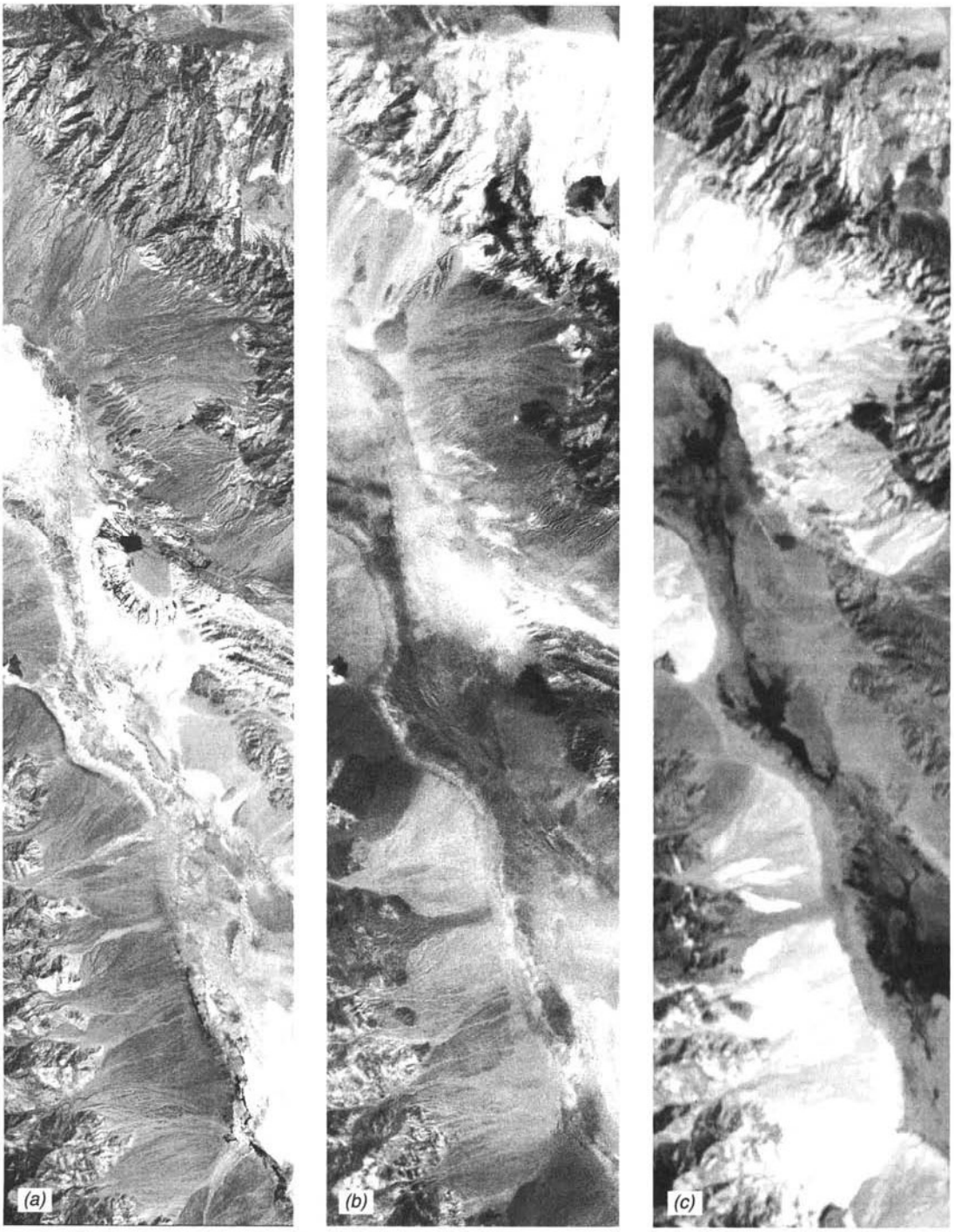

Figure 6.38 ASTER data, Death Valley, CA, early March: (*a*) band 2 (red); (*b*) band 5 (mid IR); (*c*) band 13 (thermal IR). Scale 1:300,000.

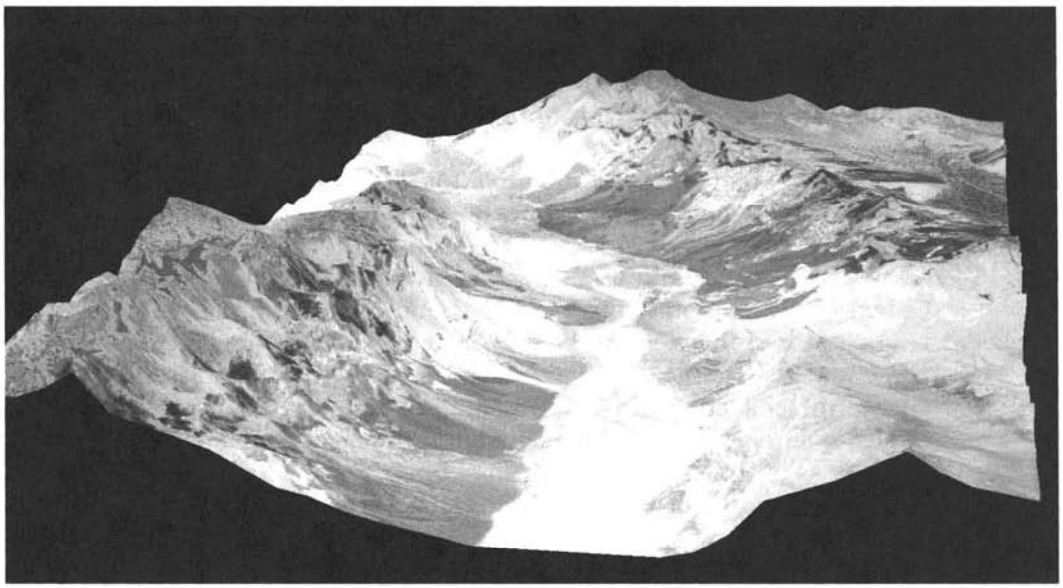

Figure 6.39 ASTER data draped over a digital elevation model, Death Valley, CA (view to the north). Black and white copy of a color composite derived from thermal IR bands. (Courtesy NASA/JPL.)

types of haze. For example, Plate 28 shows a series of MISR images of the eastern United States, acquired during a single orbit (on March 6, 2000) at four different angles. The area shown ranges from Lakes Ontario and Erie to northern Georgia, and covers a portion of the Appalachian Mountains. The eastern end of Lake Erie was covered by ice on this date, and thus appears bright in these images. Plate 28*a* was acquired at an angle of 0° (nadir-viewing), while (*b*), (*c*), and (*d*) were acquired at forward-viewing angles of 45.6°, 60.0°, and 70.5°, respectively. Areas of extensive haze over the Appalachian Mountains are almost invisible in the 0° image but have a major effect on the 70.5° image, due to the increased atmospheric path length. The images in (*c*) and (*d*) appear brighter due to increased path radiance, but also have a distinct color shift toward the blue end of the spectrum. This is a result of the fact that Rayleigh scattering in the atmosphere is inversely proportional to the fourth power of the wavelength, as discussed in Chapter 1.

6.19 SPACE STATION REMOTE SENSING

Remote sensing has been a part of previous space station missions and will likely continue in this vein in the *International Space Station* (*ISS*) program. As mentioned previously (Section 6.2), the first American space workshop, Skylab, was used to acquire numerous forms of remote sensing data in 1973.

The Russian MIR space station was fitted with a dedicated remote sensing module called PRIRODA that was launched in 1996. With contributions from 12 nations, the PRIRODA mission consisted of a broad variety of different sensors, including numerous optical systems as well as both active and passive microwave equipment.

The ISS provides an excellent platform for remote sensing from space, although its potential has barely begun to be realized. The orbital coverage of the ISS extends from 52° N to 52° S latitude. It orbits the earth every 90 min at an altitude of 400 km, and the revisit period over any given point at the equator (within 9° off nadir) is 32 hr. Hence, approximately 75 percent of the land surface of the globe, 100 percent of the rapidly changing tropics, and 95 percent of the world's population can be observed from this platform. To facilitate the collection of earth observation imagery, a 50-cm-diameter, high-optical-quality window has been installed in one of the laboratory modules on the ISS. As of the date of this writing (2002), no organized effort to collect remote sensing data from the ISS has been undertaken. However, ISS crewmembers have taken thousands of frames of imagery using a variety of film and digital cameras, sometimes in combination with telescopes. These images are being contributed to an ever-growing database of earth observation photographs at the NASA Johnson Space Center that dates back to the early years of the U.S. space program. In the future, data collected from the ISS could be used for applications ranging from validating other global terrestrial data sets to real-time monitoring of ephemeral events and human-induced global change. Real-time human oversight of the acquisition of such data complements greatly the capabilities of the various satellite systems discussed in this chapter.

SELECTED BIBLIOGRAPHY

Al-Rawi, K.R., et al., "Integrated Fire Evolution Monitoring System (IFEMS) for Monitoring Spatial-Temporal Behaviour of Multiple Fire Phenomena," *International Journal of Remote Sensing*, vol. 23, no. 10, 2002, pp. 1967–1983.

American Society of Photogrammetry (ASP), *Manual of Remote Sensing*, 2nd ed., ASP, Falls Church, VA, 1983.

American Society for Photogrammetry and Remote Sensing (ASPRS), *GAP Analysis Program Proceedings*, ASPRS, Bethesda, MD, 1996.

American Society for Photogrammetry and Remote Sensing (ASPRS), *Corona Between the Sun and the Earth: The First NRO Reconnaissance Eye in Space*, ASPRS, Bethesda, MD, 1997a.

American Society for Photogrammetry and Remote Sensing (ASPRS), *Earth Observing Platforms and Sensors*, Manual of Remote Sensing, 3rd ed. (A Series), Version 1.1, ASPRS, Bethesda, MD, 1997b (CD-ROM).

American Society for Photogrammetry and Remote Sensing (ASPRS), *Proceedings: Land Satellite Information in the Next Decade II: Sources and Applications*, ASPRS, Bethesda, MD, 1997c (CD-ROM).

American Society for Photogrammetry and Remote Sensing (ASPRS), *Remote Sensing for the Earth Sciences*, Manual of Remote Sensing, 3rd. ed., Vol. 3, Wiley, New York, 1999.

American Society for Photogrammetry and Remote Sensing (ASPRS) and Rand Corp.; *Commercial Observation Satellites at the Leading Edge of Global Trans-*